



UNIVERSITÀ DEGLI STUDI DI TRIESTE

---

DIPARTIMENTO DI FISICA  
Corso di Laurea Magistrale in Fisica  
Curriculum in Microfisica e Fisica della materia

# Tomografia quantistica applicata alle spettroscopie risolte in tempo

Quantum state tomography applied to time resolved spectroscopy

*Relatore:*  
**Dott. Daniele Fausti**

*Correlatori:*  
**Martina Esposito**  
**Prof. Fulvio Parmigiani**

*Laureanda:*  
**Francesca Giusti**

---

ANNO ACCADEMICO 2013/2014



# Contents

<b>Introduction</b>	<b>1</b>
<b>1 Fundamental concepts</b>	<b>5</b>
1.1 Field Quantization . . . . .	5
1.2 Coherent and Squeezed States . . . . .	8
1.3 The Density Operator . . . . .	13
1.3.1 <i>Example: one-dimensional harmonic oscillator</i> . . . . .	13
1.3.2 The density operator formalism . . . . .	14
1.3.3 Properties of the density operator . . . . .	15
1.3.4 <i>Example: a two level system</i> . . . . .	16
1.3.5 Time evolution of the density operator . . . . .	18
1.3.6 Liouville representation . . . . .	19
<b>2 Theory</b>	<b>23</b>
2.1 Wigner Function . . . . .	23
2.1.1 Properties of the Wigner function . . . . .	24
2.1.2 Time evolution of the Wigner Function . . . . .	27
2.2 Homodyne detection . . . . .	29
2.2.1 Beam Splitter . . . . .	30
2.2.2 From photocurrents to quadratures . . . . .	31
2.2.3 Pulsed regime . . . . .	32
<b>3 Time resolved measurements</b>	<b>35</b>
3.1 Nonlinear response function . . . . .	36
3.1.1 Time evolution operator . . . . .	37
The interaction picture . . . . .	38

3.1.2	Expansion of the density operator . . . . .	39
	Third order response . . . . .	41
3.1.3	Extended systems . . . . .	42
3.1.4	Double-sided Feynman diagrams . . . . .	43
3.2	Classification of four wave mixing techniques . . . . .	44
3.2.1	n-wave mixing . . . . .	44
	Heterodyne detection of wave mixing . . . . .	46
3.2.2	Four wave mixing . . . . .	47
3.3	Pump and probe . . . . .	49
3.4	Off-resonant Raman Scattering . . . . .	51
	<i>Brownian oscillator model</i> . . . . .	53
3.4.1	Impulsive Raman Scattering . . . . .	57
<b>4</b>	<b>Experimental apparatus</b>	<b>61</b>
4.1	Experimental set-up . . . . .	61
4.1.1	Standard time domain Raman measurements . . . . .	62
4.1.2	Homodyne detection without local oscillator . . . . .	65
4.1.3	Time resolved homodyne detection . . . . .	66
4.2	Instrumentation . . . . .	67
4.2.1	Balanced Differential Detector . . . . .	67
4.2.2	The fast digitizer . . . . .	71
<b>5</b>	<b>Experimental results</b>	<b>73</b>
5.1	Standard time domain Raman Spectroscopy . . . . .	73
	Lock-in . . . . .	74
	Fast digitizer . . . . .	75
5.2	Homodyne detection without local oscillator . . . . .	80
5.3	Time dependent Balanced Homodyne Detection . . . . .	82
5.3.1	Fixed phase difference . . . . .	82
5.3.2	Fixed time delay . . . . .	85
<b>6</b>	<b>Discussion</b>	<b>89</b>
6.1	Stimulated Raman Scattering on $\alpha$ -Quartz . . . . .	89
6.1.1	Raman active modes . . . . .	90
6.1.2	The probing process . . . . .	91

---

6.2	From the probe state to quantum fluctuation of the vibrational mode . . . . .	94
6.2.1	Squeezing of the vibrational mode in photon number fluctuations . . . . .	94
6.2.2	Full quantum state reconstruction of the probe pulses	97
6.2.3	From photon to phonon quantum state detection . . .	100
<b>A</b>	<b>Thermal states</b>	<b>105</b>
<b>B</b>	<b>Laser source</b>	<b>107</b>
B.1	Mode-Locking . . . . .	107
B.2	Kerr lens mode-locking . . . . .	108
B.3	Chirped pulse amplification . . . . .	110
B.4	The laser system . . . . .	110
<b>C</b>	<b>Autocorrelation</b>	<b>113</b>
<b>D</b>	<b>Systematic errors in BHD measurements</b>	<b>117</b>
<b>E</b>	<b>Wigner function reconstruction</b>	<b>121</b>
	<b>Conclusions</b>	<b>125</b>
	<b>Riassunto</b>	<b>127</b>
	<b>Bibliografia</b>	<b>137</b>
	<b>Ringraziamenti</b>	<b>139</b>



# Introduction

In complex systems anomalous properties can arise from the intricate interplay between the electronic, spin and magnetic degrees of freedom. Unraveling the physical mechanisms leading to such properties can be complicated as at equilibrium the interplay between specific excitation cannot be measured and is hidden under thermal fluctuations. Non-equilibrium techniques based on ultrashort ( $\sim 100$  fs) laser pulses allow to bridge this kind of limitation. The rationale of non-equilibrium approaches to complex material is the following. One ultrashort laser pulse is used to bring the sample out of the equilibrium and the relaxation processes can be measured by a second light pulse. As a matter of fact a system can be characterized by its response to a light induced perturbation: the time resolved measurement of an optical property of the perturbed system can reveal microscopic interactions, if the time interval of the sampling is much shorter than the characteristic time of thermal interactions.

Non-equilibrium studies of matter are based on the so called *pump and probe spectroscopy*. In pump and probe experiments the system is excited by an intense ultrashort light pulse, called pump, and its evolution is measured at a time delay  $\tau$  by another ultrashort pulse, the probe, reflected or transmitted by the sample. The measurement of the variation intensity of the transmitted or reflected beam provides information on the relaxation of the system and so on the evolution of its physical properties. The time delay  $\tau$  can be tuned by changing the optical path of one of the two beams.

This technique can be used to study electronic transitions in the sample, but also vibrational excitation in crystals through *Raman scattering*, that is, the

excitation (or de-excitation) of an optical phononic mode in a crystal due to electromagnetic radiation. In the Impulsive Stimulated Raman Scattering an ultrashort pump pulse excites a vibrational mode in the medium and the probe is scattered by the excited sample, providing information about the mode itself.

A "standard" time resolved experiment measures the time evolution of the material observables such as reflectivity or transmittance, which are related to the intensity and so to the variation of the mean number of photons  $\langle n \rangle = \langle a^\dagger a \rangle$  of the transmitted or reflected probe. In this kind of experiments the time domain response is typically measured integrating over subsequent repeated pump and probe measurements. So far, no significant effort has been made to measure higher order photon correlation in time domain experiments and, more specifically, to understand which significant information can be retrieved from a full time dependent quantum state characterization of the probe pulse. In this thesis we have worked in experimental conditions good enough to maintain the noise smaller than the intrinsic fluctuations of the number of photons, so that we could extend the usual measure of an "integrated" optical property to a full quantum state reconstruction of the probe pulse.

We have employed quantum state reconstruction techniques, such as *Balanced Homodyne Detection*, which are commonly used for the study of the quantum state of light. The novelty of our approach is the coupling with time resolved spectroscopy. The challenge is to understand if and eventually how the quantum state of light is affected by the phonon one in a time resolved experiment.

In this thesis work an experimental set-up which combines pump-probe spectroscopy and Balanced Homodyne Detection has been assembled in the *T-Rex* laboratory at Elettra-Sincrotrone Trieste.

The theory and the results of the experiment are collected in this thesis and are organized as follows:

- Chapter 1 and 2 contains the theoretical treatments of basic concepts of quantum optics, focusing in particular on the density operator formalism and on an experimental technique to detect the quantum state of light.
- In Chapter 3 time resolved techniques, such as pump-probe spectroscopy and Stimulated Raman Scattering are presented; the chapter is based on the S. Mukamel's treatment of four wave mixing techniques [1].
- Chapter 4 describes the experimental set-ups used for three different kinds of measurement. Particular attention has been paid on the characterization of the Balance Differential Detector with low electronic noise.
- Chapters 5 and 6 finally show and discuss experimental results.



# Chapter 1

## Fundamental concepts

The purpose of this thesis is to use the quantum state reconstruction of ultrashort light pulses as a spectroscopic mean in pump and probe experiments. In this chapter I will introduce the fundamental concepts of quantum optics which will be used further on in the thesis. In particular, the main result of this thesis is the first measurements of light quantum state in time domain experiments. In order to make the approach clear we will introduce a few basic concepts. First of all, we will specify what measuring the quantum state of a system means. In order to clarify the approach to quantum state measurements, we are going to introduce the concept of quantum state associated to the electromagnetic field, using the harmonic oscillator formalism. This rather "abstract" idea becomes more concrete through the use of appropriate formalisms. After quantizing the electromagnetic field we will introduce the density operator (defined in the last section of the chapter), that allows us to consider a larger class of quantum states: not only pure states (described simply by the wave function formalism), but also mixed states.

### 1.1 Field Quantization

Both the systems we are going to study (the modes of an electromagnetic field and the vibrational modes in condensed matter lattices) are described by the harmonic oscillator formalism. I will now consider only the electromagnetic

field quantization, but the concept can be generalized also to phononic fields. With the phrase *field quantization*, one means the substitution of classical dynamic variables of the field with operators that fulfill suitable commutation relations. We will see that each mode of the electromagnetic field can be described as a quantum harmonic oscillator, and so it can be described using the same formalism.

From classical electrodynamics we know that an electromagnetic field is defined by two physical quantities, the electric and magnetic field, which are related to each other by the Maxwell equations. We know that the same field can be described by the vector and the scalar potential. These potentials are not uniquely defined; on the contrary there are several couples of potentials that satisfy the relations with the fields and we can choose the most convenient ones (that is the most convenient *gauge*). In particular we choose the so called Coulomb gauge:  $\nabla \vec{A} = 0$  and  $\phi = 0$ , where  $\vec{A}$  is the vector potential and  $\phi$  is the scalar potential.

An electromagnetic mode is defined by its wavevector  $\vec{k}$  and its polarization  $\hat{\epsilon}$ ; for simplicity we will consider a single mode case. In order to generalize to multi mode radiation fields it is sufficient to sum over all possible  $\vec{k}$ .

Substituting the definition of the vector potential in the Maxwell equations and remembering that we are in the Coulomb gauge, we get a second order differential equation for the vector potential, whose general solution, for a single mode, is

$$\vec{A}(\vec{r}, t) = \frac{1}{V} \left[ C_0 \hat{\epsilon} e^{i(\vec{k} \cdot \vec{r} - \omega t)} + c.c. \right], \quad (1.1)$$

where  $C_0$  is a constant,  $V$  is a "normalizing" volume and *c.c.* means complex conjugate. From this expression of the vector potential  $\vec{A}$  one can obtain the electric and magnetic field.

From the classical theory we know the expression of the energy of the light field, which is (in cgs unit system)

$$\varepsilon = \frac{1}{8\pi} \int_V (E^2 + B^2) d\tau. \quad (1.2)$$

Substituting the expressions for the electric and magnetic fields, keeping in mind that the polarization vector is a versor (and so  $|\hat{\epsilon}|^2 = 1$  and  $(\vec{k} \times \hat{\epsilon}^*) \cdot$

$(\vec{k} \times \hat{\epsilon}) = \frac{\omega^2}{c^2}$  ) and integrating over the volume we get

$$\varepsilon = \frac{1}{2\pi} \frac{\omega^2}{c^2} |C(t)|^2, \quad (1.3)$$

where  $C(t) = C_0 e^{-\omega t}$ .

Let us consider now a classical harmonic oscillator, whose Hamiltonian is

$$H_{HO} = \frac{p^2}{2m} + \frac{m\omega^2}{2} q^2. \quad (1.4)$$

Rescaling  $\mathbf{p}$  and  $\mathbf{q}$  according to

$$\begin{aligned} \mathbf{p} &= \sqrt{m\omega} \mathbf{P} \\ \mathbf{q} &= \frac{\mathbf{Q}}{\sqrt{m\omega}} \end{aligned} \quad (1.5)$$

we get two new quantities ( $\mathbf{P}$  and  $\mathbf{Q}$ ), with the same dimensions, that satisfy the relations

$$\begin{aligned} H_{HO} &= \frac{\omega}{2} (Q^2 + P^2) \\ \frac{dQ}{dt} &= \omega P, \end{aligned} \quad (1.6)$$

so that they can be parametrized this way

$$\begin{aligned} Q &= \alpha_0 \cos(\omega t) \\ P &= -\alpha_0 \sin(\omega t). \end{aligned} \quad (1.7)$$

We immediately note that  $\mathbf{Q}$  and  $\mathbf{P}$  are proportional to the real and imaginary part of  $C(t)$  as defined above and rescaling  $C(t)$  with a proper constant one gets an electromagnetic field hamiltonian identical to one of the harmonic oscillator (Equation 1.6).

Since the hamiltonian of the harmonic oscillator and of the electromagnetic field is the same, we expect that also their eigenvalues and eigenstates are the same: an eigenstate  $|n\rangle$  corresponds to an eigenvalue  $E_n = \hbar\omega (n + \frac{1}{2})$ . Every photon carries an energy  $\hbar\omega$  and there is a zero point energy of  $\frac{\hbar\omega}{2}$ .

Until now we have just shown the analogies between the two considered systems: we have not quantized the electromagnetic field yet. But, because of the equivalence between our system and the harmonic oscillator, we can quantize them in the same way, i.e. using the annihilation and creation

operators, defined respectively as  $\hat{a} = \frac{\hat{Q} + i\hat{P}}{\sqrt{2\hbar}}$  and  $\hat{a}^\dagger = \frac{\hat{Q} - i\hat{P}}{\sqrt{2\hbar}}$ , that acts on the eigenstates of the hamiltonian as follows

$$\hat{a}^\dagger |n\rangle = \sqrt{n+1} |n+1\rangle \quad (1.8)$$

$$\hat{a} |n\rangle = \sqrt{n} |n-1\rangle \quad (1.9)$$

with  $[a, a^\dagger] = 1$ .

$\hat{Q}$  and  $\hat{P}$  are called *quadrature* of the electromagnetic field and, since they are function of the creation and annihilation operators, are operators themselves (from now on we will rename  $\hat{Q}$  and  $\hat{P}$  with  $\hat{q}$  and  $\hat{p}$ ). It is possible to define also *generalized quadratures*:

$$\begin{aligned} \hat{q}_\theta &= \sqrt{\frac{\hbar}{2}} (\hat{a}^\dagger e^{i\theta} + \hat{a} e^{-i\theta}) = \hat{q} \cos \theta + \hat{p} \sin \theta \\ \hat{p}_\theta &= i\sqrt{\frac{\hbar}{2}} (\hat{a}^\dagger e^{i\theta} - \hat{a} e^{-i\theta}) = -\hat{q} \sin \theta + \hat{p} \cos \theta; \end{aligned} \quad (1.10)$$

these definitions will be used in the description of quantum tomography. Keeping all these considerations in mind we can finally write the expression for the vector potential of the quantized field

$$\vec{A} = \sqrt{\frac{2\pi\hbar c^2}{\omega V}} [\hat{a}\hat{\epsilon}e^{i\vec{k}\cdot\vec{r}} + c.c.]. \quad (1.11)$$

From the commutation relation between the operators  $a$  and  $a^\dagger$  (and so between  $q$  and  $p$ ), one can rewrite the expression (1.6) for the hamiltonian

$$\hat{H}_{em} = \hbar\omega \left( \hat{a}^\dagger \hat{a} + \frac{1}{2} \right). \quad (1.12)$$

## 1.2 Coherent and Squeezed States

So far we have considered just one kind of eigenstates of the Hamiltonian of simple harmonic oscillator ( $|n\rangle$ ), that are also eigenstates of the number operator  $\hat{n} = \hat{a}^\dagger \hat{a}$  and are called Fock states; their eigenvalues  $n$  represent the number of excitations. The general expression of these states is the following

$$|n\rangle = \frac{\hat{a}^{\dagger n}}{\sqrt{n!}} |0\rangle \quad (1.13)$$

where  $|0\rangle$  is the ground state, such that

$$\hat{a} |0\rangle = 0. \quad (1.14)$$

Fock states are not the only eigenstates of the Hamiltonian (1.12). Common states which are used to describe classical like states of the harmonic oscillator are the *coherent states*. These eigenstates have some important characteristics that make them interesting to study. First of all they are the closest analogues to classical coherent oscillations and the optical states generated by the laser source during our experiment are coherent. They have also the property of saturating the Heisenberg uncertainty principle, in the sense that the product of the standard deviations is  $\sigma_q \sigma_p = \frac{\hbar}{2}$  and, moreover,  $\sigma_q = \sigma_p$ .

Coherent states can be defined as the eigenstates of the annihilation operator

$$\hat{a} |\alpha\rangle = \alpha |\alpha\rangle. \quad (1.15)$$

The eigenvalue  $\alpha$  is complex, since the annihilation operator is not hermitian, and the mean value of the number operator  $\hat{n}$  is related to  $\alpha$  as follows

$$\langle \hat{n} \rangle = \langle \alpha | \hat{a}^\dagger \hat{a} | \alpha \rangle = \alpha^* \alpha = |\alpha|^2. \quad (1.16)$$

As already seen in equation (1.14) the Fock vacuum  $|0\rangle$  is an eigenstate of the annihilation operator, so it is a coherent state. From the Fock vacuum we can generate a coherent state defining the so called *displacement operator*

$$D(\alpha) = e^{(\alpha \hat{a}^\dagger - \alpha^* \hat{a})} \quad (1.17)$$

such that  $|\alpha\rangle = D(\alpha) |0\rangle$ .

The displacement operator acts on the annihilation and creation operators as follows

$$\begin{aligned} D^\dagger(\alpha) \hat{a} D(\alpha) &= \hat{a} + \alpha \\ D^\dagger(\alpha) \hat{a}^\dagger D(\alpha) &= \hat{a}^\dagger + \alpha^*; \end{aligned} \quad (1.18)$$

from this relation we can easily evaluate the role of this operator on  $\hat{q}$  and  $\hat{p}$ . In order to better understand the action of the displacement operator, we can consider a representation in the phase space (whose dimensions are the

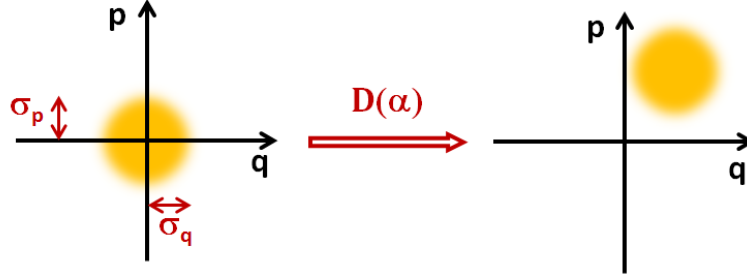


Figure 1.1: A vacuum state in phase space and a coherent state obtained applying the displacement operator on the Fock vacuum state.

expectation values  $q$  and  $p$ ) [Figure 1.1]. As we can see in Figure 1.1 the operator displaces the mean value of  $\hat{q}$  by an amount proportional to  $\Re e(\alpha)$  and the mean value of  $\hat{p}$  proportional to  $\Im m(\alpha)$ . Note that  $D(\alpha)$  changes only the mean value and not the second momentum (variance): as a matter of fact the state "shape" doesn't change in phase space [2].

Let us describe the time evolution of a coherent state, trying to understand what is its representation in the phase space. In order to calculate the time dependence of the expectation values of  $\hat{q}$  and  $\hat{p}$  we will evaluate the time evolution of the annihilation and creation operators: from the commutation relations between  $\hat{a}$  and  $\hat{a}^\dagger$  and the expression of the Hamiltonian (1.12), we get

$$\dot{\hat{a}} = \frac{i}{\hbar} [\hat{H}(t), \hat{a}] = -i\omega\hat{a} \quad (1.19)$$

and then

$$\hat{a}(t) = e^{-i\omega t}\hat{a} \quad (1.20)$$

(and analogously  $\hat{a}^\dagger(t) = e^{i\omega t}\hat{a}^\dagger$ ).

Keeping in mind that  $\hat{q} = \sqrt{\frac{\hbar}{2}}(\hat{a} + \hat{a}^\dagger)$ , we get

$$\langle \hat{q}(t) \rangle = \sqrt{\frac{\hbar}{2}} \langle \alpha | \hat{a}(t) + \hat{a}^\dagger(t) | \alpha \rangle = \sqrt{2\hbar} \Re e(\alpha e^{-i\omega t}). \quad (1.21)$$

(we can perform the same calculation for the mean value of the conjugate momentum and we obtain  $\langle \hat{p} \rangle = \sqrt{2\hbar} \Im m(\alpha e^{-i\omega t})$ ).

If we get back to the representation in the phase space (Figure 1.2), we notice that the time evolution is a rotation of the area representing the coherent state around the origin. It is quite similar to the time evolution in phase space of a classical harmonic oscillator, which is a point rotating around the origin; the difference between the two systems is due to the quantum nature of the first one and in particular to the uncertainty principle<sup>1</sup>. As we

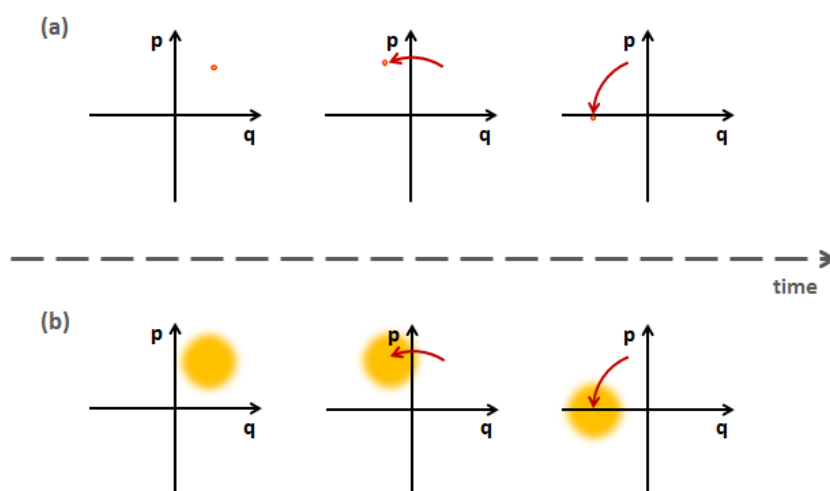


Figure 1.2: Time evolution of a classical harmonic oscillator (a) and of a coherent state (b) in phase space.

have already said *coherent states* are particular states, since they saturate the uncertainty principle and have  $\sigma_q = \sigma_p$ . Other states that saturates the

<sup>1</sup>Note that the concept of phase space cannot be simply generalized from classical physics. The first trivial observation is that in quantum mechanics we deal with operators instead of variables, but this problem can be easily avoided by using eigenvalues. Nevertheless this is not the only difference: the phase space is classically defined as the ensemble of points which univocally define the state of the system; if two operators do not commute there is no way to define a system univocally, because of the uncertainty principle (generalized uncertainty principle:  $\sigma_A^2 \sigma_B^2 \geq \left(\frac{1}{2i} \langle [\hat{A}, \hat{B}] \rangle\right)^2$ ). Since the position and momentum operators do not commute a state in quantum phase space would be described by an area instead of a point. Moreover we cannot compute the probability that a particle has both position  $q$  and momentum  $p$  as in the classical case, but only probability distributions for  $q$  and  $p$  separately. One can still define a function of both the eigenvalues, which is no more unique and can assume negative values (see section 2.1)

Heisenberg principle, for which  $\sigma_q \neq \sigma_p$ , are the so called *squeezed states*. Since they satisfy the relation  $\sigma_q \sigma_p = \frac{1}{2}$  (we have put  $\hbar = 1$  for convenience), if the uncertainty on one variable (q or p) is smaller than  $\frac{1}{\sqrt{2}}$ , the uncertainty on the other will be greater than this quantity and so the state in phase space will appear *squeezed*.

As for coherent states, also squeezed states can be obtained from the Fock vacuum state, using suitable operators. First of all one notice that a squeezed state can be seen as a coherent state (for example vacuum) modified by a "scale" transformation that compresses one dimension and dilates the other: the *squeezing operator* acts this way and is defined as follows

$$\hat{S}(\xi) = e^{\frac{1}{2}(\xi(\hat{a}^\dagger)^2 - \xi^* \hat{a}^2)}, \quad (1.22)$$

where  $\xi$  is a complex number, called *squeezing parameter*.

Acting with this operator on the Fock vacuum and then displacing it one gets the general squeezed state

$$|\alpha, \xi\rangle = \hat{D}(\alpha) \hat{S}(\xi) |0\rangle. \quad (1.23)$$

In Figure (1.3) different squeezed states are shown, in order to better understand the role of displacement and squeezing operators. Speaking about

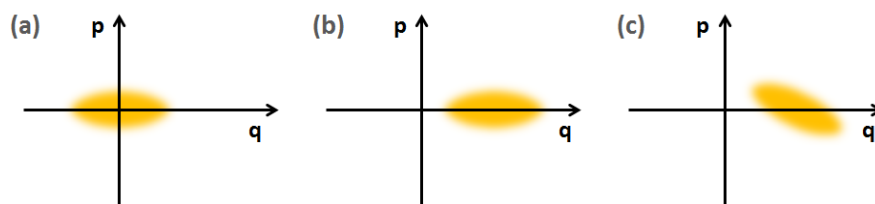


Figure 1.3: Different squeezed states: (a) no-displaced squeezed state ( $\alpha = 0$ ); (b) squeezed state with  $\alpha \neq 0$ , but null phase of the squeezing parameter (since  $\xi$  is a complex number it can be written as  $\xi = \rho e^{i\vartheta}$ , where  $\vartheta$  is the phase); (c) squeezed state with  $\alpha$  and  $\theta$  different from zero.

time dependence of a squeezed state, its evolution in the phase space is quite similar to that of a coherent state, but in this case not only the mean values of the variables change in time, but also their variances, that oscillates at

twice the frequency of the mode (that is twice the frequency of oscillation of the mean values).

### 1.3 The Density Operator

The state of a quantum system can be completely characterized by a normalized state vector  $|\psi\rangle$ , (belonging to a Hilbert space  $H$ , which contains all possible states of the considered system): as a matter of fact if we want to extract a piece of information about the system, we have just to compute the expectation value of the corresponding operator  $\hat{O}$ , that is  $\langle\psi|\hat{O}|\psi\rangle$  [3]. If the initial state and the Hamiltonian operator  $\hat{H}$  of the system are known, the previous formalism provides indeed a complete description of the system, of its time evolution and of the properties of its observables. However, there are circumstances in which we are not able to know  $|\psi\rangle$ : in these cases the system can be described in a statistical way, making the *ensemble average* over many identical systems equally prepared and introducing a new formalism [4] [3]. Let's introduce this kind of problem with a simple example [5].

#### 1.3.1 Example: one-dimensional harmonic oscillator

Let us consider a one-dimensional harmonic oscillator and suppose we want to make a position measure on an ensemble of identically prepared particles. We will first discuss the case of a particle in a single energy state  $|m\rangle$ : quantum mechanics predicts the result calculating the probability to find the particle between  $x$  and  $x + dx$

$$W(x)dx = |u_m(x)|^2 \quad (1.24)$$

(where  $u_m(x)$  is the wave function in position representation).

If we instead consider the case in which the oscillator is in a superposition of eigenstates

$$|\psi\rangle = \sum_{m=0}^{\infty} \psi_m |m\rangle \quad (1.25)$$

we get a quite different result. The probability is always the modulus square of the wave function (defined as  $\psi(x) \equiv \langle x|\psi\rangle = \sum_{m=0}^{\infty} \psi_m u_m(x)$ ) and is

defined by the expression

$$\begin{aligned} W(x)dx &= \sum_{m,n=0}^{\infty} \psi_m^* \psi_n u_m^*(x) u_n(x) \\ &= \sum_{m=0}^{\infty} |\psi_m|^2 |u_m|^2 + \sum_{m \neq n} \psi_m^* \psi_n u_m^*(x) u_n(x) \end{aligned} \quad (1.26)$$

where in the last part one divides the terms where  $m = n$  from the terms with  $m \neq n$ . Each term of the first sum represents the probability to find the particle at the position  $x$  given it is in the  $m^{\text{th}}$  eigenstate ( $|\psi|^2$  is the probability to be in the  $m^{\text{th}}$  eigenstate) and we would expect it, in a certain sense, since it is a sort of generalization of the previous case. The second sum represents something different and introduces the inadequacy of state vector formalism and to the necessity of another one.

### 1.3.2 The density operator formalism

In order to introduce the density operator formalism let us assume to have an ensemble of physical states equally prepared and to have statistical information about them, that is, we have an ensemble of eigenstates  $\psi_n$  with probabilities  $p_n$  [6]. In this case the mean value of an observable  $A$  is given by the expression

$$\langle \hat{A} \rangle = \sum_n p_n \langle \psi_n | \hat{A} | \psi_n \rangle. \quad (1.27)$$

Notice that the probability  $p_n$  demonstrates that we don't know the exact state of the system and not the quantum uncertainty due to the Heisenberg principle, that is always present [4].

As we can see in Equation 1.27, the statistic state of a system can be defined as a linear combination of the states  $|\psi_n\rangle$  with the corresponding probabilities  $p_n$  as coefficients. All these pieces of information can be summarized in just one operator, called *density operator*, which is the weighted average of the projectors on the states  $|\psi_n\rangle$ :

$$\hat{\rho} = \sum_n p_n |\psi_n\rangle \langle \psi_n|. \quad (1.28)$$

Thanks to the introduction of this operator, the mean value of an observable can be written in the more compact way

$$\begin{aligned}
 \langle \hat{A} \rangle &= \sum_n p_n \langle \psi_n | \hat{A} | \psi_n \rangle \\
 &= \sum_m \sum_n p_n \langle \psi_n | \hat{A} | m \rangle \langle m | \psi_n \rangle \\
 &= \sum_m \langle m | \hat{\rho} \hat{A} | m \rangle \\
 &= \text{Tr} (\hat{\rho} \hat{A})
 \end{aligned}
 \tag{1.29}$$

where in the second step we have introduced the completeness  $\sum_m |m\rangle \langle m|$ , and  $\text{Tr} (\hat{O})$  is the trace of  $\hat{O}$ , that is the sum of the diagonal matrix elements in any matrix representation.

Relation (1.29) implies two important consequences: the immediate knowledge of all properties of the system and the possibility of expressing all with matrix representation. As a matter of fact if we can calculate the expectation value of every observable, we know everything about the system.

The **density matrix** is the set of the matrix elements of the operator  $\hat{\rho}$  on whatever basis. There is a physical interpretation of these elements: the diagonal elements  $\rho_{nn}$  are called *populations* and represent the probability of the system to be in the eigenstate  $|n\rangle$ , while the off-diagonal elements  $\rho_{nm}$  provide the *coherence* between the states  $n$  and  $m$  (this means that  $\rho_{nn}$  is different from zero only if the system is in a coherent superposition of eigenstates  $n$  and  $m$ ) [4].

### 1.3.3 Properties of the density operator

In this section properties and observations about the density matrix (and so of the density operator too) are discussed, in order to better understand the utility of this formalism:

1. The density matrix has unitary trace:

$$\begin{aligned} \text{Tr}(\hat{\rho}) &= \sum_m \sum_n p_n \langle m | \psi_n \rangle \langle \psi_n | m \rangle \\ &= \sum_n p_n \langle \psi_n | \underbrace{\left( \sum_m |m\rangle \langle m| \right)}_{\mathbb{I}} | \psi_n \rangle \\ &= \sum_n p_n \langle \psi_n | \psi_n \rangle = \sum_n p_n = 1 \end{aligned} \tag{1.30}$$

since the probability of finding whatever state must be 1.

2. If all  $p_n$  are zero except one (that will be equal to one), the density operator is  $\hat{\rho} = |\psi\rangle \langle \psi|$ , i.e. the projector on the state with probability equal to one. In this case the wave function provides all information of the system and the new formalism becomes redundant, although still correct. The state is said to be a *pure state*, in contrast with the *mixed state*, whose properties can be described only through the density operator.
3. Let us consider the square of the density matrix and compute its trace

$$\text{Tr}(\hat{\rho}^2) = \sum_n p_n^2 \leq \sum_n p_n = 1. \tag{1.31}$$

It is a simple way to distinguish a mixed state from a pure one: in the last case the trace will be exactly equal to one (and  $\hat{\rho}^2 = \rho$  that is the density operator is a projector), while in the former it will be strictly less than one.

4. The density matrix is hermitian and its diagonal elements are positive or null (it follows from the fact that they are probabilities)

### 1.3.4 *Example: a two level system*

Let us see an *example* of a simple two level system [7] in order to understand the importance of the density operator formalism. Consider a two level system and assume for simplicity that the two levels  $|a\rangle$  and  $|b\rangle$  are symmetrically

distributed with respect to the zero. The Hamiltonian of the system in the basis  $[|a\rangle, |b\rangle]$  is

$$H = \begin{pmatrix} \Delta & 0 \\ 0 & -\Delta \end{pmatrix}. \quad (1.32)$$

Consider now two different cases:

1. At time  $t = 0$  the system is in a pure state and can be described both as an eigenstate  $|\psi\rangle$  and with the density operator  $\rho = |\psi\rangle\langle\psi|$ . If  $|\psi\rangle = \frac{1}{\sqrt{2}}(|a\rangle + |b\rangle)$ , the density matrix is

$$\rho_1 = \frac{1}{2} \begin{pmatrix} 1 & 1 \\ 1 & 1 \end{pmatrix}. \quad (1.33)$$

2. At time  $t = 0$  the state is mixed and can be described only by the density operator. Suppose that the probability for the system to be in state  $|a\rangle$  (or  $|b\rangle$ ) is  $\frac{1}{2}$ . In this case the density matrix is

$$\rho_2 = \frac{1}{2} \begin{pmatrix} 1 & 0 \\ 0 & 1 \end{pmatrix}. \quad (1.34)$$

In both cases the probability of measuring an energy  $\Delta$  or  $-\Delta$  is  $\frac{1}{2}$ , but the two states are not equal. First of all one is pure and the other is mixed, as we have already said: we can verify it computing the trace of  $\rho^2$  (in the first case we get 1 and in the second  $\frac{1}{2}$ ). In order to demonstrate that they are completely different states, let's calculate the expectation value of a general observable  $\hat{O}$ , whose representation in the chosen basis is

$$\hat{O} = \begin{pmatrix} a & b \\ c & d \end{pmatrix}. \quad (1.35)$$

Keeping in mind the relation 1.29 and knowing the two density matrices  $\rho_1$  and  $\rho_2$ , we get  $\langle\hat{O}\rangle = \frac{a+b+c+d}{2}$  in the first case and  $\langle\hat{O}\rangle = \frac{a+d}{2}$  in the second: so the mean values of the observables (that can completely characterize the system, if the set of observables is complete) are in general different, and so the states are different. Furthermore there is no wave function that characterize the second state, that is, there is no  $\psi_2$  such that  $\rho_2 = |\psi_2\rangle\langle\psi_2|$  [7].

### 1.3.5 Time evolution of the density operator

From the definition of the density operator 1.28 and the Schrödinger equation

$$i\hbar \frac{\partial \psi}{\partial t} = \hat{H} |\psi\rangle. \quad (1.36)$$

we can easily obtain the time evolution of  $\rho$

$$\begin{aligned} \frac{\partial \hat{\rho}}{\partial t} &= \sum_m \frac{\partial |\psi_m\rangle}{\partial t} p_m \langle \psi_m| + \sum_m |\psi_m\rangle p_m \frac{\partial \langle \psi_m|}{\partial t} \\ &= -\frac{i}{\hbar} \hat{H} \sum_m |\psi_m\rangle p_m \langle \psi_m| + \frac{i}{\hbar} \sum_m |\psi_m\rangle p_m \langle \psi_m| \hat{H} \\ &= -\frac{i}{\hbar} [\hat{H}, \hat{\rho}(t)] \end{aligned} \quad (1.37)$$

The previous relation is known as Liouville von Neumann equation [8].

In order to describe the time evolution of the density operator we can use the matrix representation and study the time dependence of the matrix elements. Consider for simplicity a two level system, but the results can be generalized to more complicated systems.

The hamiltonian operator in the basis of its eigenstates can be expressed with the matrix

$$H = \begin{pmatrix} \epsilon_1 & 0 \\ 0 & \epsilon_2 \end{pmatrix}. \quad (1.38)$$

where  $\epsilon_1$  and  $\epsilon_2$  are the two eigenvalues of H (that is, the two energy levels of the system). Reminding relation (1.37) and inserting the matrix H, we get

$$\frac{d}{dt} \begin{pmatrix} \rho_{11} & \rho_{12} \\ \rho_{21} & \rho_{22} \end{pmatrix} = -\frac{i}{\hbar} \begin{pmatrix} 0 & (\epsilon_1 - \epsilon_2)\rho_{12} \\ (\epsilon_2 - \epsilon_1)\rho_{21} & 0 \end{pmatrix}, \quad (1.39)$$

from which we notice that the diagonal terms are constant in time, while the off-diagonal ones have an oscillatory behavior, with frequency  $\frac{\epsilon_1 - \epsilon_2}{\hbar}$ :

$$\left\{ \begin{array}{l} \dot{\rho}_{11} = 0 \longrightarrow \rho_{11}(t) = \rho_{11}(0) \\ \dot{\rho}_{22} = 0 \longrightarrow \rho_{22}(t) = \rho_{22}(0) \\ \dot{\rho}_{12} = -\frac{i}{\hbar}(\epsilon_1 - \epsilon_2)\rho_{12} \longrightarrow \rho_{12}(t) = \rho_{12}(0)e^{-\frac{i}{\hbar}(\epsilon_1 - \epsilon_2)t} \\ \dot{\rho}_{21} = -\frac{i}{\hbar}(\epsilon_2 - \epsilon_1)\rho_{21} \longrightarrow \rho_{21}(t) = \rho_{21}(0)e^{-\frac{i}{\hbar}(\epsilon_2 - \epsilon_1)t} \end{array} \right. \quad (1.40)$$

Note that in the two level system considered as example before, the density matrices 1.33 and 1.34 become

$$\rho_1(t) = \frac{1}{2} \begin{pmatrix} 1 & e^{-2i\Delta t} \\ e^{2i\Delta t} & 1 \end{pmatrix}, \quad \rho_2(t) = \frac{1}{2} \begin{pmatrix} 1 & 0 \\ 0 & 1 \end{pmatrix}. \quad (1.41)$$

In both cases the probability of measuring an energy equal to  $\Delta$  or  $-\Delta$  is  $\frac{1}{2}$ , but the operators involve differences in the expectation values of the observables. For example let's consider an operator  $B = \begin{pmatrix} 0 & b \\ b & 0 \end{pmatrix}$  (it could be the x component of the spin in presence of an external magnetic field in the z direction). In fact we obtain

$$\left\{ \begin{array}{l} \langle B \rangle_1 = Tr(\rho_1(t)B) = b \cos(2\Delta t) \\ \langle B \rangle_2 = Tr(\rho_2(t)B) = 0 \end{array} \right. . \quad (1.42)$$

So, while in the first case we get a time dependent expectation value, in the second one it is constant: this example underlines again the difference between mixed and pure states with same probability.

### 1.3.6 Liouville representation

The matrix representation, though clearer and more concrete respect to the operator one, in this circumstance can be substituted with a simpler one, in which the time evolution of the density operator 1.37 has the form of the Schrödinger equation 1.36. This result is reached through two simple modifications of the notation used until now:

- the density matrix is no more represented by a matrix: it becomes a column vector containing all the matrix elements (for example for a 2x2 matrix we will obtain a vector of 4 elements);
- the introduction of *Liouville superoperator*  $\mathcal{L}$ , which acts on operators (that's why it is called "superoperator") in the following way

$$\mathcal{L}\hat{O} \equiv [H, \hat{O}]. \quad (1.43)$$

In practice the Liouville space is the cartesian product of two Hilbert spaces and its elements are the density operators  $\hat{\rho}$ .

In order to comprehend the use of this formalism, we will consider the usual two level system, with energy  $\epsilon_1$  and  $\epsilon_2$ ; Equation 1.45 becomes, in Liouville representation

$$\frac{d}{dt} \begin{pmatrix} \rho_{11} \\ \rho_{12} \\ \rho_{21} \\ \rho_{22} \end{pmatrix} = -\frac{i}{\hbar} \underbrace{\begin{pmatrix} 0 & 0 & 0 & 0 \\ 0 & (\epsilon_1 - \epsilon_2) & 0 & 0 \\ 0 & 0 & (\epsilon_2 - \epsilon_1) & 0 \\ 0 & 0 & 0 & 0 \end{pmatrix}}_{\mathcal{L}} \begin{pmatrix} \rho_{11} \\ \rho_{12} \\ \rho_{21} \\ \rho_{22} \end{pmatrix}, \quad (1.44)$$

that is

$$\frac{d\rho}{dt} = -\frac{i}{\hbar} \mathcal{L}\rho; \quad (1.45)$$

it is known as Liouville equation and is formally equivalent to the Schrödinger equation. Thanks to this similarity we can obtain the solution of the differential equation in analogy with the Schrödinger equation [7], so

$$\rho(t) = \mathcal{U}(t, t_0)\rho(t_0), \quad \text{with} \quad \mathcal{U}(t, t_0) = e^{-i\frac{\mathcal{L}}{\hbar}(t-t_0)} \\ \text{and} \quad \frac{\partial \mathcal{U}(t, t_0)}{\partial t} = -\frac{i}{\hbar} \mathcal{L}\mathcal{U}(t, t_0). \quad (1.46)$$

In order to distinguish the Liouville from the Hilbert space we will use, from now on, the so called **tetradic notation**. We are now going to introduce briefly this notation and some additional definition, to establish a *complete isomorphism between the time evolution in ordinary Hilbert space and the evolution of the density operator* [1].

- The state of the system, i.e. an element of the Liouville space is indicated by a double bracket  $|\rho\rangle\rangle$ . A basis set is defined as  $|jk\rangle\rangle \equiv |j\rangle\langle k|$ : it is a matrix whose element in the  $j^{\text{th}}$  row and  $k^{\text{th}}$  column is 1 while all other elements are zero. The completeness condition is  $\sum_{j,k} |jk\rangle\rangle\langle\langle jk| = 1$ .
- The operators in Hilbert space ( $\hat{O}$ ) are elements of the Liouville space: they are indicated as vectors ( $|O\rangle\rangle$ ) and can be expanded in a basis set  $|O\rangle\rangle = \sum_{j,k} |j,k\rangle\rangle O_{jk}$ . Since operators are elements in the new space, we can define a scalar product between them, namely  $\langle\langle B|A\rangle\rangle \equiv \text{Tr}(B^\dagger A)$ ; consequently the orthonormality condition is  $\langle\langle jk|mn\rangle\rangle = \text{Tr}[|k\rangle\langle j|m\rangle\langle n|] = \delta_{kn}\delta_{jm}$ . The scalar product  $\langle\langle jk|O\rangle\rangle$  provides the matrix element  $O_{jk}$ .
- The operators in Liouville space are called *superoperators* or *tetradic operators* (as the Liouville superoperator  $\mathcal{L}$ ) and are usually indicated with a calligraphic font. They are defined as

$$\mathcal{F} = \sum_{j,k,m,n} |jk\rangle\rangle\langle\langle jk|\mathcal{F}|mn\rangle\rangle\langle\langle mn|, \quad (1.47)$$

while their four indices matrix elements are  $\mathcal{F}_{jk,mn} = \langle\langle jk|\mathcal{F}|mn\rangle\rangle$ .

- The time evolution is described by the relation  $|\dot{\rho}\rangle\rangle = -\frac{i}{\hbar}\mathcal{L}|\rho\rangle\rangle$ , while the time evolution operator is defined in equation (1.46).

The tetradic notation will be useful in future, when we will introduce the four wave mixing theory.



## Chapter 2

# Theory

In this chapter the most relevant theoretical aspects of this thesis are introduced, in order to understand the kind of measurements we made, the setup (described in chapter 4) and the experimental results. In particular I will focus on the *Wigner function formalism* for describing quantum states and on the theory beyond the experimental technique of *quantum state tomography*, which allow us to "measure" the quantum state of ultrashort light pulses.

### 2.1 Wigner Function

As we have just seen, a quantum state can be identified by a state vector  $|\psi\rangle$  (in case of a pure state) or a density operator  $\hat{\rho}$ . However there exists another formalism, which derives from the previous ones, that brings us directly and "visually" the properties of the quantum state: it is the Wigner representation and lives in the phase space.

Let us go back to classical physics in order to define by analogy some important concepts. In classical mechanics a physical system is described by a point  $(q, p)$  in the phase space. A statistics of the position and the momentum a distribution  $W(q, p)$  can be introduced, which expresses the probability of finding a particular value of the two variables during their simultaneous measurement. The probability distribution  $W(q, p)$  allows us to compute, and predict, all statistical quantities and in this sense it characterizes a classical state. This concept can't be simply generalized to quantum optics because the

Heisenberg uncertainty principle asserts that we can't measure simultaneously position and momentum exactly. Nevertheless also in quantum optics we are interested in a formalism that can predict the statistic of our observations [6]. Another important difference between classical and quantum physics is the concept of phase space: in the quantum case the motion is described by the operators  $\hat{q}$  and  $\hat{p}$ , which don't commute and cannot define a phase space as we know it from the classical case. However we can construct a space whose dimensions are the eigenvalues  $q$  and  $p$  and find out a distribution depending on these two quantities. Keeping all these differences in mind, we can consider the following phase space distribution (called *Wigner function*)

$$W(q, p) = \frac{1}{2\pi\hbar} \int_{-\infty}^{+\infty} d\xi e^{-\frac{i}{\hbar}p\xi} \langle q + \frac{1}{2}\xi | \hat{\rho} | q - \frac{1}{2}\xi \rangle. \quad (2.1)$$

The previous function was introduced by E. P. Wigner in 1932 for the first time [9], without explicit motivations [5]. We are now going to justify the choice by giving an intuitive explanation and making a list of its properties. First of all let us define our aim: we want to describe the motion of a particle between the positions  $q'$  and  $q''$  (assume  $\xi = q'' - q'$ ). In analogy with the case of energy transition between two levels  $n'$  and  $n''$  (in which we compute the matrix element  $\langle n'' | \hat{\mu} | n' \rangle$ , where  $\hat{\mu}$  is the dipole operator), let us consider  $\langle q'' | \hat{\rho} | q' \rangle$ . We can redefine the states as  $q' = q - \frac{1}{2}\xi$  and  $q'' = q + \frac{1}{2}\xi$ , where  $q$  is the center of the displacement ( $q \equiv \frac{q''+q'}{2}$ ). In order to obtain a momentum distribution we perform a Fourier transform and finally get the Wigner function ( $\frac{1}{2\pi\hbar}$  is just a normalization factor).

The expression (2.1) is the most general one: in case of a pure state it becomes

$$W(q, p) = \frac{1}{2\pi\hbar} \int_{-\infty}^{+\infty} d\xi e^{-\frac{i}{\hbar}p\xi} \psi^* \left( q - \frac{1}{2}\xi \right) \psi \left( q + \frac{1}{2}\xi \right); \quad (2.2)$$

this definition will be useful to introduce the concept of quasiprobability distribution.

### 2.1.1 Properties of the Wigner function

At the beginning of this section the Wigner representation was introduced with the scope of being a pictorial representation of the quantum state; it is truth and we will see why, but the Wigner function gives us much more

information: it allows us to calculate expectation values of observable, and so to characterize quantitatively the state. However in this respect it is not unique: infinite other functions satisfy this request [5]. Nevertheless the Wigner function is unique for its important properties; we are now going to list some of them, from to the most "mathematical" ones to those with interesting physical meaning.

1. First of all the Wigner function is *real*, that is  $W^*(q, p) = W(q, p)$ : it can be simply demonstrated by considering the complex conjugate of the function (keeping in mind that the density operator  $\rho$  is hermitian) and replacing  $q$  with  $-q$ .
2. Thanks to the factor  $\frac{1}{2\pi\hbar}$  the Wigner function is *normalized*, namely

$$\int_{-\infty}^{+\infty} \int_{-\infty}^{+\infty} W(q, p) dq dp = 1; \quad (2.3)$$

(it derives from the properties of the density operator (1.30) and of the Dirac delta  $\delta(x) = \frac{1}{2\pi} \int_{-\infty}^{+\infty} e^{ikx} dk$  and  $\delta(\alpha x) = \frac{1}{|\alpha|} \delta(x)$ ).

3. This property deals with the *marginals* of the Wigner function and represents the connection of this variable with probability distributions. Marginals are the integral of the function over one of the dimensions of the phase space: we will demonstrate that they represent the probability distribution function on the other variable. Let us consider for example the integration over  $p$ :

$$\begin{aligned} \int_{-\infty}^{+\infty} W(q, p) dp &= \int_{-\infty}^{+\infty} d\xi \langle q + \frac{1}{2}\xi | \hat{\rho} | q - \frac{1}{2}\xi \rangle \underbrace{\frac{1}{2\pi\hbar} \int_{-\infty}^{+\infty} dp e^{-\frac{i}{\hbar} p \xi}}_{2\pi\hbar\delta(\xi)} \\ &= \int_{-\infty}^{+\infty} d\xi \langle q + \frac{1}{2}\xi | \hat{\rho} | q - \frac{1}{2}\xi \rangle \delta(\xi) \\ &= \langle q | \hat{\rho} | q \rangle \equiv W(q). \end{aligned} \quad (2.4)$$

$W(q)$  is the probability distribution for the position; analogously one gets the momentum distribution integrating over the position  $q$  [5].

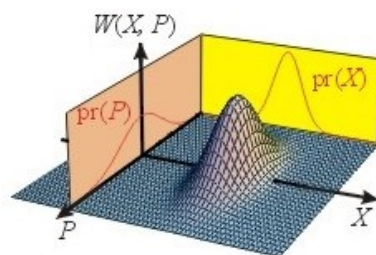


Figure 2.1: Example of Wigner function and relative position and momentum distribution [10]

4. Another important property of the Wigner function is the so called **overlap formula** [6] (or **trace product rule** [5]), since it has three remarkable consequences. Its expression is

$$Tr(\hat{A}\hat{B}) = 2\pi\hbar \int_{-\infty}^{+\infty} \int_{-\infty}^{+\infty} W_A(q, p) W_B(q, p) dqdp, \quad (2.5)$$

where  $W_A$  and  $W_B$  are the Wigner transforms of the operators  $\hat{A}$  and  $\hat{B}$  (the same as in relation 2.1, with one of the operators instead of  $\rho$ ): it can be easily demonstrated with the usual trick of the Dirac delta, as in the case of the marginals, and simple changes of variables [6].

A consequence of this formula is the calculation of the *expectation value* of a general observable  $\hat{O}$ . Remembering the relation (1.29), we get

$$\langle \hat{O} \rangle = Tr(\hat{\rho}\hat{O}) = 2\pi\hbar \int_{-\infty}^{+\infty} \int_{-\infty}^{+\infty} W(q, p) W_{\hat{O}}(q, p) dqdp. \quad (2.6)$$

In this sense there is a strictly connection with the classical probability distribution; nevertheless the next consequence underlines the differences between the two cases.

In the case of pure states  $\hat{\rho}_j = |\psi_j\rangle\langle\psi_j|$  the trace of the product is

$$\begin{aligned} Tr(\rho_1\rho_2) &= Tr(|\psi_1\rangle\langle\psi_1|\psi_2\rangle\langle\psi_2|) = |\langle\psi_1|\psi_2\rangle|^2 \\ &= 2\pi\hbar \int_{-\infty}^{+\infty} \int_{-\infty}^{+\infty} W_1(q, p) W_2(q, p) dqdp, \end{aligned} \quad (2.7)$$

i.e. the transition probability between the pure states  $|\psi_1\rangle$  and  $|\psi_2\rangle$ . If the two states are orthogonal their scalar product is zero. From the second line of relation 2.7 we find out that, in order to have a

null integral, at least one of the two Wigner function should have some negative values (excluding particular cases); this represents one of the main differences with the classical distribution and that's why the Wigner function is called *quasiprobability distribution*. Note that this statement doesn't exclude the possibility of a non-negative Wigner function: in particular Gaussian states (for example coherent and squeezed states) are positive everywhere.

### 2.1.2 Time evolution of the Wigner Function

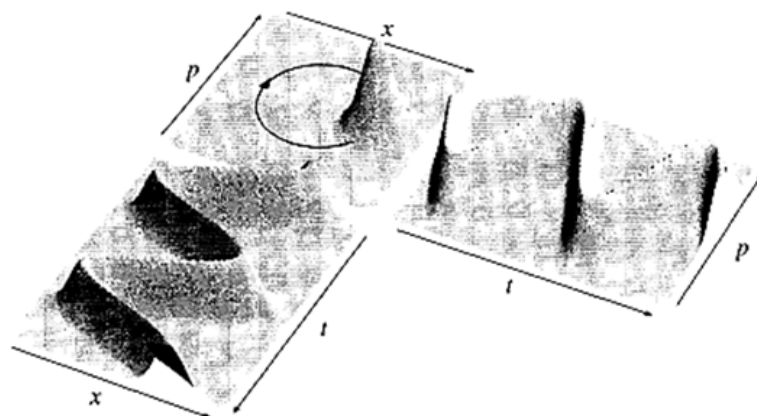
We have already shown the evolution of a quantum state expressed as the density operator time evolution. Since the Wigner function depends on the density operator, starting from the Liouville von Neumann equation (1.37), we can get the time evolution of the Wigner function, that is

$$\frac{\partial W}{\partial t} = \frac{-i}{\hbar} \frac{1}{2\pi\hbar} \int_{-\infty}^{+\infty} d\xi e^{-\frac{i p \xi}{\hbar}} \langle q + \frac{1}{2}\xi | [\hat{H}, \hat{\rho}] | q - \frac{1}{2}\xi \rangle. \quad (2.8)$$

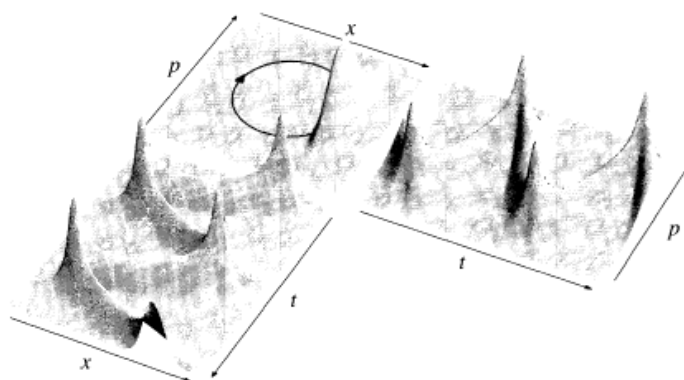
The hamiltonian is the sum of a kinetic ( $\frac{p^2}{2m}$ ) and potential part  $U$  and the previous equation can be rewritten in this way

$$\begin{aligned} \frac{\partial W}{\partial t} &= \mathcal{T} + \mathcal{U}, \quad \text{where} \\ \mathcal{T} &= -\frac{p}{M} \frac{\partial}{\partial q} W(q, p, t), \\ \mathcal{U} &= \sum_{l=0}^{\infty} \frac{(i\hbar/2)^{2l}}{(2l+1)!} \frac{d^{2l+1}U(q)}{dq^{2l+1}} \frac{\partial^{2l+1}}{\partial p^{2l+1}} W(q, p, t). \end{aligned} \quad (2.9)$$

as demonstrated by W. P. Schleich [5]. In order to show the time evolution for Gaussian states let us first consider the ground state of a harmonic oscillator and provide a sudden displacement: the so obtained state is coherent. If we know the initial Wigner function (that is a two-dimensional Gaussian with the same width along  $q$  and  $p$ ) and the harmonic potential, we can solve the differential equation 2.9 and finally get the time dependence of a coherent state in phase space. This procedure demonstrates [5] that a coherent state evolves in time by rotating in the phase space (similarly to the classical case); if we compute the marginals for every time instant  $t$ , we observe that the variables  $q$  and  $p$  perform harmonic oscillation with constant width, as shown



(a)



(b)

Figure 2.2: Time evolution of the Wigner function of a coherent state (a) and a squeezed state (b) in phase space [5]

in Figure 2.2 (a). With a similar procedure one can calculate also the time evolution of a squeezed state. The result is always a rotation in phase space, and the marginals oscillate harmonically in time, but their width is no more constant: it oscillates in time too and a large width in momentum implies a small one in position and vice versa. The frequency of this oscillation is twice that of the  $q$  and  $p$  mean values oscillations, in agreement with what we found out in section 1.2.

## 2.2 Homodyne detection

Now the question is how can we measure a quantum state, i.e. its Wigner function? In this section we are going to introduce the method for quantum state tomography based on the Balanced Homodyne Detection (BHD). To introduce the technique we will show that BHD, under low noise conditions, provides the measurements of the projection of the Wigner function on different planes. This characteristic will be used to achieve a tomographic reconstruction of the optical quantum state. A schematic set-up is showed in figure 2.3. We want to know the quantum state of the *signal*  $a$ , while  $b$  (the so

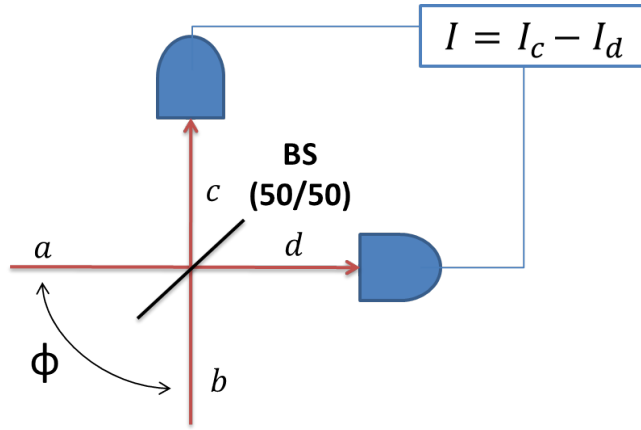


Figure 2.3: Schematic diagram of Balanced Homodyne Detection [11]

called *local oscillator*) is a known coherent state  $|z\rangle$ . The two modes interfere in a balance (50:50) beam splitter. The intensities of the output modes  $c$  and  $d$  are measured and subtracted by a differential detector repeatedly<sup>1</sup>. It can be shown that the values of the quadratures of the signal fields, as they have been defined in section (1.1)

$$\hat{x}_\Phi = \frac{1}{\sqrt{2}} \left( \hat{a} e^{-i\Phi} + \hat{a}^\dagger e^{i\Phi} \right), \quad (2.10)$$

for every phase difference  $\Phi$  (the phase difference is obtained by changing the optical path of the local oscillator) allow to reconstruct the Wigner function.

<sup>1</sup>In the pulse regime, the interferometric measurements are performed for every single light pulse. Under this condition the experiment can be described as a repeated measurement on equally prepared quantum state.

Let us consider in details this technique, starting from the beam splitter: we have to understand how the quantum states transform under the action of a beam splitter operator.

### 2.2.1 Beam Splitter

The description of the beamsplitter will proceed as follows. Consider a generic beam splitter using a classical treatment, we will focus on a 50:50 beam splitter and, finally we will discuss to the quantum case.

In our model a beam splitter is essentially a dielectric medium localized in space: light impinge on and emerge from it. We know that the Maxwell equations should be valid both out and inside the medium and that the solution should be continuous on the boundaries. The most simple model is that of a linear dielectric medium, in which there is a linear coupling between the modes

$$a_{l'} = \sum_l U_{l'l} a_l, \quad (2.11)$$

where  $a_l$  is the amplitude of the  $l$ th mode on one side of the beam splitter (in our case  $a$  and  $b$ ), while  $l'$  refers to the other side ( $c$  and  $d$ ).

As we can see in Figure 2.3 in homodyne detection there are two input and two output modes, and, therefore, we have to compute a  $2 \times 2$  transformation matrix (whose elements are the  $U_{l'l}$  defined before). In general

$$\begin{pmatrix} c \\ d \end{pmatrix} = \begin{pmatrix} t_1 & r_2 \\ r_1 & t_2 \end{pmatrix} \begin{pmatrix} a \\ b \end{pmatrix}, \quad (2.12)$$

where  $t_i$  and  $r_i$  are the transmission and reflection coefficients.

For the energy conservation, assuming a lossless beam splitter,  $|a|^2 + |b|^2 = |c|^2 + |d|^2$ ; substituting  $c$  and  $d$  in the right hand side with their expression in (2.12) one gets the equations

$$\begin{aligned} |t_1|^2 + |r_1|^2 &= |t_2|^2 + |r_2|^2 = 1 \\ t_1 r_2^* + t_2^* r_1 &= t_1^* r_2 + t_2 r_1^* = 0. \end{aligned} \quad (2.13)$$

Now consider a 50:50 beam splitter: one can easily imagine that  $|t_1|^2 = |r_1|^2 = |t_2|^2 = |r_2|^2 = \frac{1}{2}$ , while the second equation of 2.13 connects the

phases of the transmission and reflection coefficients. The phase depends on some characteristics of the beam splitter itself; nevertheless we can consider a particular condition and get the phase difference. Assume a symmetric situation  $t_1 = t_2 = \frac{1}{\sqrt{2}}$ : in this case the reflection is asymmetric and, if  $r_1 = \frac{1}{\sqrt{2}}$ , one obtains  $r_1 = -r_2$ . The transformation matrix becomes

$$U_{BS} = \frac{1}{2} \begin{pmatrix} 1 & -1 \\ 1 & 1 \end{pmatrix}. \quad (2.14)$$

In making the transition to quantum mechanics we replace the amplitude  $a_l$  with the operators  $\hat{a}_l$  [5] and we get

$$\begin{aligned} \hat{c} &= \frac{1}{\sqrt{2}} (\hat{a} - \hat{b}) \\ \hat{d} &= \frac{1}{\sqrt{2}} (\hat{a} + \hat{b}). \end{aligned} \quad (2.15)$$

### 2.2.2 From photocurrents to quadratures

Once the two beams have interfered in the beam splitter the intensities of the output beams are measured and then subtracted. Let  $\hat{I}$  be the differential current operator, defined as  $\hat{I} = \hat{c}^\dagger \hat{c} - \hat{d}^\dagger \hat{d}$ , where  $c$  and  $d$  are the annihilation operators of the modes  $c$  and  $d$  while  $c^\dagger c$  and  $d^\dagger d$  are their photon number observables (the nomenclature of the modes is referred to Figure 2.3). Using equations (2.15) one obtains

$$\hat{I} = \hat{a}^\dagger \hat{b} + \hat{b}^\dagger \hat{a}. \quad (2.16)$$

The phase difference  $\Phi$  between the signal and the local oscillator can be varied changing the optical path of the latter; to introduce this concept we make the substitution  $\hat{b} \rightarrow \hat{b}e^{i\Phi}$  in equation (2.16) and get

$$\hat{I}_\Phi = \hat{a}^\dagger \hat{b}e^{i\Phi} + \hat{b}^\dagger \hat{a}e^{-i\Phi}. \quad (2.17)$$

We will now demonstrate how this operator, and in particular its expectation value, is related to the quadrature  $\hat{x}_\Phi$  (Equation 2.10). The procedure is the

following

$$\begin{aligned}
 \langle \hat{I}_\Phi \rangle &= \text{Tr} \left[ \hat{\rho}_s \otimes |z\rangle\langle z| \hat{I}_\Phi \right] = \text{Tr} \left[ \hat{\rho}_s \otimes |z\rangle\langle z| (\hat{a}^\dagger \hat{b} e^{i\Phi} + \hat{b}^\dagger \hat{a} e^{-i\Phi}) \right] \\
 &= \text{Tr} \left[ \hat{\rho}_s \otimes |z\rangle\langle z| (\hat{a}^\dagger \hat{b} e^{i\Phi}) \right] + h.c. = \left( \text{Tr}[\hat{\rho}_s \hat{a}^\dagger] \cdot \text{Tr}[|z\rangle\langle z| \hat{b} e^{i\Phi}] \right) + h.c. \\
 &= \left( \text{Tr}[\hat{\rho}_s \hat{a}^\dagger] \cdot \langle z| \hat{b} e^{i\Phi} |z\rangle \right) + h.c. = \left( \text{Tr}[\hat{\rho}_s \hat{a}^\dagger] \cdot z e^{i\Phi} \right) + h.c. \\
 &= \text{Tr} \left[ \hat{\rho}_s (\hat{a}^\dagger z e^{i\Phi} + \hat{a} z^* e^{-i\Phi}) \right] = |z| \text{Tr} \left[ \hat{\rho}_s \underbrace{(\hat{a}^\dagger e^{i\Phi} + \hat{a} e^{-i\Phi})}_{\sqrt{2}\hat{x}_\Phi} \right] \\
 &= \sqrt{2} |z| \langle \hat{x}_\Phi \rangle, \tag{2.18}
 \end{aligned}$$

where  $\text{Tr}[\hat{\rho}_s \otimes |z\rangle\langle z| \hat{I}_\Phi]$  is the expectation value of the photocurrent  $\hat{I}_\Phi$  on the total input state  $\hat{\rho}_s \otimes |z\rangle\langle z|$  and at the end, since  $z$  is a complex number  $z = |z|e^{i\theta}$  we have redefined  $\Phi \rightarrow \Phi + \theta$ . The separation of the trace in the second line is possible since the two states belong to different Hilbert spaces. Nevertheless this demonstration is valid under certain conditions dealing with the local oscillator. The first observation is that the operator  $\hat{I}$  has a discrete spectrum, but if the local oscillator is in a strong semiclassical state (high intensity) its quantum fluctuation can be neglected and  $\hat{b} \rightarrow z$ . Moreover the expectation values of the moments of order greater than one are different from the quadratures ones: it can be demonstrated [12] that

$$\langle \hat{I}_\Phi^n \rangle = \langle \hat{x}_\Phi^{n-2} \left( \hat{x}_\Phi^2 + \frac{\hat{a}^\dagger \hat{a}}{2|z|^2} \right) \rangle. \tag{2.19}$$

They tend to the quadrature moments only if  $\langle \hat{a}^\dagger \hat{a} \rangle \ll |z|^2$ .

In conclusion we can perform a balanced homodyne detection only if two conditions on the local oscillator are satisfied:

$$\begin{aligned}
 1) \quad &|z| \gg 1 \\
 2) \quad &|z|^2 \gg \langle \hat{a}^\dagger \hat{a} \rangle.
 \end{aligned} \tag{2.20}$$

### 2.2.3 Pulsed regime

The previous description of Balanced Homodyne Detection does not treat explicitly the case of pulsed laser sources. However performing *time domain* measurement (with a pulsed source of light) can be interesting in order to study states of light with non classical features, which can be created by non

linear interactions. Since the high peak intensity of pulsed laser enable a large variety of non linear effects, pulsed laser sources are the ideal playground to look for non classical states of light. In addition to this, the intrinsic advantage of pulses sources is that they can be used in pump and probe measurements. This possibility will be exploited here to study in time domain to analyze coherent vibrational states in condensed matter.

On the other hand the use of pulsed sources entails some technical challenges for the detector:

1. The electronics should be fast enough to separate the signals coming from different laser pulses
2. The detector must subtract precisely the two photocurrents in order to eliminate the classical noise of the local oscillator, even at high energy (since we work in the semiclassical regime of the local oscillator)
3. It should be able to measure the *shot noise*, which is due to the quantization of the electromagnetic field (and not to characteristics of the detector) and describes the fluctuation of the number of photons. This means that the detector should provide very low noise to the signal, that is, should have efficiency  $\eta$  close to 1. In particular we define efficiency the ratio between the shot noise and the total noise at a certain intensity of the beam (the highest one which does not present other noise contributions). Fortunately verifying this property of the photodetector is quite simple, since the shot noise varies linearly with the power of the beam, while the classical noise scales quadratically and the electronic noise is constant [11] (see Figure (2.4)).

There is another problem which is not connected with the detector: since both the signal and the local oscillator are pulsed, they cannot be monochromatic and the theory of Balanced Homodyne Detection might not be valid anymore. Nevertheless a mathematical formalism has been developed that generalizes the treatment of the single mode Balanced Homodyne Detection to the pulsed regime [13].

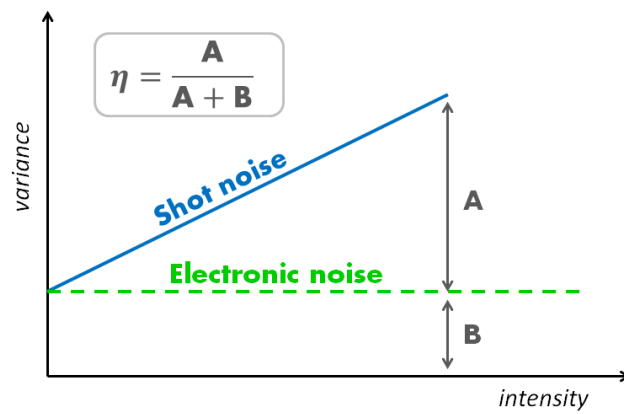


Figure 2.4: Schematic result of a noise measurement: the linear component (blue) represent the shot noise, while the constant one (green) is the electronic noise.  $\eta$  is the efficiency of the detector.

## Chapter 3

# Time resolved measurements

So far we have introduced concepts of quantum optics and an experimental technique to measure the quantum state of light. The project of this work is to couple these quantum optics aspects with time resolved spectroscopy and in particular with pump and probe experiments and Raman spectroscopy.

In a *pump and probe* experiment an ultrashort pulse ( $\sim 100$  fs) called *pump* impinges on the sample and injects excitation in the system; a second pulse, called *probe*, is then transmitted (or reflected) by the sample during its relaxation, in order to measure the variation of optical properties of the sample (transmittance or reflectivity). The time delay between the two pulses can be tuned by changing mechanically the optical path of one of the beams (through a slit, for example):  $1 \mu\text{m}$  difference corresponds to a time delay of 3.3 fs. This variation allows to measure the dynamics of the transmitted or reflected probe after the system excitation.

*Raman scattering* is an inelastic scattering process from vibrational modes of molecules or lattice in crystals. Naively we can imagine an experiment in which a light pulse impinges on the sample: the energy difference between the incident and the final beams is due to the excitation or de-excitation of vibrational modes. In particular Raman spectroscopy gives information about the frequencies of optical phononic modes near the Brillouin zone center.

To determine Raman active modes one needs a complete treatment in group theory; nevertheless the *rule of mutual exclusion* tells us that in a centrosymmetric crystal even parity modes are Raman active [14]. We will consider *stimulated* Raman Spectroscopy, in which a pump pulse excites nuclear vibrations in the sample and then the probing beam is scattered by the excited system.

In this chapter these concepts are introduced, following the formalism suggested by S. Mukamel in his work *Principles of nonlinear optical spectroscopy* [1].

### 3.1 Nonlinear response function

We could say naively that the aim of optical spectroscopy is to understand the features of a sample studying the variation of the properties of the light passing through (or reflected by) it. So, in order to define a theory that describes this experimental technique, it is "sufficient" to focus on an optical quantity which connects the properties of the material with that of the electromagnetic radiation: the polarization  $P(\mathbf{r}, t)$  seems to be a good candidate, since it is a material quantity and appears in the Maxwell equations. In this section we are going to develop the *nonlinear response theory*, a formalism used in the calculation of optical polarization.

Before starting with our purpose we will make some approximations in order to simplify the calculations:

1. We will adopt the semiclassical approximation, that is, the electromagnetic field is considered classical and the sample is treated quantum mechanically.
2. We will consider a perturbative expansion, which is valid only if the radiation field is weak enough. The approximation of *weak field* is not so restrictive, since the field must be compared with the internal fields (in an hydrogen atom it is of the order of  $10^{17} \text{ W/cm}^2$ , while the maximum intensity of our fields is about  $10^3 \text{ W/cm}^2$ ).

3. The argument will be introduced in *dipole approximation*: we assume the samples dimension to be much smaller than the optical wavelength: consequently the field can be considered homogeneous in the interested region. This assumption is used in the first calculation and then the results are generalized to more complex systems.

In dipole approximation the semiclassical Hamiltonian describing the radiation-matter interaction is

$$H' = - \int E(\mathbf{r}, t) P(\mathbf{r}) d\mathbf{r} = -E(\mathbf{r}, t) V, \quad (3.1)$$

where  $V$  is the dipole operator  $V = \sum_{\alpha} q_{\alpha} (\mathbf{r} - \mathbf{r}_{\alpha})$  (we sum over all nuclei and electrons  $\alpha$  with charge  $q_{\alpha}$  and positions  $\mathbf{r}_{\alpha}$ ).

The total Hamiltonian is  $H = H_0 + H'$  and its time evolution is defined by the equation

$$\begin{aligned} \frac{d\hat{\rho}}{dt} &= -\frac{i}{\hbar} [\hat{H}_0, \hat{\rho}] - \frac{i}{\hbar} [\hat{H}', \hat{\rho}] \\ &= -\frac{i}{\hbar} \mathcal{L}_0 \rho - \frac{i}{\hbar} \mathcal{L}' \rho, \end{aligned} \quad (3.2)$$

where  $\rho$  is the density operator and the first line is written in Hilbert space notation, while the second in Liouville one; as a consequence of equation (1.43)  $\mathcal{L}'(t)A = [H', A]$ .

Let us introduce a new superoperator, that will be useful to simplify the notation in Liouville space:

$$\mathcal{V}A = [V, A]. \quad (3.3)$$

Our first aim is to write the power series of the density operator, but, in order to do this, let us before focus on the time evolution operator.

### 3.1.1 Time evolution operator

From the differential equation (1.46)

$$\frac{\partial \mathcal{U}(t, t_0)}{\partial t} = -\frac{i}{\hbar} \mathcal{L} \mathcal{U}(t, t_0), \quad (3.4)$$

we can get an expression for the Liouville time evolution superoperator  $\mathcal{U}(t, t_0)$ , with initial condition  $\mathcal{U}(t_0, t_0) = 1$ . If we are considering a system

described by a *time independent Hamiltonian*, the time evolution superoperator is simply

$$\mathcal{U}(t, t_0) = e^{-\frac{i}{\hbar}\mathcal{L}(t-t_0)} \quad (3.5)$$

whose representation in Hilbert space is

$$\mathcal{U}(t, t_0)\rho(t_0) = e^{-\frac{i}{\hbar}H(t-t_0)}\rho(t_0)e^{\frac{i}{\hbar}H(t-t_0)}. \quad (3.6)$$

If we consider instead a more general case, in which the Hamiltonian is time dependent, the solution of the time evolution operator becomes

$$\mathcal{U}(t, t_0) = \text{exp}_T \left[ -\frac{i}{\hbar} \int_{t_0}^t d\tau \mathcal{U}(\tau) \right], \quad (3.7)$$

where the subscript T means *time-ordered exponential*, i.e. a short notation for

$$\begin{aligned} \mathcal{U}(t, t_0) &= 1 + \sum_{n=1}^{\infty} \left( -\frac{i}{\hbar} \right)^n \int_{t_0}^t d\tau_n \int_{t_0}^{\tau_n} d\tau_{n-1} \dots \int_{t_0}^{\tau_2} d\tau_1 \times \\ &\times \mathcal{L}(\tau_n)\mathcal{L}(\tau_{n-1})\dots\mathcal{L}(\tau_1) \end{aligned} \quad (3.8)$$

$$\begin{aligned} \mathcal{U}(t, t_0)\rho(t_0) &= \rho(t_0) + \sum_{n=1}^{\infty} \left( -\frac{i}{\hbar} \right)^n \int_{t_0}^t d\tau_n \int_{t_0}^{\tau_n} d\tau_{n-1} \dots \int_{t_0}^{\tau_2} d\tau_1 \times \\ &\times [H(\tau_n), \dots [H(\tau_2), [H(\tau_1), \rho(t_0)]] \dots], \end{aligned} \quad (3.9)$$

where we have used the definition of the Liouville superoperator (1.43).

### The interaction picture

So far we treated the entire Hamiltonian perturbatively (as a matter of fact it compares "entirely" in the expansion of  $\mathcal{U}(t, t_0)$  (3.9)), but this method is usually valid for short times and it breaks down at longer times. The *interaction picture*, instead, treats one part of the Hamiltonian ( $H_0$ ) exactly and expands only the remaining part  $H_1$ . If the Hamiltonian is conveniently divided in the two parts, that is if the Hamiltonian  $H_0$  is "simple" and its time evolution can be calculated exactly, the expansion is valid for longer times. This representation can be considered intermediate between the Schrödinger picture and the Heisenberg one, since in this case both state vectors and

operators are function of time and contribute to the time dependence of observables; they are represented in Hilbert space as follows

$$\begin{aligned} |\psi_I(t)\rangle &= e^{\frac{i}{\hbar}\hat{H}_0 t} |\psi_S(t)\rangle \\ \hat{A}_I(t) &= e^{\frac{i}{\hbar}\hat{H}_0 t} \hat{A}_S(t) e^{-\frac{i}{\hbar}\hat{H}_0 t}. \end{aligned} \quad (3.10)$$

One can introduce the same picture in Liouville space, by partitioning the Liouville superoperator as suggested by equation (3.2)

$$\mathcal{L} = \mathcal{L}_0 + \mathcal{L}'. \quad (3.11)$$

Consequently also the time evolution operator can be split in two parts

$$\begin{aligned} \mathcal{U}_0(t, t_0) &= \exp_T \left[ -\frac{i}{\hbar} \int_{t_0}^t d\tau \mathcal{L}_0(\tau) \right] \\ \mathcal{U}_{int}(t, t_0) &= \exp_T \left[ -\frac{i}{\hbar} \int_{t_0}^t d\tau \mathcal{L}'_{int}(\tau) \right] \end{aligned} \quad (3.12)$$

(where  $\mathcal{L}'_{int}(\tau) = \mathcal{U}^\dagger(\tau, t_0) \mathcal{L}' \mathcal{U}(\tau, t_0)$ ), whose product gives the total time evolution superoperator; finally we can express the total operator as

$$\begin{aligned} \mathcal{U}(t, t_0) &= \mathcal{U}_0(t, t_0) + \sum_{n=1}^{\infty} \left( -\frac{i}{\hbar} \right)^n \int_{t_0}^t d\tau_n \int_{t_0}^{\tau_n} d\tau_{n-1} \dots \int_{t_0}^{\tau_2} d\tau_1 \times \\ &\times \mathcal{U}_0(t, \tau_n) \mathcal{L}'(\tau_n) \mathcal{U}_0(\tau_n, \tau_{n-1}) \mathcal{L}'(\tau_{n-1}) \dots \\ &\dots \mathcal{U}_0(\tau_2, \tau_1) \mathcal{L}'(\tau_1) \mathcal{U}_0(\tau_1, t_0). \end{aligned} \quad (3.13)$$

### 3.1.2 Expansion of the density operator

Let us come back to the time dependent density operator and consider its expansion in powers of the electric field, i.e.

$$\rho(t) \equiv \rho^{(0)}(t) + \rho^{(1)}(t) + \rho^{(2)}(t) + \dots \quad (3.14)$$

where  $\rho^{(0)}(t) = \rho(-\infty)$ . Keeping in mind the time evolution of the elements of Liouville space (1.46) and the evolution of the superoperator  $\mathcal{U}(t, t_0)$  (3.13) we get

$$\begin{aligned} \rho^{(n)}(t) &= \left( -\frac{i}{\hbar} \right)^n \int_{t_0}^t d\tau_n \dots \int_{t_0}^{\tau_2} d\tau_1 \mathcal{G}(t - \tau_n) \mathcal{L}_{int}(\tau_n) \mathcal{G}(\tau_n - \tau_{n-1}) \cdot \\ &\cdot \mathcal{L}_{int}(\tau_{n-1}) \dots \mathcal{G}(\tau_2 - \tau_1) \mathcal{L}_{int}(\tau_1) \mathcal{G}(\tau_1 - t_0) \rho(t_0) \end{aligned} \quad (3.15)$$

where  $\mathcal{G}(\tau) = \theta(\tau)e^{-\frac{i}{\hbar}\mathcal{L}\tau}$  is the Liouville space Green function in absence of radiation fields and  $\theta(\tau)$  is the Heavyside step function.

Since  $\rho(t_0)$  represents the equilibrium density operator, it does not evolve in time in absence of external fields, so  $\mathcal{G}(\tau_1 - t_0)\rho(t_0) = \rho(t_0)$ . Furthermore  $\mathcal{L}'_{int} = -E(t)\mathcal{V}$ , as follows from equations (3.1) and (3.3). The equation for the  $n^{th}$  contribution of the density operator then becomes

$$\begin{aligned} \rho^{(n)}(t) &= \left(\frac{i}{\hbar}\right)^n \int_{t_0}^t d\tau_n \dots \int_{t_0}^{\tau_2} d\tau_1 E(\mathbf{r}, \tau_n) E(\mathbf{r}, \tau_{n-1}) \dots E(\mathbf{r}, \tau_1) \times \\ &\quad \times \mathcal{G}(t - \tau_n) \mathcal{V} \mathcal{G}(\tau_n - \tau_{n-1}) \mathcal{V} \dots \\ &\quad \dots \mathcal{G}(\tau_2 - \tau_1) \mathcal{V} \mathcal{G}(\tau_2 - \tau_1) \mathcal{V} \rho(t_0). \end{aligned} \quad (3.16)$$

Finally if we change the time variables with  $t_k \equiv \tau_{k+1} - \tau_k$  (and  $\tau_{n+1} = t$ ), send  $t_0 \rightarrow -\infty$  and define  $\mathcal{V}(\tau) \equiv e^{\frac{i}{\hbar}\mathcal{L}\tau} \mathcal{V} e^{-\frac{i}{\hbar}\mathcal{L}\tau}$ , we get

$$\begin{aligned} \rho^{(n)}(t) &= \left(\frac{i}{\hbar}\right)^n \int_0^{+\infty} dt_n \dots \int_0^{+\infty} dt_1 E(\mathbf{r}, t - t_n) E(\mathbf{r}, t - t_n - t_{n-1}) \dots \\ &\quad \dots E(\mathbf{r}, t - t_n - t_{n-1} \dots t_1) \mathcal{G}(t_n + t_{n-1} + \dots + t_1) \mathcal{V}(t_{n-1} + \dots + t_1) \dots \\ &\quad \dots \mathcal{V}(t_1) \mathcal{V}(0) \rho(t_0). \end{aligned} \quad (3.17)$$

The knowledge of the perturbative expansion of the density operator is useful since it allows to compute the expectation value (or more precisely, its expansion) of any observable on the considered state [Equation (1.29)]; in particular we developed it in order to find out the polarization  $P(\mathbf{r}, t)$ , i.e. the expectation value of the dipole operator  $V$ .

We are interested in this expansion because every order represents a different kind of measurement: the linear polarization determines linear optics,  $P^{(2)}$  represents second order processes, such as frequency sum generation and third order concerns techniques including four wave mixing and pump-probe spectroscopy. The  $n^{th}$  order contribution to the polarization is

$$\begin{aligned} P^{(n)}(\mathbf{r}, t) &= \langle V \rangle = Tr[V\rho] = \langle \langle V | \rho \rangle \rangle \\ &= \int_0^{+\infty} dt_n \dots \int_0^{+\infty} dt_1 S^{(n)}(t_n, t_{n-1}, \dots t_1) E(\mathbf{r}, t - t_n) \cdot \\ &\quad \cdot E(\mathbf{r}, t - t_n - t_{n-1}) \dots E(\mathbf{r}, t - t_n - t_{n-1} \dots t_1), \end{aligned} \quad (3.18)$$

where

$$\begin{aligned}
 S^{(n)}(t_n, t_{n-1}, \dots, t_1) &= \left(\frac{i}{\hbar}\right)^n \langle\langle V | \mathcal{G}(t_n) \mathcal{V} \mathcal{G}(t_{n-1}) \mathcal{V} \dots \mathcal{G}(t_1) \mathcal{V} | \rho(-\infty) \rangle\rangle \\
 &= \left(\frac{i}{\hbar}\right) \theta(t_1) \theta(t_2) \dots \theta(t_n) \cdot \\
 &\quad \cdot \langle\langle V(t_n + \dots + t_1) | \mathcal{V}(t_n + \dots + t_1) \dots \mathcal{V}(t_1) \mathcal{V}(t_0) | \rho(-\infty) \rangle\rangle
 \end{aligned} \tag{3.19}$$

is the  $n^{\text{th}}$  order response function and sum up the total microscopic information for the calculation of optical measurement. We can define the same quantity in the Hilbert space and, using the definition of  $\mathcal{V}$ , one obtains

$$\begin{aligned}
 S^{(n)}(t_n, t_{n-1}, \dots, t_1) &= \left(\frac{i}{\hbar}\right) \theta(t_1) \theta(t_2) \dots \theta(t_n) \cdot \\
 &\quad \cdot \langle V(t_n + \dots + t_1) [V(t_n + \dots + t_1), [\dots [V(t_1), [V(t_0), \rho(-\infty)]] \dots]] \rangle.
 \end{aligned} \tag{3.20}$$

Note that the Heaviside step functions  $\theta(t)$  guarantee the causality principle in the calculation of the polarization, since it depend only on the fields at earlier times.

### Third order response

Since in definition (3.19) every  $\mathcal{V}$  represents a commutator, the nonlinear response function  $S^{(n)}$  is made up of  $2^n$  terms, but only half of them are independent: the others are the complex conjugates of the former.

In this thesis we are particularly interested in the *third order response function*, because it is used to treat four wave mixing techniques (described in section 3.2). Let us rewrite equation (3.19) for  $n = 3$ :

$$\begin{aligned}
 S^{(3)}(t_3, t_2, t_1) &= \left(\frac{i}{\hbar}\right)^3 \theta(t_1) \theta(t_2) \theta(t_3) \langle\langle V(t_3 + t_2 + t_1) | \\
 &\quad \mathcal{V}(t_3 + t_2 + t_1) \mathcal{V}(t_2 + t_1) \mathcal{V}(t_1) \mathcal{V}(0) | \rho(-\infty) \rangle\rangle \\
 &= \left(\frac{i}{\hbar}\right)^3 \theta(t_1) \theta(t_2) \theta(t_3) \langle V(t_3 + t_2 + t_1) \\
 &\quad [V(t_2 + t_1) [V(t_1) [V(t_0), \rho(-\infty)]]] \rangle,
 \end{aligned} \tag{3.21}$$

which can be redefined as

$$S^{(3)}(t_3, t_2, t_1) = \left(\frac{i}{\hbar}\right)^n \theta(t_1)\theta(t_2)\theta(t_3) \sum_{\alpha=1}^4 [R_\alpha(t_3, t_2, t_1) - R_\alpha^*(t_3, t_2, t_1)], \quad (3.22)$$

where

$$\begin{aligned} R_1(t_3, t_2, t_1) &= \langle V(t_1 + t_2 + t_3)V(0)\rho(-\infty)V(t_1)V(t_1 + t_2) \rangle \\ R_2(t_3, t_2, t_1) &= \langle V(t_1 + t_2 + t_3)V(t_1)\rho(-\infty)V(0)V(t_1 + t_2) \rangle \\ R_3(t_3, t_2, t_1) &= \langle V(t_1 + t_2 + t_3)V(t_1 + t_2)\rho(-\infty)V(0)V(t_1) \rangle \\ R_4(t_3, t_2, t_1) &= \langle V(t_1 + t_2 + t_3)V(t_1 + t_2)V(t_1)V(0)\rho(-\infty) \rangle. \end{aligned} \quad (3.23)$$

are the so called Liouville paths.

### 3.1.3 Extended systems

Up to now we have considered a simple model of an isolated small particle for which the adiabatic approximation is valid; let us generalize the obtained result to a more realistic system with arbitrary size. In this case the interaction Hamiltonian is

$$H' = - \int d\mathbf{r} E(\mathbf{r}, t) \cdot V(\mathbf{r}), \quad (3.24)$$

where  $V(\mathbf{r})$  is a polarization operator. From the generalization of equation (3.18) one gets

$$\begin{aligned} P_{\nu_s}^{(n)}(\mathbf{r}, t) &= \int d\mathbf{r}_n \int d\mathbf{r}_{n-1} \dots \int d\mathbf{r}_1 \int_0^{+\infty} dt_n \dots \\ &\dots \int_0^{+\infty} dt_1 S_{\nu_1, \dots, \nu_n, \nu_s}^{(n)}(\mathbf{r}; \mathbf{r}_n, \dots, \mathbf{r}_1, t_n, t_{n-1}, \dots, t_1) E_{\nu_n}(\mathbf{r}_n, t - t_n) \times \\ &\times E_{\nu_{n-1}}(\mathbf{r}_{n-1}, t - t_n - t_{n-1}) \dots E_{\nu_1}(\mathbf{r}_1, t - t_n, t_{n-1} \dots t_1), \end{aligned} \quad (3.25)$$

with nonlinear response function

$$\begin{aligned} S_{\nu_1, \dots, \nu_n, \nu_s}^{(n)}(\mathbf{r}; \mathbf{r}_n, \dots, \mathbf{r}_1, t_n, t_{n-1}, \dots, t_1) &= \\ &= \left(\frac{i}{\hbar}\right)^n \langle \langle V_{\nu_s}(\mathbf{r}) | \mathcal{G}(t_n) V_{\nu_n}(\mathbf{r}_n) \mathcal{G}(t_{n-1}) \dots \mathcal{G}(t_1) \mathcal{V}_{\nu_1}(\mathbf{r}_0) | \rho(-\infty) \rangle \rangle. \end{aligned} \quad (3.26)$$

In the previous equations  $E_{\nu_i}(\mathbf{r}_j, t)$  is the field polarized in the  $\nu_i$  direction and  $S^{(n)}$  describes the  $\nu_s$  component of the polarization induced at point  $\mathbf{r}$  and time  $t$  by  $n$  interactions with the field at times  $t - t_n, t - t_n - t_{n-1}, \dots, t - t_n - \dots - t_1$  and points  $\mathbf{r}_n, \dots, \mathbf{r}_1$ .

### 3.1.4 Double-sided Feynman diagrams

We have just obtained the optical polarization, both for point-like and extended systems, which contains the total information about the interaction we want to study. Nevertheless the physical interpretation of its expression is not so clear, even for simple systems. So let us introduce a graphic representation, containing a lot of information about the interaction, the so called *double-sided Feynman diagram*. This representation is based on the concepts of response function and density operator. In order to introduce it we will consider the third order response function analyzed in section [3.1.2], not only because it is simpler to be represented, but also because the third order of the polarization perturbative expansion is useful to treat four wave mixing techniques [section (3.2)], as already anticipated.

Let us consider expression 3.22: we are looking for a graphic representation of  $R_i$  (equations 3.23). The double-sided Feynman diagram can be constructed using the following rules:

1. Two vertical lines represent the density operator, and, in particular, the left line is the ket, while the right one is the bra.
2. Time is running from the bottom to the top of the lines (so we could say that the lines represent the time evolution of the density operator).
3. The interaction with the field is represented by wavy arrows pointing towards or away from the system.
4. As a convention the last interaction (in this case at time  $t_1 + t_2 + t_3$ ) "goes out" from the left side (the ket).
5. The sign of  $R_i$  is  $(-1)^n$ , where  $n$  is the number of interaction on the right (bra), because any of them represents the second term of a commutator. In our situation in  $R_1$ ,  $R_2$  and  $R_3$  there are 2 interactions on the right and in  $R_1$  there is no interaction on the right, so in both cases the sign is plus.
6. An arrow pointing to the right stands for the contribution of the field  $E_j e^{i(\mathbf{k}_j \cdot \mathbf{r} - \omega_j t)}$  and the action of the photon annihilation operator  $\hat{a}$ ,

while an arrow pointing to the left represent its complex conjugate and the action of the creation operator  $\hat{a}^\dagger$ . As a consequence an arrow pointing towards the system symbolizes photon absorption, while an arrow pointing away describes photon emission

7. The last interaction must end in a population state.

Following these rules one can draw the Feynman diagram for any light-matter interaction. The third order response function, in particular, gives these contributions:

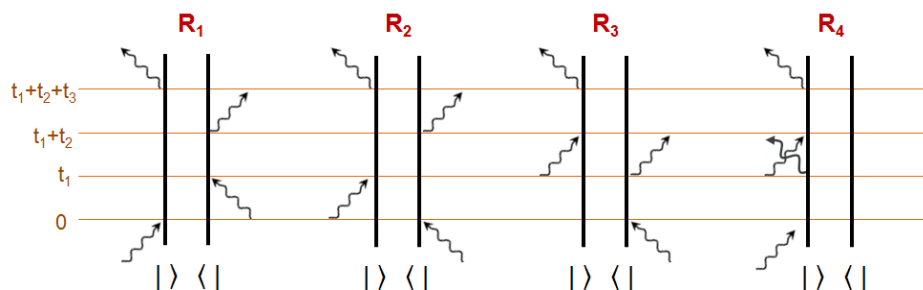


Figure 3.1: Feynman diagrams representing the contributions of the third order response function (3.23).

## 3.2 Classification of four wave mixing techniques

In this section we are going to treat low order nonlinear optical techniques, connected with the nonlinear polarization  $P^{(n-1)}$ ; the simplest and most common ones are related to *multiwave mixing*. The  $n$ -wave mixing process is due to the interaction between  $n - 1$  electromagnetic fields, with wave vectors  $\mathbf{k}_1 \dots \mathbf{k}_n$  and frequencies  $\omega_1 \dots \omega_n$ : a coherently generated signal should have wave vector  $\mathbf{k}_s = \pm \mathbf{k}_1 \pm \mathbf{k}_2 \pm \dots \pm \mathbf{k}_n$  and frequency  $\omega_s = \pm \omega_1 \pm \omega_2 \pm \dots \pm \omega_n$ .

### 3.2.1 n-wave mixing

Let us compute the contribution to the  $n^{th}$  order of the signal generated by many electromagnetic fields. In general the total electric field can be written

as

$$\mathbf{E}(\mathbf{r}, t) = \sum_{j=1}^n E_j(\mathbf{r}, t) e^{i(\mathbf{k}_j \cdot \mathbf{r} - \omega_j t)}. \quad (3.27)$$

If the signal field is outside the absorption spectrum, the dielectric function is real, i.e.  $\epsilon(\omega_j) = n_j^2$ , where  $n_j$  is the refractive index of the medium for light at frequency  $\omega_j$  (note that  $k_j = \frac{\omega_j}{c} n_j$ ). From the Maxwell equations we get

$$\vec{\nabla} \times \vec{\nabla} \times \mathbf{E}(\mathbf{r}, t) + \frac{n^2}{c^2} \frac{\partial^2 \mathbf{E}(\mathbf{r}, t)}{\partial t^2} = -\frac{4\pi}{c^2} \frac{\partial^2 \mathbf{P}_{NL}(\mathbf{r}, t)}{\partial t^2}, \quad (3.28)$$

where  $P_{NL}(\mathbf{r}, t)$  is the nonlinear polarization generated by the interaction between the incoming modes and the medium. Let us rewrite the nonlinear polarization in the form

$$P_{NL}(\mathbf{r}, t) = \sum_n \sum_s P_s^{(n)}(t) e^{i(\mathbf{k}_s \cdot \mathbf{r} - \omega_s t)}, \quad (3.29)$$

and focus only on one term of the previous sum, that experimentally means that we fix the position of the detector (index  $s$ ) and we choose a particular technique, which allows us to see a specific order of the signal (index  $n$ ). In order to simplify the calculation we change the coordinate system, such that  $\mathbf{k}_s$  is parallel to the  $z$ -axis; as a consequence  $\mathbf{k}_s \cdot \mathbf{r} = k_s z$ .

Assuming that the solution of equation (3.28) is of the form

$$\mathbf{E}(\mathbf{r}, t) = \mathbf{E}_s(z, t) e^{i(\mathbf{k}'_s \cdot \mathbf{r} - \omega_s t)} + c.c., \quad (3.30)$$

that  $P_s(t)$  varies very slowly (i.e.  $\left| \frac{\partial P_s(t)}{\partial t} \right| \ll |\omega_s P_s(t)|$ ) and inserting all information in (3.28), one gets that

$$E_s(l, t) = \frac{2\pi i}{n(\omega_s)} \frac{\omega_s}{c} l P_s(t) \text{sinc} \left( \frac{\Delta k \cdot l}{2} \right) e^{i \frac{\Delta k \cdot l}{2}}, \quad (3.31)$$

where  $l$  is the "thickness" of the sample along the  $z$ -axis, with  $k_s \cdot l \ll 1$  (which means that the wavelength of the incident beam should be much smaller than the dimension of the sample),  $\Delta k = \mathbf{k}_s - \mathbf{k}'_s$  and  $\text{sinc}(x) = \frac{\sin x}{x}$ , as shown in Figure (3.2).

Note that for  $l \rightarrow \infty$   $\text{sinc} \left( \frac{\Delta k \cdot l}{2} \right) \rightarrow (2\pi)^3 \delta(\Delta k \cdot l)$ : the last limit represent the *phase matching condition*.

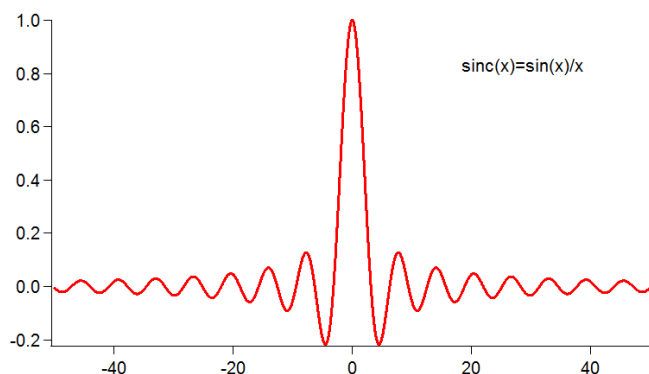


Figure 3.2: Function  $\text{sinc}(x) = \frac{\sin x}{x}$ .

### Heterodyne detection of wave mixing

We already know that performing a spectroscopic experiment we finally get a signal proportional to the square of the polarization. The advantage of wave mixing is that the signal can be generated in a direction different from that of the incoming fields, reducing considerably the background and giving a more sensitive response, but it is also much weaker. For this reason another technique is usually coupled to wave mixing, the *heterodyne detection*, which allows us to amplify the signal (and so the sensibility) by adding a new field, called *local oscillator*. The local oscillator should have the same wave vector direction of the output signal: in this way the measured intensity ( $I(t)$ ) is a superposition of the local oscillator and the signal fields ( $E_{LO}$  and  $E_S$  respectively), i.e.

$$\begin{aligned} I(t) &= \frac{n(\omega_s) \cdot c}{8\pi} |E_{LO}(t) + E_S(t)|^2 \\ &= I_{LO} + I_S(t) + \frac{n(\omega_s) \cdot c}{4\pi} \mathcal{R}e [E_{LO}^*(t) \cdot E_S(t)]. \end{aligned} \quad (3.32)$$

As already said this technique is used when the signal is weak, so we can always choose an intense local oscillator: in this case the term  $I_S$  is negligible when compared to  $I_{LO}$  or to the product of the two fields, while  $I_{LO}$  can be easily subtracted, since the field is known and does not interact in the sample.

A particular case of this technique occurs when the field is generated along one of the incoming beams: in this case we have an intrinsic heterodyne

detection and one measures the intensity

$$I(t) = \frac{n(\omega_s) \cdot c}{4\pi} \Re e [E_3^*(t) \cdot E_S(t)] \propto \omega_2 l \Im m [E_3^*(t) \cdot P_S(t)], \quad (3.33)$$

where  $I_2$  is the incoming field intensity (with frequency  $\omega_2$ ); the notation is in accordance with that used to describe pump and probe [section 3.3] and Raman [section 3.4] spectroscopy.

### 3.2.2 Four wave mixing

Different orders of the polarization allow to study different phenomena. For the second order polarization  $P^{(2)}$  we get three wave mixing processes, such as the second harmonic generation ( $\mathbf{k}_s = 2\mathbf{k}_1$  and  $\omega_s = 2\omega_1$ ), or more generally sum or difference frequency generation ( $\mathbf{k}_s = \mathbf{k}_1 \pm \mathbf{k}_2$  and  $\omega_s = \omega_1 \pm \omega_2$ ). However second order non linearities vanish for isotropic media with inversion symmetry: in this case the first order non linearity is the third one and one gets *four wave mixing processes*.

In general when light-matter interactions take place we don't know exactly what happens to the density operator (that is how it evolves in time), since the polarization contains all the possible Liouville paths. Nevertheless a convenient choice of some experimental conditions allows us to get a lot of information about the process itself. We will initially consider an ideal time domain four wave mixing measurement performed with three *well separated pulses*: as a matter of fact controlling the time ordering of the pulses and selecting the wave vector direction of the output signal, we can choose a particular Liouville space path.

Let us consider an electric field made up of three pulses

$$E(\mathbf{r}, t) = E_1(t+\tau+\tau')e^{i(\mathbf{k}_1 \cdot \mathbf{r} - \omega_1 t)} + E_2(t+\tau)e^{i(\mathbf{k}_2 \cdot \mathbf{r} - \omega_2 t)} + E_3(t)e^{i(\mathbf{k}_3 \cdot \mathbf{r} - \omega_3 t)} + c.c., \quad (3.34)$$

where  $E_j$  is the envelope of the  $j$ -th pulse and  $\omega_j$  is its mean frequency; suppose the time delays  $\tau$  and  $\tau'$  between the pulses to be much longer than the duration of the pulses (Figure (3.3)).

As one can simply observe from the definition of  $k_s$ , there are eight possible directions for the output signal; nevertheless some opportune approximations can reduce their number.

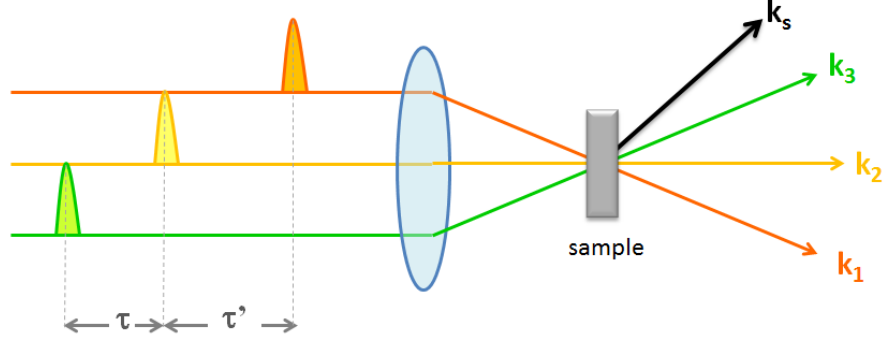


Figure 3.3: Simplified scheme of a four wave mixing process.

Suppose that our system is a two-electronic level one and that the frequencies of the electromagnetic fields are near resonance, i.e.  $\omega_1, \omega_2, \omega_3 \approx \omega_{eg}$  (where  $\hbar\omega_{eg}$  is the energy difference between the levels). Considering the transition due to the three fields, if we compute the third order polarization, we obtain terms with frequency  $(\omega_j - \omega_{eg})$  or  $(\omega_j + \omega_{eg})$ . The latter oscillate much faster than the former and performing a time integration over the signal (present in the calculation of the polarization), it gives a small contribution and can be neglected: this is the so called *rotating wave approximation*.

For the same reason the first two fields ( $E_1$  and  $E_2$ ) must have opposite sign of frequency, otherwise we get a highly oscillatory term  $e^{i(\omega_1 + \omega_2)t_2}$  which disappear with the integration over the period  $t_2$ . This means that the only possible wave vectors for the resulting field are  $\pm k_3 \pm (k_2 - k_1)$ : it is possible to interpret the signal in terms of a grating formed by the first two beams, while the third undergoes a Bragg diffraction from that grating.

Finally the dominant components of the polarization are:

$$\begin{aligned}
 P^{(3)}(\mathbf{k}_a \equiv \mathbf{k}_3 + \mathbf{k}_2 - \mathbf{k}_1, t) &= \left(\frac{i}{\hbar}\right)^3 \int_0^{+\infty} dt_3 \int_0^{+\infty} dt_2 \int_0^{+\infty} dt_1 \\
 & [R_2(\mathbf{k}_3, \mathbf{k}_2, \mathbf{k}_1) + R_3(\mathbf{k}_3, \mathbf{k}_2, \mathbf{k}_1)] E_3(t - t_3) E_2(t + \tau - t_3 - t_2) \\
 & E_1^*(t + \tau + \tau' - t_3 - t_2 - t_1) e^{i(\omega_3 + \omega_2 - \omega_1)t_3} e^{i(\omega_2 - \omega_1)t_2} e^{-i\omega_1 t_1}
 \end{aligned} \quad (3.35)$$

$$\begin{aligned}
 P^{(3)}(\mathbf{k}_b \equiv \mathbf{k}_3 - \mathbf{k}_2 + \mathbf{k}_1, t) &= \left(\frac{i}{\hbar}\right)^3 \int_0^{+\infty} dt_3 \int_0^{+\infty} dt_2 \int_0^{+\infty} dt_1 \\
 & [R_1(\mathbf{k}_3, \mathbf{k}_2, \mathbf{k}_1) + R_4(\mathbf{k}_3, \mathbf{k}_2, \mathbf{k}_1)] E_3(t - t_3) E_2^*(t + \tau - t_3 - t_2) \\
 & E_1(t + \tau + \tau' - t_3 - t_2 - t_1) e^{i(\omega_3 - \omega_2 + \omega_1)t_3} e^{-i(\omega_2 - \omega_1)t_2} e^{i\omega_1 t_1}
 \end{aligned} \tag{3.36}$$

and their complex conjugates. Positioning the detector along a specific direction ( $\mathbf{k}_a$ ,  $\mathbf{k}_b$ ,  $-\mathbf{k}_a$  or  $-\mathbf{k}_b$ ), one can select the desired contribution of the polarization. Moreover if the duration of the pulse is short enough, its envelope tends to a Delta function and the calculation of the third order polarization becomes easier.

We must keep in mind that this result is due to some relevant simplifications. First of all we have considered a two level system: in a three level system, for example, also  $\mathbf{k}_1 + \mathbf{k}_2 + \mathbf{k}_3$  and  $\omega_1 + \omega_2 + \omega_3$  can be a resonant combination! Moreover if the pulses overlap we can get additionally contributions, due to the permutations of  $\mathbf{k}_1$ ,  $\mathbf{k}_2$  and  $\mathbf{k}_3$ . In order to obtain different spectroscopic techniques we have to change some of these experimental conditions: in particular we are interested in pump-probe spectroscopy, in which we will consider pulses that overlap, and off-resonance Raman scattering, in which the frequencies are far from  $\omega_{eg}$  and their difference is equal to a vibrational transition ( $\omega_1 - \omega_2 = \omega_{\nu\nu'}$ ).

### 3.3 Pump and probe

Let us consider now a four wave mixing technique in which we have only partial control on time ordering, that is to say that the time interval  $\tau$  is sufficiently large to distinguish the third pulse from the first two, whose time order is not completely defined. Pulses 1 and 2 interfere in the medium creating a grating of matter response of  $\mathbf{k}$ -vector  $\mathbf{k}_1 - \mathbf{k}_2$ , while pulse 3 undergoes a Bragg diffraction which generates a scattering beam with  $\mathbf{k}_s = \mathbf{k}_1 \pm (\mathbf{k}_3 - \mathbf{k}_2)$ .

The present situation seems to be quite different from a typical pump and probe experiment, first of all because it involves three or even four (if we consider also a local oscillator to detect the signal better), instead of two pulses (the pump and the probe). Let  $E_1(t + \tau)$  be the envelope of the pump,

centered at time  $t = -\tau$  and  $E_3(t)$  the probe one, peaked at  $t = 0$ : the hypothesis on the time delay  $\tau$  ensures that the pump comes before the probe. One can consider the effect of the pump on the sample as the interaction of more pulses on it: therefore  $E_2$  is the pump envelope too ( $E_1 = E_2$ ), just arriving at a slightly different time. Since  $\mathbf{k}_1 = \mathbf{k}_2$ , the two possible signal wave vectors are  $\mathbf{k}_s = \mathbf{k}_3$  and  $\mathbf{k}_s = 2\mathbf{k}_1 - \mathbf{k}_3$ , but in the usual configuration of a pump-probe experiment the field measured propagates along the probe direction, therefore only the first possibility is correct. Moreover in this particular situation the probe field acts as a local oscillator too, as described in the section about heterodyne detection.

Using equations (3.18), (3.22) and (3.23), reminding that in the present case we have a partial time ordering, so the only condition on time is that  $E_3$  interacts last, that  $E_3$  acts as a local oscillator too (and the measured intensity is given by equation (3.33) integrated in time), and performing the change of variable  $t \rightarrow t - \tau + t_3$ , one finally gets the following signal

$$\begin{aligned}
 I_{PP}(\omega_1, \omega_2, \tau) = & \left(\frac{1}{\hbar}\right)^3 2\omega_2 \mathcal{R}e \left\{ \int_{-\infty}^{+\infty} dt \int_0^{+\infty} dt_3 \int_0^{+\infty} dt_2 \int_0^{+\infty} dt_1 \right. \\
 & [E_3^*(t - \tau + t_3) E_3(t - \tau) E_1^*(t - t_2) E_1(t - t_2 - t_1) \cdot \\
 & \cdot e^{i(\omega_2 t_3 + \omega_1 t_1)} [R_1(t_3, t_2, t_1) + R_4(t_3, t_2, t_1)] + \\
 & + E_3^*(t - \tau + t_3) E_3(t - \tau) E_1(t - t_2) E_1^*(t - t_2 - t_1) \cdot \\
 & \left. e^{i(\omega_2 t_3 - \omega_1 t_1)} [R_2(t_3, t_2, t_1) + R_3(t_3, t_2, t_1)] \right\}
 \end{aligned} \tag{3.37}$$

In the previous expression only contributions that are second order in the pump and probe fields has been considered. Obviously there are also terms of fourth order in the probe and zeroth in the pump field with the same wave vector ( $\mathbf{k}_s = \mathbf{k}_3 - \mathbf{k}_3 + \mathbf{k}_3$ ), but since we want to measure the probe difference absorption (that is the difference between the probe in presence of the pump and in absence of the latter) they do not contribute to the difference signal.

### 3.4 Off-resonant Raman Scattering

Raman scattering is an inelastic diffusion of photons in which the energy difference between the incident and the scattered beam corresponds to vibrational levels of the sample. In impulsive Raman spectroscopy experiments a laser pulse is applied (pump) and coherent vibrations are observed in the variation in time domain of the optical properties of a second pulse (the probe), due to the excitation of coherent phonons. The term off-resonant refers to the fact that the involved energies are far from electronic transitions. Off-resonant Raman spectroscopies are a simple class of non-linear techniques related to  $P^{(3)}$ : we look for two photon resonance, whose frequency difference is resonant with vibrational transitions ( $\omega_{\nu\nu'} = \omega_1 - \omega_2$ ). As we have already anticipated we use only two pulses, even if we want to observe two photon resonances. As in the case of pump-probe measurements the first two fields are both provided by the first pulse, but there is an important difference with the previous case: this time the frequencies ( $\omega_1$  and  $\omega_2$ ) cannot be the same, otherwise no phonon can be excited. The solution comes from the pulsed nature of laser radiation: since the beams are limited in time (that is they are not continuous), they present a frequency dispersion. If the bandwidth is large enough to contain a vibrational energy gap of the sample, we will observe Raman scattering. In our case the laser radiation has a bandwidth of  $\Delta\lambda \approx 30$  nm, which corresponds to  $\Delta\omega \approx 8 \cdot 10^{13}$  Hz, which is larger than the lowest energy Raman active modes in our sample (whose energy is of the order of some Terahertz), but is lower than the energy gap of  $\alpha$ -quartz ( $\hbar\Delta\omega \approx 0.06$  eV, while the energy gap is several electronvolts). Raman experiments are performed using ultrafast laser pulses, shorter than the relevant vibrational periods and relaxation times (which appears in the signal as broadening).

Assume to have two simultaneous pumps, with central frequencies  $\omega_1$  and  $\omega_2$  (and wave vector  $\mathbf{k}_1$  and  $\mathbf{k}_2$ ) respectively, which interacts in the sample creating a dynamic grating with wave vector  $\mathbf{k}_1 - \mathbf{k}_2$ . After a time delay  $\tau$  a third pulse with frequency  $\omega_3$  (and wave vector  $\mathbf{k}_3$ ) impinges on the sample and is scattered from it. The Raman signal wave vector is  $\mathbf{k}_s = \mathbf{k}_3 + \mathbf{k}_1 - \mathbf{k}_2$ ,

corresponding to the Bragg diffraction from the grating. Note that in our case  $\mathbf{k}_1$  and  $\mathbf{k}_2$  have the same direction and similar modulus, and the angle between  $\mathbf{k}_1$  and  $\mathbf{k}_3$  is as small as possible, therefore the direction of the Raman scattering is close to the probe one ( $\mathbf{k}_3$ ) [see Figure (3.4)].

The total electric field in a Raman experiment is

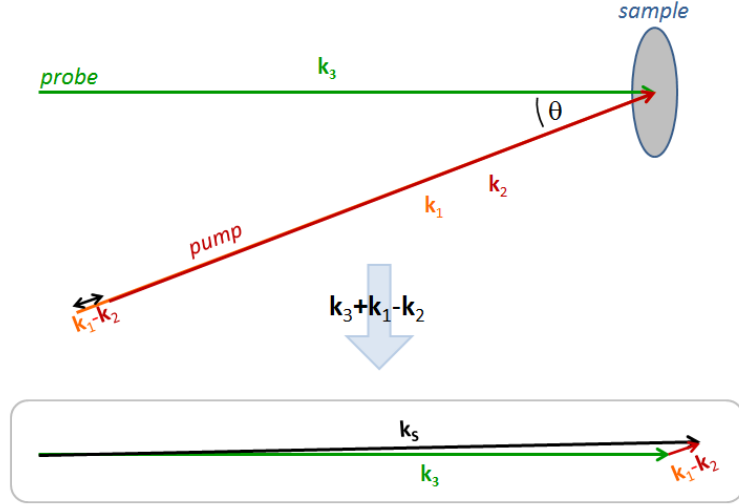


Figure 3.4: Scheme of Stimulated Raman Scattering on the sample. Red lines represent the two pump pulses with same direction but slightly different modulus, while the green line is the probe pulse. Inserting the data of our experiment (wavelength  $\lambda = 800$  nm, Raman active mode with frequency  $\nu = 3.9$  THz), the modulus of  $\mathbf{k}_3$  is two order of magnitude bigger than the modulus of  $\mathbf{k}_1 - \mathbf{k}_2$ . Even if we consider an angle  $\theta$  between the pump and the probe propagation direction of  $20^\circ$  (in our experimental set-up it is surely less) the ratio between the  $\mathbf{k}_s$  component parallel to  $\mathbf{k}_3$  and the perpendicular one is about 300, therefore the propagation direction of the signal can be considered the same of the probe one.

$$E(\mathbf{r}, t) = E_1(t-\tau)e^{i(\mathbf{k}_1 \cdot \mathbf{r}_1 - \omega_1 t)} + E_2(t-\tau)e^{i(\mathbf{k}_2 \cdot \mathbf{r}_2 - \omega_2 t)} + E_3(t)e^{i(\mathbf{k}_3 \cdot \mathbf{r}_3 - \omega_3 t)} + c.c., \quad (3.38)$$

where pulses 1 and 2 are coincident in time and centered in  $t = -\tau$ , while the third pulse is peaked at  $t = 0$ ; the time delay  $\tau$  is large enough to consider the first pulses well separated from the last. The measured signal will depend

on the third order nonlinear polarization through the relation

$$I_{RS}(\tau) = \int \left| P^{(3)}(\mathbf{k}_s, t, \tau) \right|^2 dt, \quad (3.39)$$

with polarization

$$\begin{aligned} P^{(3)}(\mathbf{k}_s, t, \tau) = & \int_0^{+\infty} dt_1 \int_0^{+\infty} dt_2 \int_0^{+\infty} dt_3 S^{(3)}(t_3, t_2, t_1) \left\{ E_3(t - t_3) \cdot \right. \\ & \cdot E_2^*(t + \tau - t_2 - t_3) E_1(t + \tau - t_1 - t_2 - t_3) e^{i\omega_s t_3} e^{i\omega_1 t_1} e^{i(\omega_1 - \omega_2) t_2} + \\ & \left. + E_3(t - t_3) E_2^*(t + \tau - t_1 - t_2 - t_3) E_1(t + \tau - t_2 - t_3) e^{i\omega_s t_3} e^{-i\omega_2 t_1} e^{i(\omega_1 - \omega_2) t_2} \right\}, \end{aligned} \quad (3.40)$$

where we have considered that  $E_3$  is always the last pulse.  $S^{(3)}$  has eight terms (Equation 3.22), which depend on the Hamiltonian of the system. Let us now introduce the Brownian oscillator model which allows the description of the dynamics of nuclei in a crystal in order to calculate the response function.

### *Brownian oscillator model*

The Brownian oscillator model describes the nuclear dynamics both in the case of coherent and damped motions and so represents a general way to study the coupling between nuclear motions and optical transitions.

Let us consider a two electronic-level system, with a ground state  $|g\rangle$  and an excited state  $|e\rangle$  and with nuclear coordinates  $\mathbf{q}_j$  coupled linearly with the electronic system. The Brownian oscillator Hamiltonian is

$$H = |g\rangle H_g \langle g| + |e\rangle H_e \langle e| + H' \quad (3.41)$$

where

$$\begin{aligned} H_g &= \sum_j \left[ \frac{p_j^2}{2m_j} + \frac{1}{2} m_j \omega_j^2 q_j^2 \right] \\ H_e &= \hbar\omega_{eg}^0 + \sum_j \left[ \frac{p_j^2}{2m_j} + \frac{1}{2} m_j \omega_j^2 (q_j + d_j)^2 \right] \end{aligned} \quad (3.42)$$

and  $q_j$ ,  $p_j$ ,  $m_j$  represent the coordinate, momentum and mass of the  $j^{th}$  nuclear mode, while  $\hbar\omega_{eg}^0$  is the electronic energy gap at the equilibrium

and  $d_j$  is the displacement of the equilibrium configuration of the  $j^{\text{th}}$  mode. Moreover the nuclear degrees of freedom are coupled to a bath of harmonic oscillators with coordinates  $x_n$  and momenta  $p_n$ . The interaction between the two kinds of oscillators is assumed to be linear, with strength  $c_n$ , and is described by

$$H' = \sum_n \left[ \frac{p_n^2}{2m_j} + \frac{m_n \omega_n^2}{2} \left( x_n - \sum_j \frac{c_{nj} q_j}{m_n \omega_n^2} \right)^2 \right] \quad (3.43)$$

Suppose that the total system is initially at equilibrium in the ground electronic state

$$\hat{\rho}_g = |g\rangle \langle g| \frac{e^{-\beta(H_g + H')}}{\text{Tr}(e^{-\beta(H_g + H')})} \quad (3.44)$$

and define

$$C_j = \langle q_j(t) q_j(0) \rho_g \rangle. \quad (3.45)$$

The latter quantity is related to the response function through the so called *cumulant expansion*, which is a method to calculate the response function perturbatively: in this case the expansion is performed directly on the response function rather than on the time evolution operator. In this thesis we are not going to derive it; anyway it is important to know that the term of the expansion (and so also the  $R_i$  of equation (3.23)) are exponential of the function  $g(t) \equiv \int_0^t d\tau_2 \int^{\tau_2} d\tau_1 \mathbf{C}(\tau_1)$ , and  $\mathbf{C}(\tau) = \sum_j \left( \frac{m_j \omega_j^2 d_j}{\hbar} \right) C_j$ .

One can separate  $C_j$  in its real and imaginary part

$$\begin{aligned} C'_j(t) &= \frac{1}{2} [\langle q_j(t) q_j(0) \rho_g \rangle + \langle q_j(0) q_j(t) \rho_g \rangle] \\ C''_j(t) &= \frac{-i}{2} [\langle q_j(t) q_j(0) \rho_g \rangle - \langle q_j(0) q_j(t) \rho_g \rangle]. \end{aligned} \quad (3.46)$$

Computing the Fourier transform of these coefficients and considering high frequency vibrations and the ideal case of absence of friction in the oscillator, the latter experiences a coherent motion and we get

$$C''_j = -\frac{\hbar}{2m_j \omega_j} \sin(\omega_j t). \quad (3.47)$$

---

<sup>1</sup>Thermal states are discussed in Appendix A

In order to have a more compact notation let us define

$$\begin{aligned}
 \rho_D(t) &= e^{-\frac{i}{\hbar}H_e t} V_{eg} \rho_g e^{\frac{i}{\hbar}H_g t} V_{ge} \\
 \rho_W(t) &= e^{\frac{i}{\hbar}H_e t} V_{eg} e^{-\frac{i}{\hbar}H_g t} V_{ge} \\
 \rho'_D(t) &= V_{ge} e^{-\frac{i}{\hbar}H_e t} V_{eg} \rho_g e^{\frac{i}{\hbar}H_g t} \\
 \rho'_W(t) &= V_{ge} e^{\frac{i}{\hbar}H_e t} V_{eg} e^{-\frac{i}{\hbar}H_g t}
 \end{aligned} \tag{3.48}$$

(where  $V$  is the usual dipole operator), such that

$$\begin{aligned}
 R_1 &= \langle \rho_W(t_3) \mathcal{G}_{ee}(t_2) \rho_D(t_1) \rangle \\
 R_2 &= \langle \rho_W(t_3) \mathcal{G}_{ee}(t_2) \rho_D^\dagger(t_1) \rangle \\
 R_3 &= \langle \rho'_W(t_3) \mathcal{G}_{gg}(t_2) \rho_D^\dagger(t_1) \rangle \\
 R_4 &= \langle \rho'_W(t_3) \mathcal{G}_{gg}(t_2) \rho'_D(t_1) \rangle
 \end{aligned} \tag{3.49}$$

and, from equation (3.22),

$$\begin{aligned}
 S^{(3)}(t_1, t_2, t_3) &= \left(\frac{i}{\hbar}\right)^3 \theta(t_1) \theta(t_2) \theta(t_3) \cdot \\
 &\cdot \left\{ \langle [\rho_W(t_3) - \rho_W^\dagger(t_3)] \mathcal{G}_{ee}(t_2) [\rho_D(t_1) - \rho_D^\dagger(t_1)] \rangle + \right. \\
 &\left. + \langle [\rho'_W(t_3) - \rho'_W^\dagger(t_3)] \mathcal{G}_{gg}(t_2) [\rho'_D(t_1) - \rho'_D^\dagger(t_1)] \rangle \right\}.
 \end{aligned} \tag{3.50}$$

Keeping in mind this new notation one finally gets

$$\begin{aligned}
 P^{(3)}(\mathbf{k}_s, t, \tau) &= \frac{i}{\hbar^3} E_3(t) \int_0^{+\infty} dt_2 e^{i(\omega_1 - \omega_2)t_2} E_1(t + \tau - t_2) E_2^*(t + \tau - t_2) \cdot \\
 &\cdot \langle \langle \rho'_W(\omega_s) - \rho_W^\dagger(\omega_s) | \mathcal{G}_{gg}(t_2) | \rho_D(\omega_1) - \rho'_D(-\omega_2) + \rho_D^\dagger(\omega_1) - \rho_D^\dagger(-\omega_2) \rangle \rangle,
 \end{aligned} \tag{3.51}$$

where  $\rho(\omega)$  is the Fourier transform of  $\rho(t)$  and  $\omega_s = \omega_3 + \omega_1 - \omega_2$ .

In general the third order polarization should depend on  $\omega_1$ ,  $\omega_2$  and  $\omega_s$ ; however under off-resonant conditions this dependence is weak and all the frequencies can be replaced by  $\omega_p = \frac{\omega_1 + \omega_2}{2}$ . The previous approximation is valid only during  $t_1$  and  $t_3$  periods; that's why we kept the term  $e^{i(\omega_1 - \omega_2)t_2}$ , which represents the two photon resonance.

Equation (3.51) can be rewritten also using the polarizability operator at the

average frequency

$$\alpha \equiv \frac{1}{\hbar} V_{ge} \mathcal{G}_{eg}(\omega_p) V_{eg} + V_{ge} \mathcal{G}_{eg}(-\omega_p) V_{eg}$$

and

$$(3.52)$$

$$\alpha(t) \equiv e^{\frac{i}{\hbar} H_g t} \alpha e^{-\frac{i}{\hbar} H_g t} = \alpha \mathcal{G}_{gg}(t)$$

(the previous expression is obtained by calculating the linear response function and remembering that the dipole moment  $V = \alpha E$  at the first order).

From the previous relation one gets

$$\begin{aligned} \rho'_W(\omega_p) - \rho'^{\dagger}_W(\omega_p) &= \hbar \alpha \\ \rho'_D(\omega_p) - \rho'^{\dagger}_D(-\omega_p) &= \hbar \alpha \rho_g \\ \rho'^{\dagger}_W(\omega_p) - \rho'^{\dagger}_D(-\omega_p) &= \hbar \rho_g \alpha. \end{aligned} \quad (3.53)$$

Substituting the previous operators in equation (3.51) one gets

$$\begin{aligned} P^{(3)}(\mathbf{k}_s, t, \tau) &= -E_3(t) \int_0^{+\infty} dt_2 e^{i(\omega_1 - \omega_2)t_2} E_1(t + \tau - t_2) \cdot \\ &\cdot E_2^*(t + \tau - t_2) \underbrace{\left\langle -\frac{i}{\hbar} [\alpha(t_2), \alpha(0)] \rho_g \right\rangle}_{\chi_{\alpha\alpha}(t_2)}, \end{aligned} \quad (3.54)$$

where  $\chi_{\alpha\alpha}$  is the linear response function associated to the polarizability.

The measured signal can be calculated by performing the modulus square of the polarization and then integrating over time t

$$I_{RS} = \int_{-\infty}^{+\infty} dt |E_3(t)|^2 \left| \int_0^{+\infty} dt_2 e^{i(\omega_1 - \omega_2)t_2} E_1(t + \tau - t_2) E_2^*(t + \tau - t_2) \chi_{\alpha\alpha}(t_2) \right|^2. \quad (3.55)$$

Off-resonant Raman Scattering is due to the dependence of the electronic polarizability on the nuclear coordinates ( $\alpha(\mathbf{q})$ ), which is totally contained in the term  $\chi_{\alpha\alpha}$ . The dependence is usually weak (but not completely negligible, as of resonant excitations), so one can expand  $\alpha(\mathbf{q})$  around some equilibrium positions  $\mathbf{q}_0$ :

$$\alpha(\mathbf{q}) = \alpha(\mathbf{q}_0) + \sum_j k_j q_j + \dots, \quad (3.56)$$

where  $k_j \equiv \frac{\partial \alpha}{\partial q_j}$  evaluated in  $\mathbf{q}_0$ . The previous expansion is usually justified for phonons in crystals, since the relevant values of the positions are confined

in a small region close to the equilibrium ones. If we truncate the expansion to linear order in  $\mathbf{q}$ , we get

$$\chi_{\alpha\alpha}(t) = -\frac{i}{\hbar} \sum_j k_j^2 \langle [q_j(t), q_j(0)] \rho_g \rangle \quad (3.57)$$

with

$$q_j(t_2) \equiv e^{\frac{i}{\hbar} H_g t_2} q_j e^{-\frac{i}{\hbar} H_g t_2} \quad (3.58)$$

(note that the zeroth order of the expansion does not contribute, since it is a number and commutes with all operators).

From relation (3.45) we notice that this result is connected to the harmonic Brownian oscillator through the relation

$$\chi_{\alpha\alpha}(t) = \frac{2}{\hbar} \sum_j k_j^2 C_j''(t) \quad (3.59)$$

### 3.4.1 Impulsive Raman Scattering

Impulsive pulses (of the order of femtoseconds) have a sufficiently broad bandwidth to excite high frequency vibrations coherently. Let us first take  $E_1$  and  $E_2$  to have identical envelopes  $E_p$  and the same frequency; the third order polarization becomes

$$P^{(3)}(\mathbf{k}_s, t, \tau) = -E_3(t) \int_0^{+\infty} dt_2 |E_p(t + \tau - t_2)|^2 \chi_{\alpha\alpha}(t_2). \quad (3.60)$$

If both the pump and the probe pulses are impulsive, they can be approximated by a Dirac delta and one obtains

$$\begin{aligned} P_{IRS} &= -E_3(t) \int_0^{+\infty} |\delta(t + \tau - t_2)|^2 \chi_{\alpha\alpha}(t_2) = -E_3(t) \chi_{\alpha\alpha}(t + \tau) \\ I_{IRS} &= \int_{-\infty}^{+\infty} \underbrace{|E_3(t)|^2}_{\delta(t)} \left| \frac{1}{2\pi} \int_{-\infty}^{+\infty} d\omega e^{-i\omega(t+\tau)} \chi_{\alpha\alpha}(\omega) \right|^2 \\ &= \left| \frac{1}{2\pi} \int_{-\infty}^{+\infty} d\omega e^{-i\omega\tau} \chi_{\alpha\alpha}(\omega) \right|^2 = |\chi_{\alpha\alpha}(t)|^2, \end{aligned} \quad (3.61)$$

where  $\chi_{\alpha\alpha}(\omega)$  is the Fourier transform of the linear response function associated to the polarizability.

Inserting the expression of the linear response function associated to the polarizability (3.59) in (3.61) and keeping in mind the relation that connects the coefficients  $C_j''$  of the Cumulant expansion with the field frequency (in absence of friction) (3.47), one notice that the scattered field has the same Fourier components of the excited Raman active modes of the medium, and

$$I_{IRS} \approx \left[ \sum_j \frac{1}{m_j \omega_j} \sin(\omega_j t) \right]^2. \quad (3.62)$$

Note that low frequency modes are more visible than high frequency ones, since the amplitude of the single mode contribution is proportional to  $\omega_j^{-1}$ .

The previous result is based on the implicit assumption of a perfect homodyne configuration, in which the initial probe beam is totally extinguished; a more realistic treatment would consider a coupling between the emitted field and the probe, in heterodyne configuration (3.2.1). In this case the measured field is the sum of the emitted field (which is very weak) and the initial probe, which acts as local oscillator:

$$P_{TOT} = -E_3(t)\chi_{\alpha\alpha}(t + \tau) + AE_3(t)e^{i\omega_3 t}, \quad (3.63)$$

(where A is a dimensional constant) and, inserting the previous equation in 3.61,

$$I_{IRS} = \int_{-\infty}^{+\infty} dt \underbrace{|E_3(t)|^2}_{\delta(t)} \left\{ \left| \frac{1}{2\pi} \int_{-\infty}^{+\infty} d\omega e^{-i\omega(t+\tau)} \chi_{\alpha\alpha}(\omega) \right|^2 + \underbrace{|Ae^{i\omega_3 t}|^2}_{A^2} + 2A\Re e \left[ \frac{1}{2\pi} \int_{-\infty}^{+\infty} d\omega e^{-i\omega(t+\tau)} \chi_{\alpha\alpha}(\omega) e^{i\omega_3 t} \right] \right\}. \quad (3.64)$$

Under the action of the Dirac delta and because of relation (3.47), the previous equation becomes

$$I_{IRS} \approx A^2 + \left[ \sum_j \frac{1}{m_j \omega_j} \sin(\omega_j t) \right]^2 + 2A \sum_j \frac{1}{m_j \omega_j} \sin(\omega_j t), \quad (3.65)$$

where the only relevant term is the last one, since the second is much smaller and the first is constant. Therefore performing this kind of measure we will

obtain an intensity which is essentially the sum of signals that oscillates with the same frequency of the Raman active modes in the material. In our case, as we will see in chapter 5, just one mode is visible and the output signal is exactly a sine wave.



## Chapter 4

# Experimental apparatus

As already anticipated the scope of this work is to combine different techniques: the pump-probe Raman spectroscopy and quantum tomography. The latter is commonly used to study the quantum state of light in quantum optics laboratories. Our aim is to study the quantum state of ultrashort probe pulses after they have interacted with a photoexcited material. To this purpose we combine the two techniques of pump and probe and tomographic reconstruction of the light quantum state. In this chapter I will describe the set-ups we used both for "simple" time domain Raman scattering experiments and for time-resolved tomography.

### 4.1 Experimental set-up

In this work several kinds of measurements on the sample ( $\alpha$ -quartz) have been performed. In the present section I will describe the different experimental set-ups. The main structure for the pump and probe setup is depicted in Figure (4.1).

The laser source produces ultrashort pulses with wavelength  $\lambda = 800$  nm and repetition rate 250 KHz. The beam is divided by a beam splitter (BS) in a pump and a probe beam. The probe is then reflected by some mirrors, impinges on the sample and is finally detected. The pump is also deflected to impinge on the sample, but two of the mirrors along its path are positioned

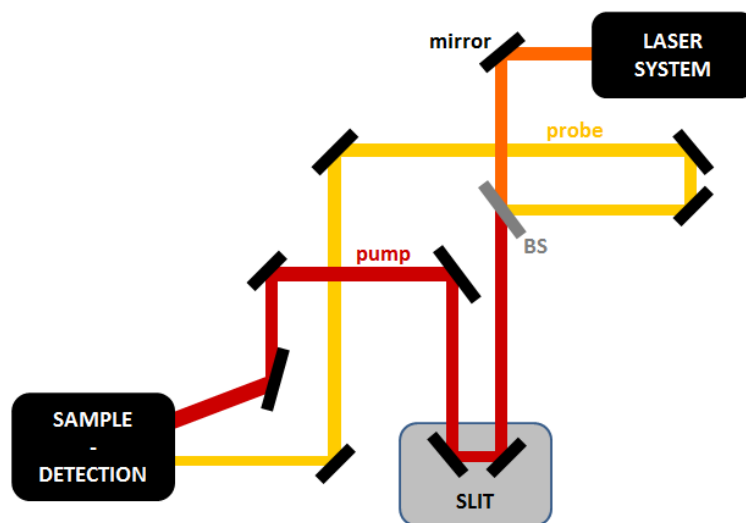


Figure 4.1: Simplified scheme of the experimental set-up of the time resolved measurement.

on a mechanical translator stage used to change the time delay between the pump and the probe. The optical paths of the two beams are chosen to have the same length for a translator position close to the center one. Filters, half-wave plates and polarizers are put along the beams paths to control their intensity and polarization.

In order to measure different observables in the same excitation conditions, variations in the last part of the set-up (represented as the box *sample-detection* in Figure 4.1) should be performed. In details we made “Standard” time domain Stimulated Raman Scattering spectroscopy measurements, a sort of noise measurement (with the same set-up of the Balance Homodyne Detection, but without the local oscillator) and time resolved BHD. The three set-ups are now presented.

#### 4.1.1 Standard time domain Raman measurements

In the first kind of measurements a "simple" time domain Raman spectroscopy is performed: the pump pulse excites optical vibrations in the sample that are detected by the probe pulse. Both the pump and the probe are focused on the sample by a lens and after the interaction a second lens collimates the

transmitted beam. The pulse passes through a polarizer in order to select the emitted field (as described in section 6.1.2) and finally reaches the photodiode and the detector. We made two kinds of Raman measurements which mainly differ for the detection system.

- In the first measurement (Figure 4.2) the output of the photodiode is sent to a *lock-in amplifier*, which measure the AC component of a signal integrated over different subsequent pulses. That's why in this measurement the signal is modulated by using a mechanical chopper (whose output is sent to the lock-in, in order to select the correct frequency) in the pump path. The result of the experiment is the intensity of the transmitted probe as a function of the delay between the pump and probe <sup>1</sup>.

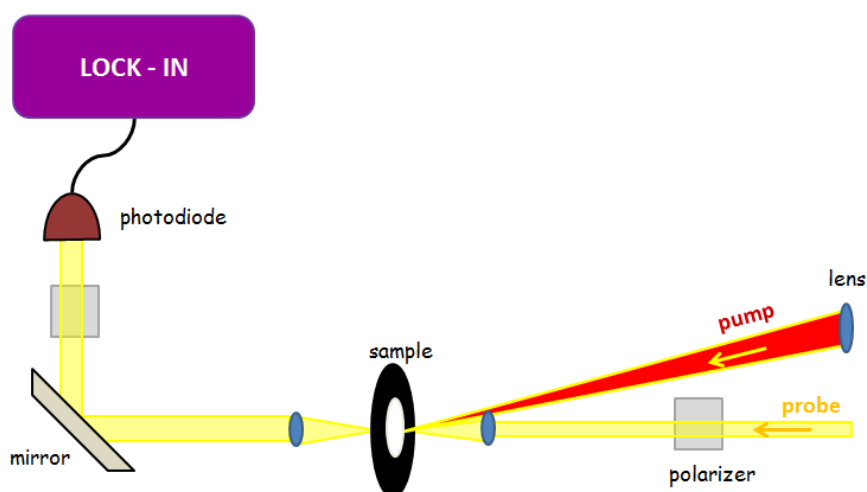


Figure 4.2: Simplified scheme of the experimental set-up of the Raman measurement with lock-in amplifier.

<sup>1</sup>It is important to note that in this configuration the response is integrated over a large number of pulses determined by the lock-in acquisition times (typically we used acquisition times of 100 ms, corresponding to 25000 pulses). This configuration allows for a very precise measurement of the mean photon number transmitted by the sample as a function of the pump-probe delay, but doesn't allow for the measurements of intrinsic noise due to pulse to pulse intensity fluctuation.

- In the second measurement (Figure 4.3) the noise is eliminated first of all by making the subtraction between the transmitted signal and a reference one (the probe before the interaction). For this reason a beam splitter (BS) is put before the sample and the intensities of the two beams are finally subtracted by a balanced amplified differential detector. Two wedged plates are put in the path of the reference signal to balance it with the transmitted field one. A *fast digitizer* allows to acquire hundreds of pulses: a software can then average their intensities (eliminating the noise contribution), but also calculate the variance and higher momenta, in order to make also a statistical analysis.

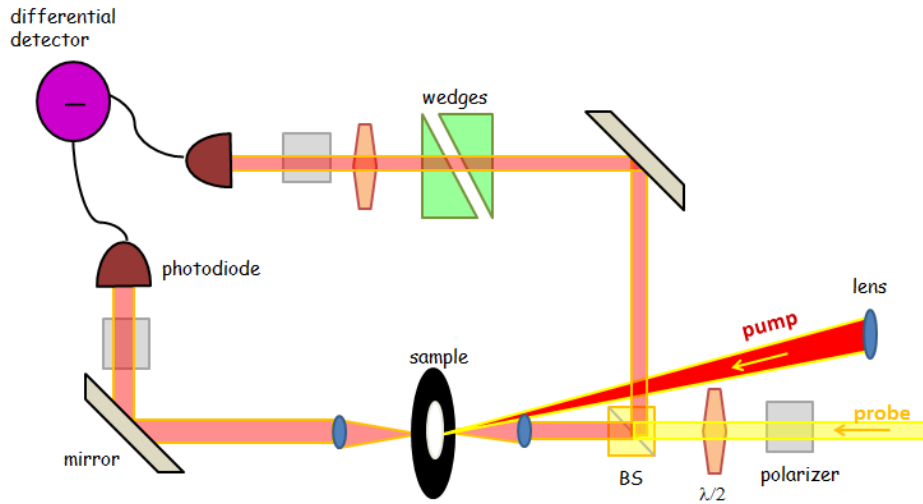


Figure 4.3: Simplified scheme of the experimental set-up of the Raman measurement with differential detector and reference beam. In the figure BS is a beam splitter, while  $\lambda/2$  is a half wave plate, used to tune the probe power of both the branches

### 4.1.2 Homodyne detection without local oscillator

In order to measure the shot noise of the transmitted light pulses we made use of a sort of Homodyne detection without local oscillator (Figure 4.4). The scheme is similar to the first we have analyzed, but in this case after the sample and the polarizer there is a non-polarizing beam splitter which divides the beam in two with same intensity (the last two polarizers and half wave plates ensure the balance between them). A balanced differential detector measures the difference between the intensity of every couple of pulses and the data are acquired by a fast digitizer as in the previous case.

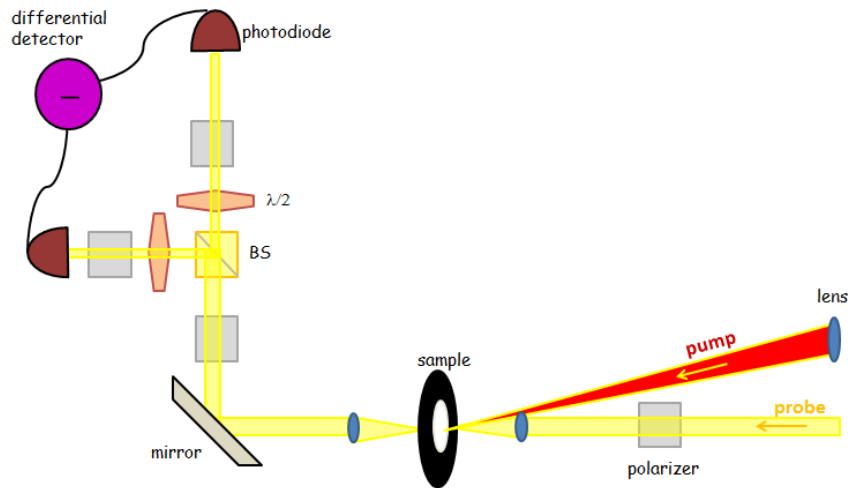


Figure 4.4: Simplified scheme of the experimental set-up of the "Homodyne detection without local oscillator".

### 4.1.3 Time resolved homodyne detection

The last measurements we made are time-resolved balanced homodyne detection (section 2.3) in which the signal passes through the sample previously excited by the pump pulse (Figure 4.5). The phase difference between the signal and the local oscillator (LO) is provided by a mirror put on a piezoelectric translator, that slightly modifies the path of the LO. The wedge plates balance the paths of the two branches; one of them is mounted on a slit that allows to vary in a quite precise way the optical path of the local oscillator, so that the two beams interfere on the beam splitter. The differential detector measures the difference between the intensity of the two new pulses. The result of this measurement is the value of the quadrature  $\langle \hat{x}_\phi \rangle$  both as a function of the phase difference  $\phi$  provided by the piezoelectric translator and the time delay between the pump and the probe, experimentally due to the motion of the slit. As in the previous cases many pulses are analyzed in order to get average, variance and higher momenta.

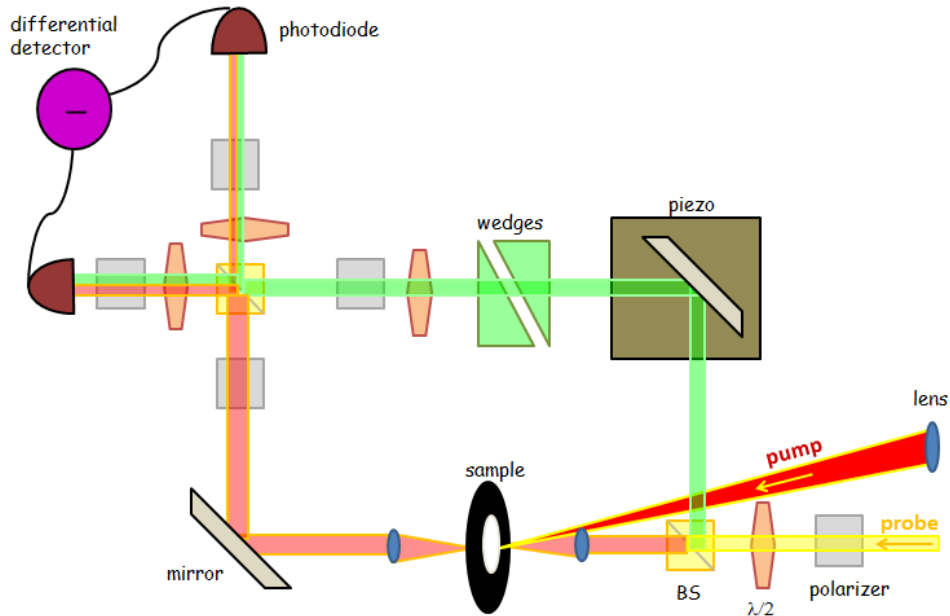


Figure 4.5: Simplified scheme of the experimental set-up of the time resolved BHD. In the figure BS represents a beam splitter, while  $\lambda/2$  is a half wave plate

## 4.2 Instrumentation

In this section I will give more details about some instruments and parts of the set-ups previously described. In particular I will focus on the differential detector and the digitizer <sup>2</sup>.

### 4.2.1 Balanced Differential Detector

As already anticipated we need a balanced amplified differential photodetector, which is able to measure the difference between the photocurrents (proportional to the intensities of the signals) provided by two photodiodes. Since the detector is amplified its response is proportional to the quantity we want to measure.

In quantum optics experiments low-noise conditions are very important and therefore the detector must have some characteristics and in particular high shot-to-electronic noise ratio (that is low electronic noise; this feature is relevant also for common time resolved measurement as we shall see later). For the first measurements we used a commercial detector (*Thorlabs PDB430A*); however it did not completely satisfy our noise requests and so we finally decided to use a "home-made" detector, based on the work of H. Hansen [15]. We have made some tests on the detector in order to verify its adequacy to our measurements (see section 2.2.3).

1. First of all we deal with pulses of about 80 fs with repetition rate 250 KHz, which means a pulse every 4  $\mu s$ . The electronics of the detector should be fast enough to separate the signals coming from different laser pulses, that means that the duration of the response of the detector should be shorter than 4  $\mu s$ ; this condition is fulfilled, since the response length is about 1  $\mu s$  as one can see in Figure (4.6).
2. The second test deals with the characterization of the two photodiodes independently: we expect that their output voltage is proportional to

---

<sup>2</sup>The laser system is described in appendix B.3. In order to understand the following sections it is sufficient to know that it is a pulsed laser source and its output beam has  $\lambda = 800$  nm, with spectral width  $\sim 30$  nm, repetition rate of 250 KHz and about 1.5 W mean power.

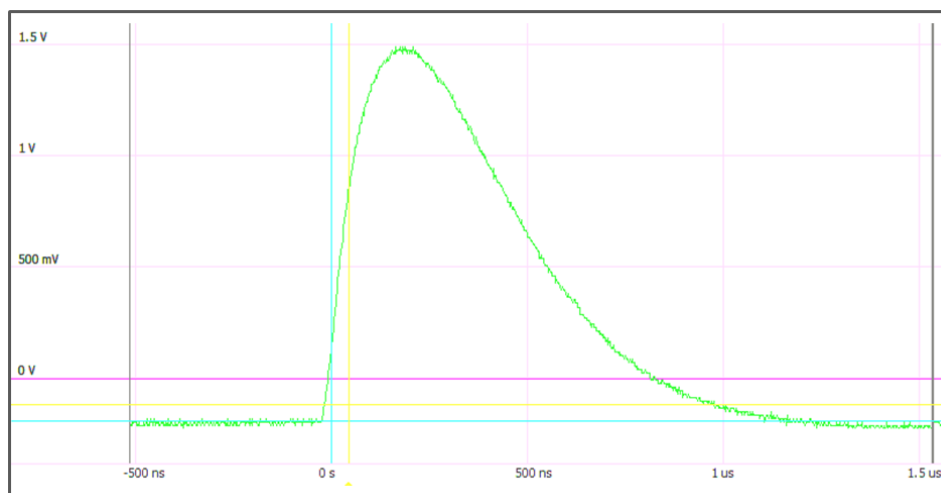


Figure 4.6: Detector response of a single laser pulse of  $\sim 100$  fs. In order to analyze the detector response just one diode measurements have been performed.

the intensity we want to measure, but this property should be verified. Therefore we keep the photodiodes open one at a time and measure the output voltage as a function of the local oscillator intensity (the signal beam is blocked during the measurement). The result is reported in Figure 4.7. One can immediately note that until  $6 \cdot 10^4$  photons per pulse the diodes present a linear behavior. For higher intensities of the local oscillator the diodes saturate: this effect is immediately visible, since the detector response results deformed (Figure 4.8)

3. The previous points describe just preliminary analyses, which ensure the validity of the measurements, but the scope of the new detector is a high shot-to-electronic noise ratio, which we will now consider. The electronic noise is a detector feature and does not depend on the signal, while the shot noise is determined by the quantum nature of light and is the quantity we want to measure. Its dependence on the intensity of the signal can be easily calculated for a coherent state. The shot noise can be defined as the variance ( $var(A) = \langle A^2 \rangle - \langle A \rangle^2$ ) of the number operator  $\hat{n} = \hat{a}^\dagger \hat{a}$ . Keeping in mind the definition of coherent state (1.15), the relation (1.16) and the commutation rule  $[\hat{a}, \hat{a}^\dagger] = 1$ ,

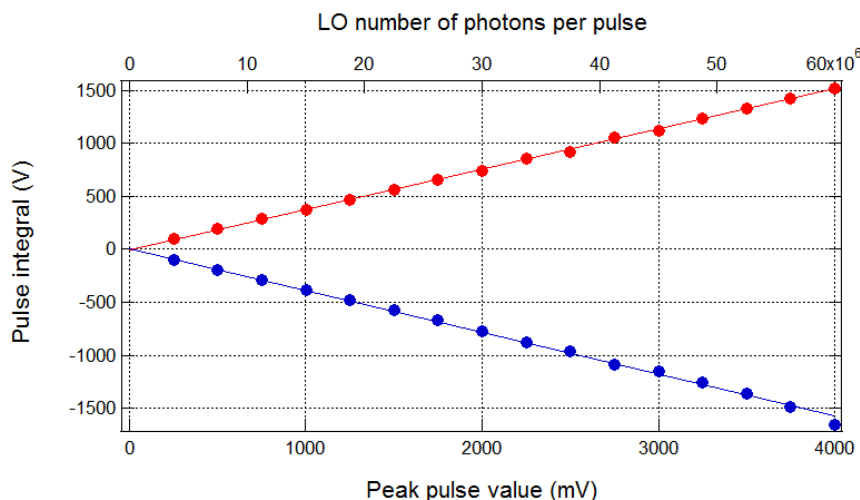


Figure 4.7: Integral of the detector output over the pulse region as function of the local oscillator intensity. The signal has been blocked.

one gets  $\text{var}(\hat{n}) = \langle \hat{n} \rangle$ . Since the current output of the photodiodes is proportional to the intensity of the signal,  $\hat{I} = c\hat{n}$  (where  $c$  is a constant) and therefore

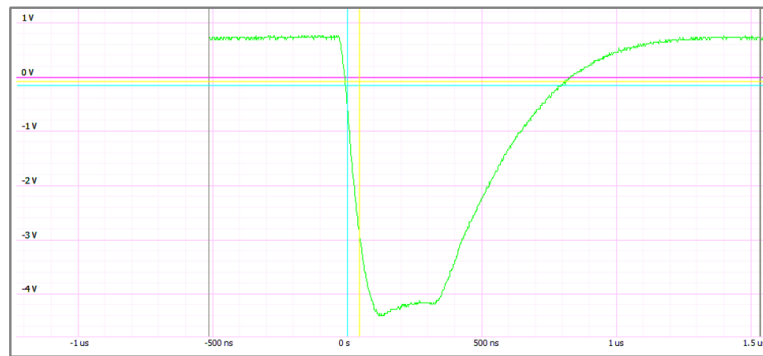
$$\text{var}(\hat{I}) = c^2 \text{var}(\hat{n}) = c^2 \langle \hat{n} \rangle = c \langle \hat{I} \rangle. \quad (4.1)$$

The shot noise scales linearly with the intensity of the beam impinging on the photodiode and is distinguishable from the electronic noise.

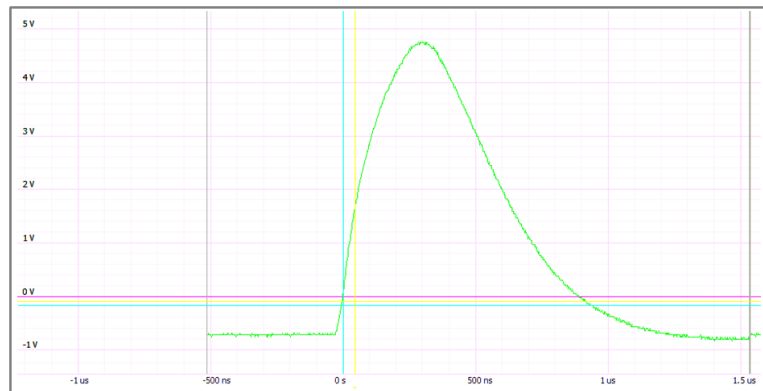
In order to compare the two noises we measured a set of pulses (with both the photodiodes) and computed the variance of their time integral (Figure 4.9). The linear dependence on the intensity represents the shot noise, while the contribution to the noise when the intensity tends to zero is due only to the detector (electronic noise).

For relative high intensities the noise has higher order contribution, so we can perform measurements with maximum intensity corresponding to about 1.5 V peak output ( $\sim 1.5 \cdot 10^7$  photon per pulse). At this intensity value the shot-to-electric noise ratio is 8.3 dB (to be compared with 2 dB of the commercial detector).

Another quantity that allows to test the sensibility of the detector is the so called *efficiency* (see section 2.2.3), which is the ratio between



(a)



(b)

Figure 4.8: Single diode response for high intensities of the probe: the pulse is deformed with respect to low intensities (in Figure 4.6).

the shot and the total noise at a specific intensity of the beam. The measured efficiency for our detector is 0.88.

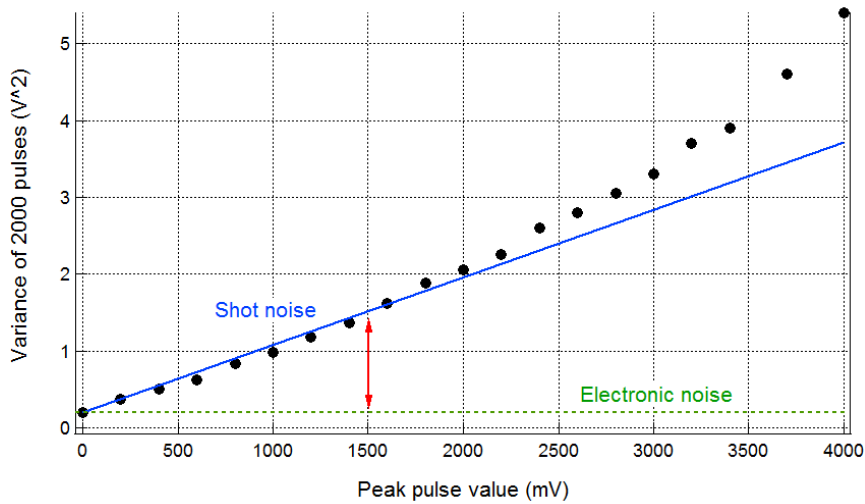


Figure 4.9: Variance of the time integral of 2000 acquired pulses. Different noise contribution are visible: constant electronic noise (green), shot noise, which depends linearly on the intensity, and higher order contributions for intensities higher than 1.5 V.

#### 4.2.2 The fast digitizer

Once the balanced differential detector has subtracted and amplified the two input signals, the output voltage is sent to a fast 8-bit ADC, which has a sampling rate of 1 GSample/s, that means that it can acquire up to one difference current value every nanosecond.

The ADC is mounted on a 500 MByte memory board, with a specific option called *Multiple Recording*; it allows to acquire only for a limited time, in order to limit the data to collect. In our case, for example, the laser repetition rate is 250 KHz, that means a pulse every 4  $\mu$ s. Nevertheless the response of the detector lasts about 1  $\mu$ s; the other 3  $\mu$ s are not useful for our purpose and so can be discarded. This selection is possible by choosing an appropriate trigger and "duration" of the acquisition after the trigger itself. The Multiple Recording is sketched on Figure (4.10).

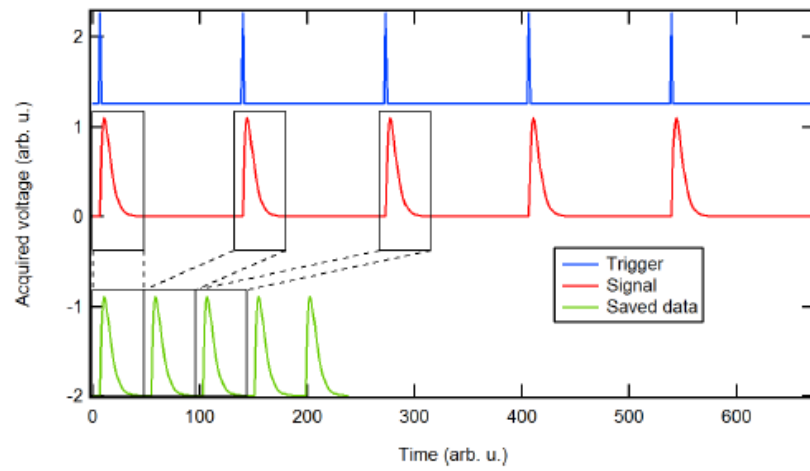


Figure 4.10: Multiple recording acquisition: only a defined time interval (which contains the relevant data) of the signal is saved. The beginning of the acquisition is determined by a trigger [16].

## Chapter 5

# Experimental results

In this chapter I will show the experimental results; as in the previous chapter they will be divided in three kinds of measurements: time domain Raman Spectroscopy (both detected by a lock-in amplifier and a fast digitizer), Homodyne detection without local oscillator and time resolved Balanced Homodyne Detection.

### 5.1 Standard time domain Raman Spectroscopy

The first measurement is a "typical" time resolved Impulsive Stimulated Raman Spectroscopy, in which phonons are excited in the medium by the pump pulse, while the probe detects the sample optical properties after the excitation. The result of the measure is the intensity of the emitted field as function of the time delay between the pump and the probe (provided mechanically by a slit). We expect to measure an oscillating field, whose frequency is the same of the excited vibrational mode. Raman active modes in  $\alpha$ -quartz are represented in Figure (6.1): since the dispersion of our mode-locked laser pulse is about  $\Delta\lambda = 30$  nm the maximum energy difference between the pump pulses 1 and 2 (so named in section 3.4), i.e. the maximum energy of the excited phonon, is about  $460$   $cm^{-1}$  and the signals related to high energy modes are less intense than the low energy ones (equation 3.62). Moreover, As described earlier, the polarizer after the sample selects only the contribution of only E-modes of  $\alpha$ -quartz.

### Lock-in

First measurements have been performed with a lock-in amplifier, as described in section (4.1.1). They represented preliminary measurements that allow us to find the "zero" of the pump probe, that is, the slit position for which the pump and the probe pulses impinge on the sample at the same instant. The other aim of these measurements was to find the polarizer rotation for which the probe contributions vanishes (in order to see only the emitted field one and select just Raman active E-modes).

A typical result of this measurement is shown in Figure (5.1): after the

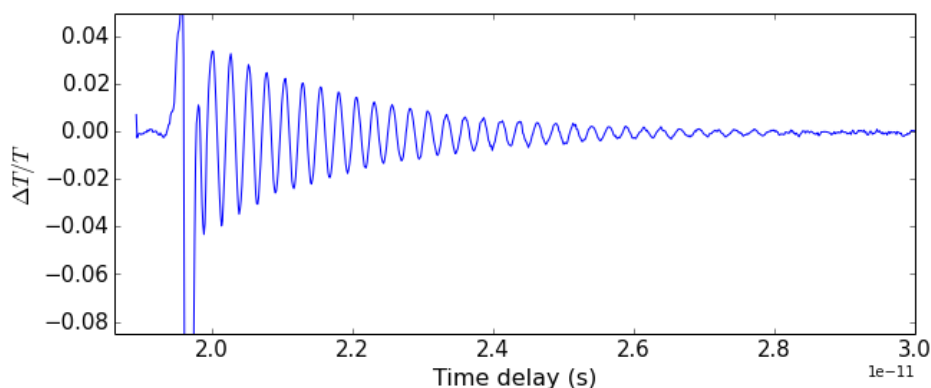


Figure 5.1: Emitted field in a standard time resolved Raman Scattering experiment. The most intense peak represents the time coincidence between the pump and the probe, while the following oscillations have the same frequency of the nuclear vibration due to the pump.

pump (the coincidence between the pump and the probe determines the peak) oscillations in the signal are visible. They are quite definite and the period of the oscillation can be directly measured. Anyway, in order to get more precise and complete information one can perform a Fourier analysis, which clearly provides the frequency components of the signal. The Fourier transform of the signal represented in Figure 5.1 is shown in Figure 5.2: only one peak at frequency  $\nu = 3.9$  THz is visible. It corresponds to a Raman active mode of  $\alpha$ -quartz (Figure (6.1)), and in particular a E-mode with wave number  $128 \text{ cm}^{-1}$ .

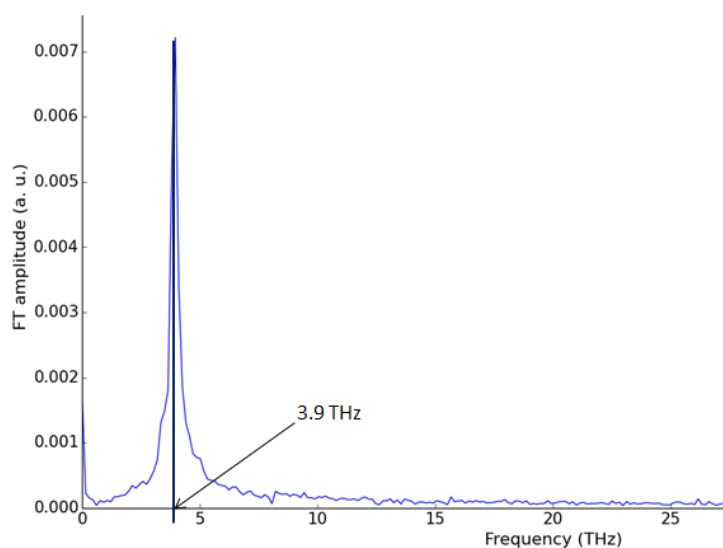


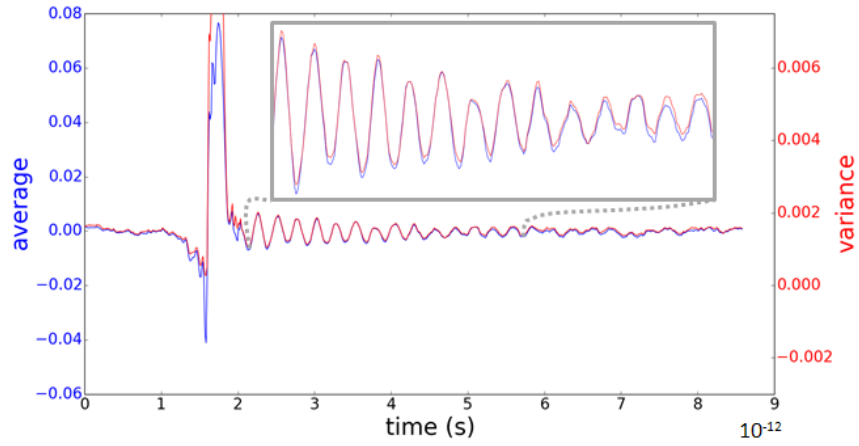
Figure 5.2: Fourier transform of the signal after the pump. Only one E-mode is evident at frequency 3.9 THz ( $128 \text{ cm}^{-1}$ ).

### Fast digitizer

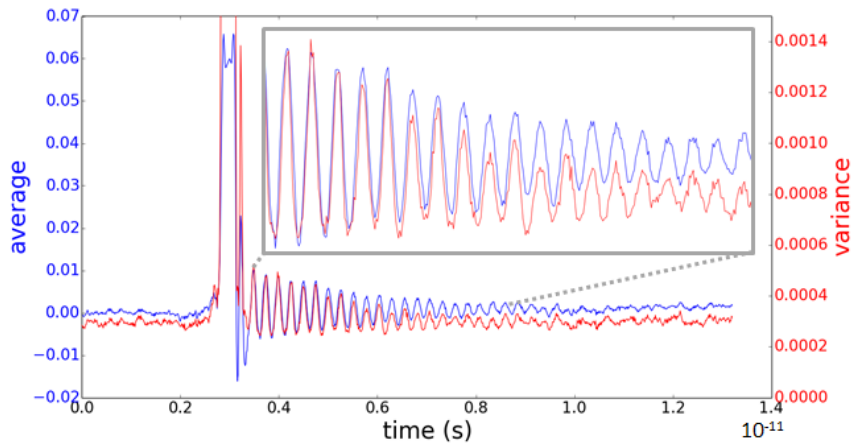
The same measurement can be performed with a different acquisition system: in particular we used a fast digitizer which allows to collect many values of the same quantity (referred of different pulses at the same time delay between the pump and the probe) in order to get not only the signal, but also a statistical analysis (Figure 4.3). We especially considered the mean signal and its variance. For the relevant cases we computed also the third and fourth momentum.

The analysis of the variance provides a useful contribution to the study of the quantum state of light, which is not accessible simply from the emitted field. As a matter of fact we expect the variance to have the same behavior of the signal, since the noise will be higher when also the field has greater values, but other frequency components can appear in this case. For example a peak at twice the frequency of the excited mode can be related to squeezing, as discussed in section (1.2).

The results are shown in figure (5.3): both the average signal and the variance are plotted. Observations on the mean are the same as for the



(a)



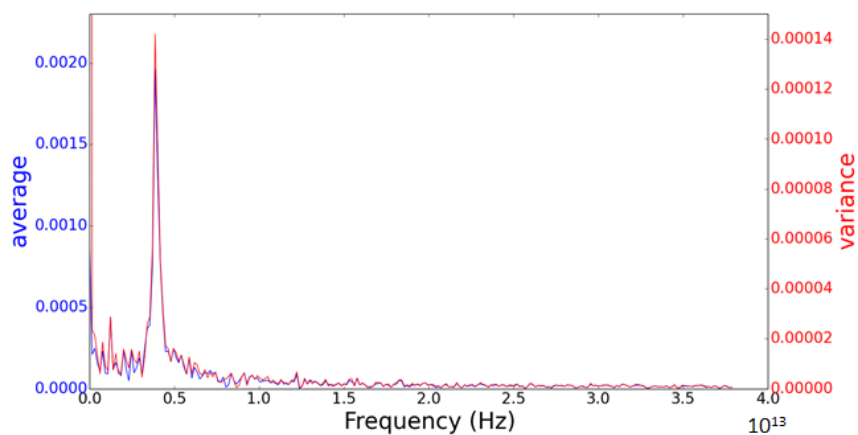
(b)

Figure 5.3: Average differential transmitted signal (blue) and variance (red) in two different measurements. In both cases the variance follows the oscillation of the average. The details of the measurements are: (a) pump power 680 mW, 4000 pulses per time delay, 100 scans of the slit; (b) pump power 620 mW, 4000 pulses per time delay, 50 scans of the slit

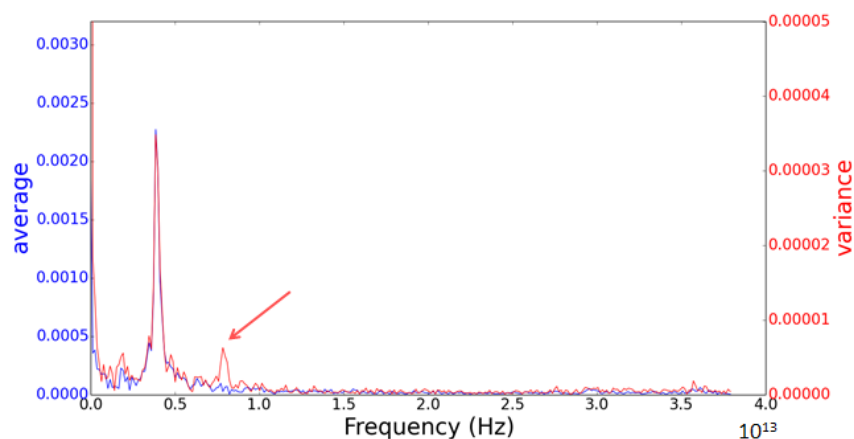
lock-in measurements: after the pump pulse, which is evident since produces the only high peak in the signal, quite regular oscillations, with defined period, can be seen. The same behavior characterizes the variance, which is in phase with the measured mean field. No significant difference between the two sets

of data is visible in time domain.

Nevertheless in Fourier space the two measurements give quite different results (Figure 5.4): in both cases one notices a strong frequency contribution at



(a)



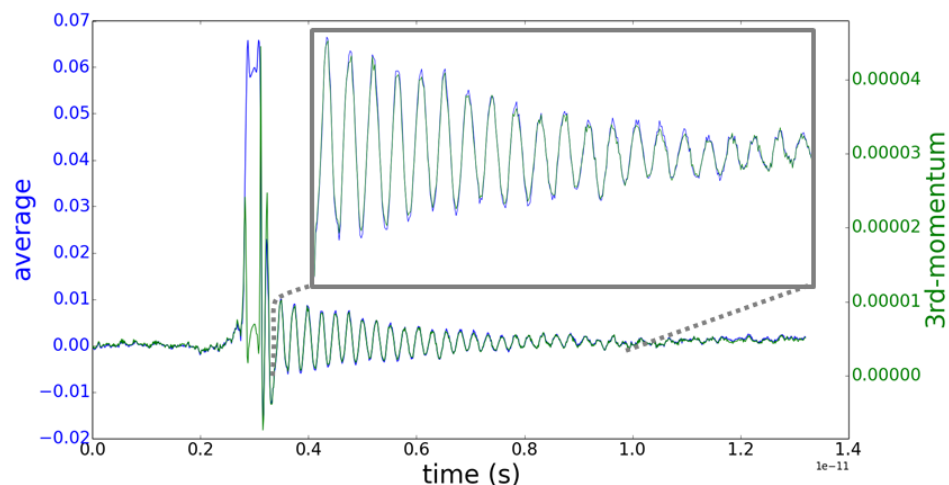
(b)

Figure 5.4: Fourier transforms of the signal reported in Figure (5.3). While the first measure (a) shows only a Fourier component at about 3.9 THz (which corresponds to a Raman active mode of  $\alpha$ -quartz) both in the signal and the average, in the second one (b) a peak at 7.84 THz in the variance is visible.

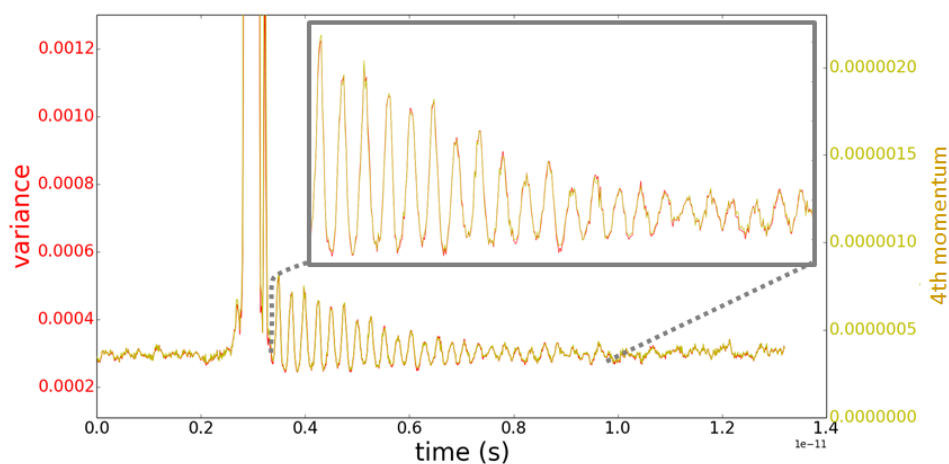
about 3.9 THz, both in the average (as we have already seen in the lock-in measurements) and the variance, but in Figure 5.4.b the variance shows

also a small peak at frequency 7.84 THz, which is about the double of the frequency of the E-mode we have already observed. As already anticipated it is probably related to the squeezing of the phonon mode (see chapter 6).

The major difference between the two measurements is in the noise level:



(a)



(b)

Figure 5.5: Comparison between (a) signal and  $3^{rd}$  momentum and (b) variance and  $4^{th}$  momentum as function of the time delay between the pump and the probe. In both graphics the two quantities have almost the same time dependence.

in the first case the noise is higher (about one order of magnitude larger, as one can see from the values of the variance) and so the oscillation at  $2\omega$  is hidden within the noise level and cannot be observed.

The acquisition of many pulses allows also to compute higher momenta, which should provide information on the symmetry and the "width" of the distribution of measured data near the expected values: in Figure 5.5 (a) and (b)  $3^{\text{rd}}$  and  $4^{\text{th}}$  momentum are compared with the signal and the variance respectively. We notice that higher momenta do not add information, since their time dependence is essentially proportional to lower momenta; this fact is confirmed also by their Fourier transform (Figure 5.6).

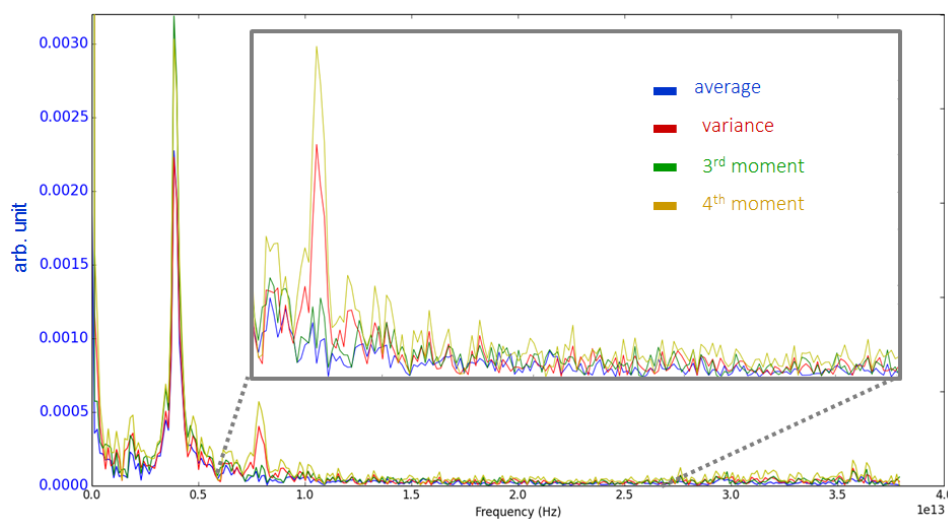


Figure 5.6: Fourier transforms of the four momenta represented in Figure (5.5): they confirm the similarity of momenta with the same parity.

For this reason, from now on only the contributions of the signal and of the variance will be shown.

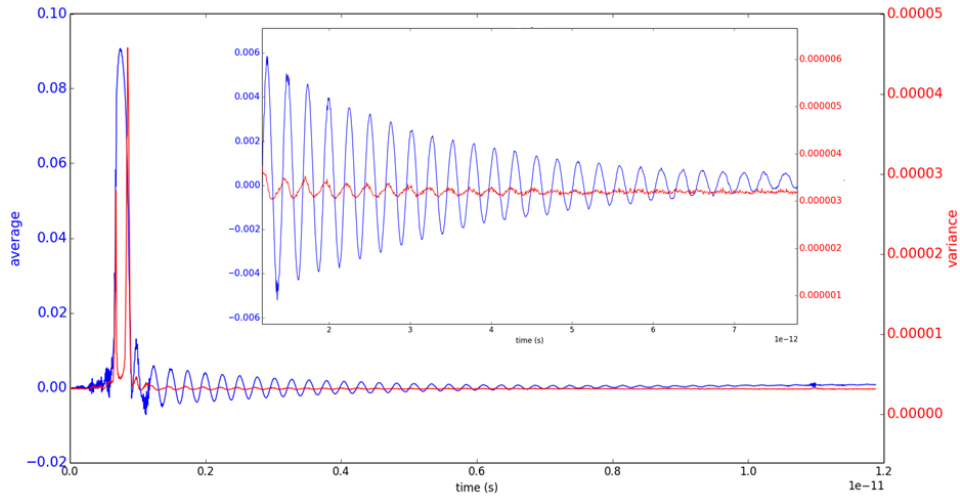
## 5.2 Homodyne detection without local oscillator

In order to consolidate the evidence of a squeezing of the phonon mode produced by photoexcitation in this condition we performed a measurements of the time evolution of the probe shot noise after the interaction with the sample. In the experimental configuration 4.4 the sample is excited by the pump and then the probe measures the variation of the optical properties of the medium, as in the previous case. After the sample and the polarizer a 50:50 beam splitter divides the beam and the intensities of the two branches are measured and subtracted by a differential detector (see Figure 4.4).

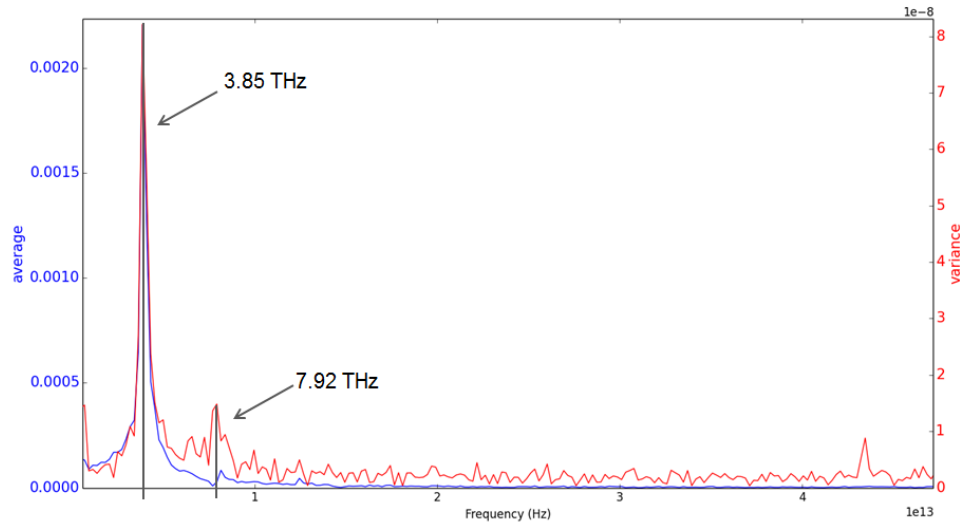
The result of the measurement is the difference of intensities as function of the time delay between pump and probe: in Figure 5.7 the data are shown. Also in this case after the pump (which causes the highest peak) the signal and its variance oscillate with the same frequency, as demonstrated by their Fourier transform (Figure 5.7 (b)), in which the usual frequency component (at about 3.9 THz) appears both in the average and in the variance. Also in this case the variance presents also a second Fourier component at about 7.9 THz. The difference with the results of the previous set-up is visible in time domain (Figure 5.7 (a)), where a difference in the phase of the two quantities is evident.

We still do not know the causes of these results, since we would expect a zero mean value for this measure (one can prove it through the homodyne detection theory 2.18 inserting a vacuum state  $|0\rangle$  as local oscillator). Oscillations in the average are probably due to the unbalance of the two beam branches which enter the detector, but even in this case there is no apparent explanation for the phase shift of the variance.

5.2. Homodyne detection without local oscillator



(a)



(b)

Figure 5.7: Results of the measurement *Homodyne without local oscillator*: comparison (a) between the average signal and its variance, which underlines the phase difference in the oscillations after the pump and (b) between their Fourier transforms, which show the same frequency contribution.

### 5.3 Time dependent Balanced Homodyne Detection

Up to now we have made hypothesis about the quantum state of light just considering intensity measurements as function of the time delay between the pump and the probe and analyzing both the signal (i.e. the average oh hundreds of pulses for each time delay) and the variance. Our set-up (see Figure 4.5) allows to have much more complete information about the quantum state of light by combining time-resolved Raman spectroscopy and Balanced Homodyne Detection. The coupling of the two techniques provides the value of the quadrature  $x_\Phi$  as a function of both the phase difference  $\Phi$  between the emitted field and the local oscillator (determined by the piezoelectric translator) and of the time after the excitation. The result of the measurement is a two-dimensional image, since the quadrature depends on two variables: typical data are shown in Figure 5.8

We performed a preliminary analysis of the time evolution of the quadrature at a fixed phase difference (that is we considered a single horizontal line in Figure 5.8) and then for each time delay we analyzed the quadrature and reconstruct the Wigner function in order to get the quantum state of light after the interaction with the excited sample as function of time. Moreover, from the Wigner function one gets the expectation values of every observable of the system through relation 2.6.

#### 5.3.1 Fixed phase difference

Let us consider first of all the case of fixed phase difference, that is, let us select a line in the two-dimensional image (Figure 5.8).

From a first analysis we noticed that "structures" in the measure are more visible in the minimum of the quadrature value <sup>1</sup>.

Also in this case the coincidence between the pump and the probe is represented by the highest peak in time dependence and, as in the previous cases, we get one spike in frequency domain at  $\nu = 3.9$  THz, which is the usual Raman active E-mode.

---

<sup>1</sup>If we perform a measurement at a fixed position of the slit and we vary only the piezoelectric translator position we get a sine function, which, of course, presents periodic minima (see Figure 5.10). In Figure 5.8 the minimum is represented by the blue zone.

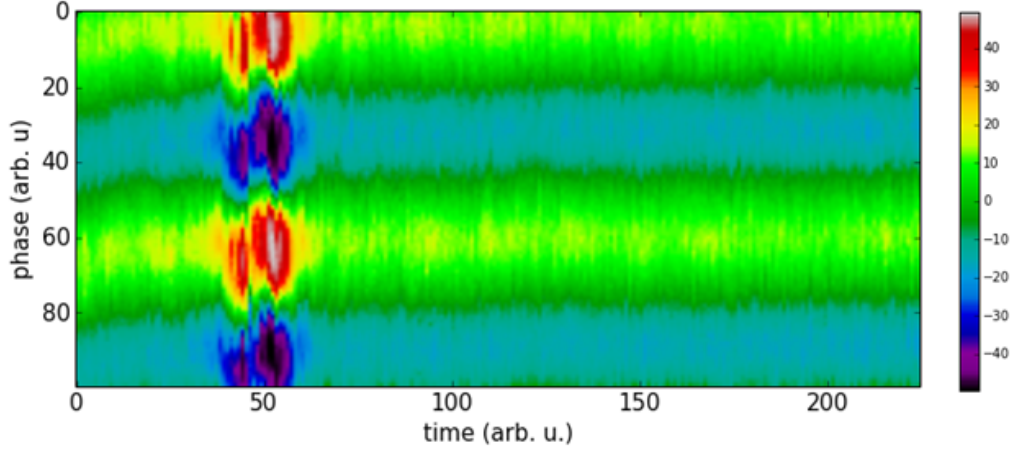
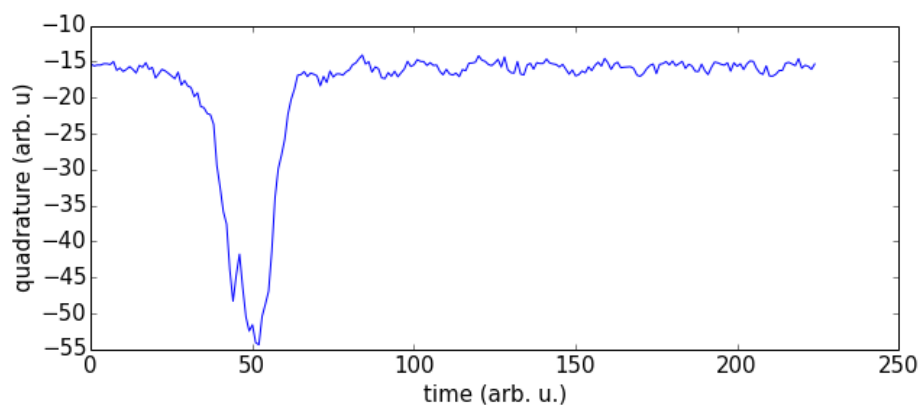
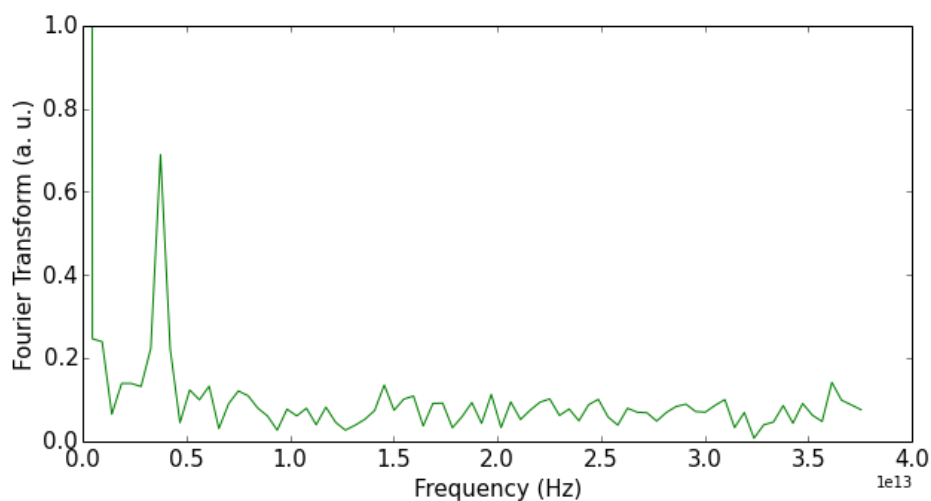


Figure 5.8: Image of the quadratures  $x_\phi$  as function of time and phase difference  $\Phi$  (both expressed as the number of steps of the slit and the piezoelectric translator respectively). The step of the slit is  $2 \mu m$ , which corresponds to a time delay of  $13.5 fs$ , while the piezoelectric translator one is of  $10 nm$ ; every point value is the average of 800 pulses. The powers of the pump and probe beams are respectively  $700 mW$  and  $2 \mu W$ , which corresponds to intensities of  $5.7 mJ/cm^2$  and  $45 nJ/cm^2$  per pulse respectively. The zone around  $time=50$  is due to the interaction of the pump with the sample. Every row in the figure represents the time dependence of the quadrature at a fixed phase, while the columns are the usual quadrature, which are function of the phase difference, and can be used to reconstruct the quantum state of light at a specific time delay.

Even if every value of the quadrature is the average of many pulses, a single measurement is not precise enough and so several scans in the same conditions have been performed; we have then computed the Fourier transform of the time dependent quadrature at the same phase difference and finally performed the average.



(a)



(b)

Figure 5.9: (a) Time dependent values of the quadrature  $x_\Phi$  at fixed phase difference between the signal and the local oscillator (remember that the step of the slit corresponds to a delay of 13.5 fs). One can observe that after the coincidence on the sample of the pump and the probe, these values are modulated by the excited phonons. The frequencies of the latter can be measured performing the Fourier transform of the signal (b), which underlines just one component at about 3.9 THz, as in the previous measurements.

### 5.3.2 Fixed time delay

Our set-up allows measure the field quadrature  $x_\Phi$  of the transmitted signal for every time delay between the pump and the probe (Figure 5.10).

For every phase difference 800 values have been collected, which are sta-

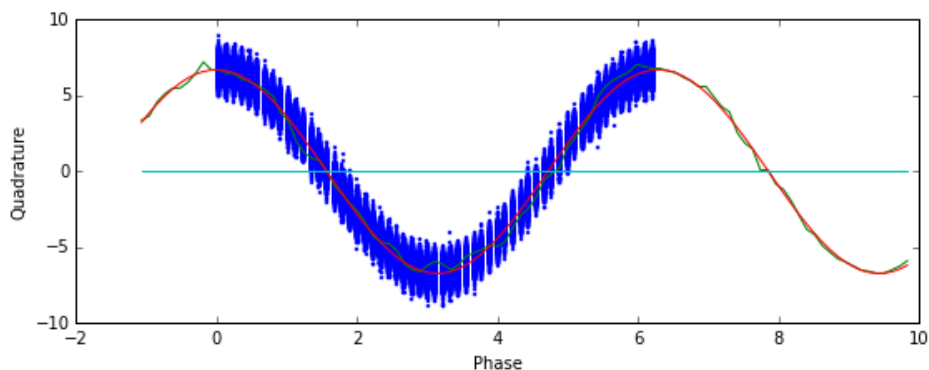


Figure 5.10: Quadrature of the measure represented in Figure 5.8. Every blue point represent the photocurrent generated by a single pulse. The green represents the mean values for each phase difference and the red one is a sine wave fit. Axis has been rescaled with the procedure described in this section.

tistically distributed around their mean value. In Figure 5.10 the average of the pulses is a sine wave, while its "thickness" is of course related to the variance. Subtracting the mean value for each phase difference to the corresponding quadrature value, one may observe also a modulation in the standard deviation (and so in the variance).

Notice that the values measured by the differential detector and the corresponding piezo positions should be rescaled in order to obtain the couple  $(x_\Phi, \Phi)$ . We already know that the value provided by the photodetector is a measurement of the differential photocurrent (see equation 2.18), which is proportional to the quadrature:

$$x_\Phi^M = \gamma x_\Phi, \quad (5.1)$$

where  $x_\Phi^M$  is the measured value at phase  $\Phi$ .

Our aim is the calculation of the coefficient  $\gamma$ : to obtain it we need some reference data, whose quadrature is known *a priori*.

Consider the quadrature of the vacuum state  $|0\rangle$ : its expectation value is zero for  $\Phi$ , since

$$x_\Phi = \langle \hat{x}_\Phi \rangle = \langle 0 | \frac{\hat{a}e^{-i\Phi} + \hat{a}^\dagger e^{i\Phi}}{\sqrt{2}} | 0 \rangle = 0, \quad (5.2)$$

but its variance is

$$\begin{aligned} \sigma_0^2 &= \langle \hat{x}_\Phi^2 \rangle - \underbrace{\langle \hat{x}_\Phi \rangle}_0^2 \\ &= \frac{1}{2} \left\{ \langle 0 | \hat{a}^2 e^{-2i\Phi} | 0 \rangle + \langle 0 | \hat{a}^{\dagger 2} e^{2i\Phi} | 0 \rangle + \langle 0 | \hat{a}^\dagger \hat{a} | 0 \rangle + \langle 0 | \hat{a} \hat{a}^\dagger | 0 \rangle \right\} \\ &= \frac{1}{2}. \end{aligned} \quad (5.3)$$

The previous equation demonstrates that the variance of a vacuum state is independent on the phase  $\Phi$  and is equal to  $\frac{1}{2}$ .

Therefore the measure of the quadrature of a vacuum state (obtained by blocking the signal and performing a BHD measurement) provides a set of data  $x_\Phi^0$ , such that

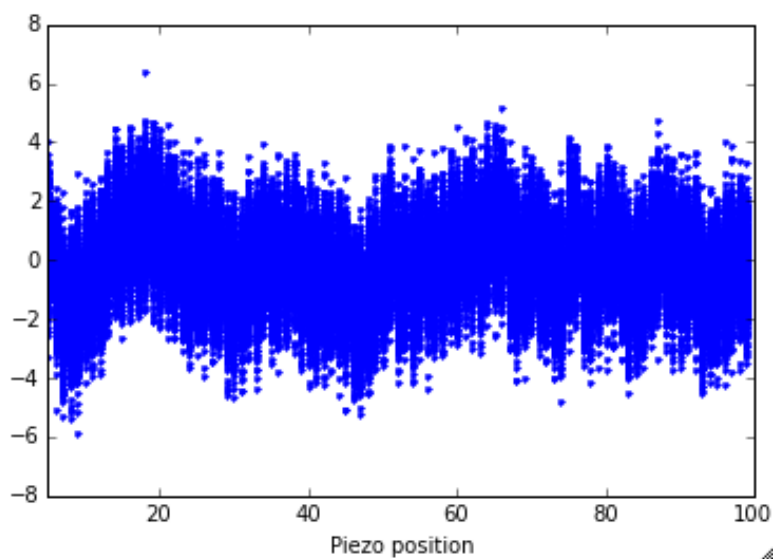
$$(\sigma_0^M)^2 = \gamma^2 \cdot \frac{1}{2} \implies \gamma = \sqrt{2 (\sigma_0^M)^2}, \quad (5.4)$$

where  $(\sigma_0^M)^2$  is the (constant, in principle) variance of the detected quadrature  $x_\Phi^M$ .

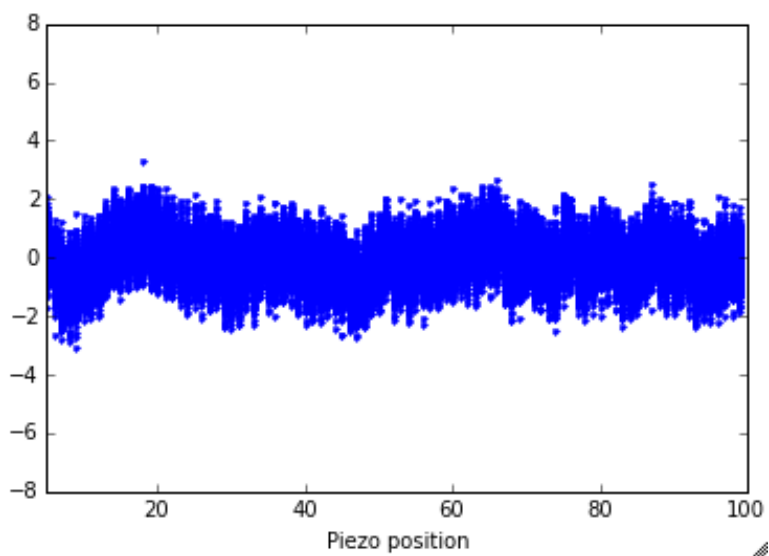
The previous treatment is based on the hypothesis of an ideal detection; on the contrary the efficiency of the detector affects the measurement. To take into account also the electronic noise contribution, one can compute another coefficient  $\gamma'$ , which is related to  $\gamma$  by the relation

$$\eta = \frac{A}{A+B} = \left( \frac{\gamma}{\gamma'} \right)^2, \quad (5.5)$$

where the efficiency  $\eta$  and coefficients  $A$  and  $B$  are defined in Figure 2.4 [13]. In order to rescale the axis of the phase difference  $\Phi$  one can perform a fit of the quadrature  $x_\Phi$  with the function  $f = A_0 + A \cos(\xi t + \Phi_0)$  where  $t$  represents the piezo position. From the obtained parameter one can subtract  $A_0$  to all the data and consider two consecutive points in which the fit function is equal to zero. In this way one gets  $\xi t_1 + \Phi_0 - \xi t_2 - \Phi_0 = \pi$ , from which derives the scaling factor  $\xi = \frac{\pi}{t_1 - t_2}$ . We have so obtained the rescaled values



(a)



(b)

Figure 5.11: Quadrature of a vacuum state: (a) data obtained by Balance Homodyne Detection; (b) rescaled data.

of the phase difference, the quadrature and its variance.

All these data (both mean quadratures and variances) enable the recon-

struction the Wigner function and so to completely characterize the quantum state of the signal at each time delay. In particular the quadrature distribution at each phase is connected to the marginals of the Wigner function and so to its "shape", while its mean value provides the position of the peak of the function in phase space. More details about the Wigner function reconstruction are given in Appendix E, while the results will be discussed in the next chapter.

## Chapter 6

# Discussion

The central task of my work has been to investigate the quantum nature of the vibrational states observed in time domain experiments. The approach taken is twofold. A full quantum state reconstruction of the probe pulses as a function of pump-probe delay has been experimentally achieved and realistic models to link the quantum fluctuations in the probe photon state to the intrinsic quantum fluctuations on the vibrational mode have been developed. The structure of this concluding chapter is representative of such an approach. We start by giving a description of Impulsive Stimulated Raman Scattering specific for the generation and detection of coherent phonon in quartz. Subsequently we address how the measurements of intrinsic fluctuation in the probe photon number could be related to non classical vibrational states in photoexcited matter. Finally, we show through a full quantum state reconstruction of the ultrashort probe pulses that the quantum state of the vibrational modes can be used to manipulate the probe quantum state.

### 6.1 Stimulated Raman Scattering on $\alpha$ -Quartz

Quartz is often used as a paradigmatic example for the generation of coherent phonons via Impulsive Stimulated Raman Scattering and it represents the ideal playground to test the coupling of the two techniques described above. In particular we used  $\alpha$ -quartz, that is the low-temperature (less than 848 K)

phase of quartz, which has trigonal structure and  $D_3$  symmetry (see Figure 6.2 (a)), with 9 atoms for unit cell [17].

### 6.1.1 Raman active modes

Group theory calculations shows that the 27 degrees of freedom (3 times the atoms for unit cell) are divided in 2 acoustic vibration with  $A_2$  and  $E$  symmetry and 16 optical vibrations:  $4A_1 + 4A_2 + 8E$ . We are interested in the latter, and in particular in the four totally symmetric modes  $A_1$  and 8 doubly degenerate modes of symmetry  $E$ .

In our experiment the sample is 1 mm thick and the front and back faces are

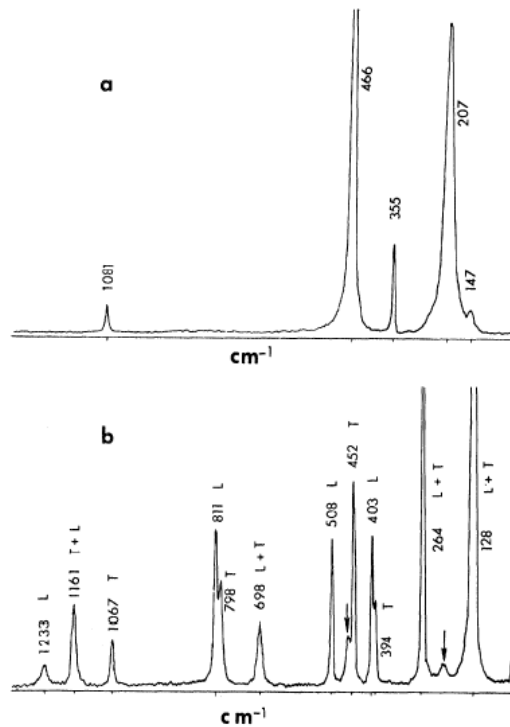


Figure 6.1: Raman spectra of  $\alpha$ -quartz at room temperature; the label L indicates Longitudinal modes, while T Transverse ones. In Figure (a)  $A_1$  modes are presented, while in Figure (b) one can see the  $E$  modes (the arrows point on intense  $A_1$  modes, visible also in the second spectrum by reason of imperfect alignment). [18]

orthogonal to the  $c$ -axis. In this way the laser propagates along the  $c$ -axis (in order to avoid complications arising from linear birefringence [19]) and the only accessible vibrational modes are those of a system with  $C_3$  symmetry (see Figure 6.2 (b) and (c)).

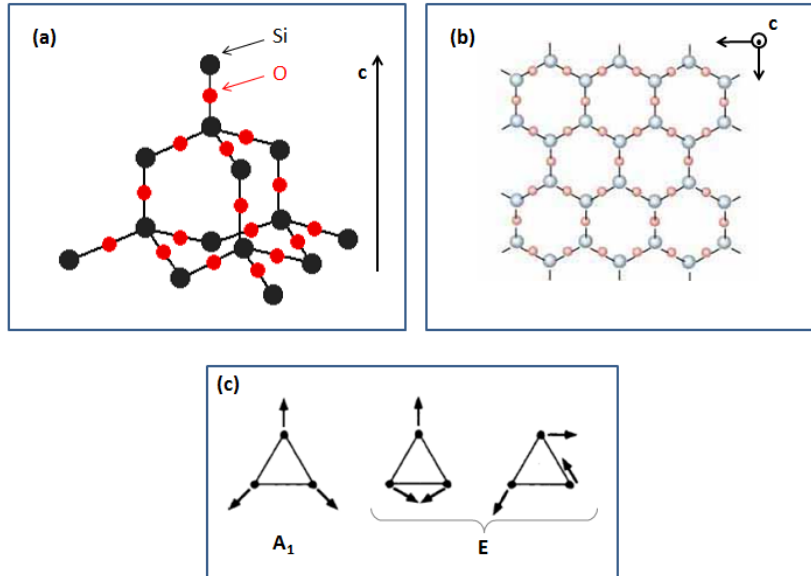


Figure 6.2: (a) Crystal structure of  $\alpha$ -quartz [20] and (b) its projection on the plane perpendicular to the  $c$ -axis [21]. (c) Normal mode vibrations for a  $C_3$  symmetry crystal or molecule [17].

### 6.1.2 The probing process

In Stimulated Raman Scattering Spectroscopy a first pulse impinges on the sample exciting vibrational states and a second one probes the process. As a consequence of the interaction between the probe and the sample after the excitation a new electric field is generated (as described in chapter 3): if the angle between the pump and the probe propagation directions is small this *emitted field* propagates in the direction of the probe wave vector and its modulus is given by equation (3.31).

In our case we have an intrinsic heterodyne configuration, since the probe acts as local oscillator too. This configuration allow us to amplify the emitted

field, as described in equation 3.32. In order to distinguish the contribution of the emitted field from that of the probe we exploit the Optical Kerr Effect, which acts on the polarization of the beams.

The  $i^{th}$  component of the third order polarization can be generally written as

$$P_i^{(3)}(z, \omega) \propto \sum_{j,k,l} \chi_{i,j,k,l}^{(3)} E_{1,j}(z, \omega_1) E_{2,k}(z, \omega_2) E_{3,l}(z, \omega_3), \quad (6.1)$$

where  $\chi_{i,j,k,l}^{(3)}$  is the four-rank susceptibility tensor and in our configuration it has three terms, reported in figure (6.3). The Stimulated Raman Scattering

$$\begin{array}{ccc} \begin{pmatrix} a & 0 & 0 \\ 0 & a & 0 \\ 0 & 0 & b \end{pmatrix} & \begin{pmatrix} c & 0 & 0 \\ 0 & -c & d \\ 0 & d & 0 \end{pmatrix} & \begin{pmatrix} 0 & -c & -d \\ -c & 0 & 0 \\ -d & 0 & 0 \end{pmatrix} \\ A\text{-mode} & E_T\text{-mode} & E_L\text{-mode} \end{array}$$

Figure 6.3: Susceptibility tensor components in our experimental configuration, one for each normal mode if  $\alpha$ -quartz. [19]

can be seen as a two step process: in the first one phonons are created from the pump photons, while in the second probe photons interact with the newly created phonons, producing the final scattered photons. The complete four-rank tensor is so given by  $\chi_{ijkl}^{(3)} = A_{ij}A_{kl} + E_{ij}^T E_{kl}^T + E_{ij}^L E_{kl}^L$ ; the result is represented in figure (6.4). In the previous representation the outer level

$$\left[ \begin{array}{cc} \begin{pmatrix} a^2 + c^2 & 0 \\ 0 & a^2 - c^2 \end{pmatrix} & \begin{pmatrix} 0 & c^2 \\ c^2 & 0 \end{pmatrix} \\ \begin{pmatrix} 0 & c^2 \\ c^2 & 0 \end{pmatrix} & \begin{pmatrix} a^2 - c^2 & 0 \\ 0 & a^2 + c^2 \end{pmatrix} \end{array} \right]$$

Figure 6.4: Complete four-rank susceptibility tensor [19].

rows and columns correspond to the analyzer and the probe polarizations and the inner ones to the pump polarizations [19]. Since in our case we have just one pump pulse, we consider only tensor elements for which  $j=k$ . The

most general expression for the polarization in this case is:

$$\begin{pmatrix} p_x \\ p_y \end{pmatrix} = \begin{pmatrix} c^2 \cos(\alpha - 2\beta) + a^2 \cos(\alpha) \\ -c^2 \cos(\alpha - 2\beta) + a^2 \cos(\alpha) \end{pmatrix}, \quad (6.2)$$

where  $\alpha$  is the angle of the probe and  $\beta$  of the pump (both above the x axis). If the probe pulse is vertically polarized ( $\alpha = 90^\circ$ ) and the pump has  $\beta = 45^\circ$  the emitted field is horizontally polarized: positioning a polarizer after the sample one can separate the emitted field from the probe (Figure 6.5 and (6.6)).

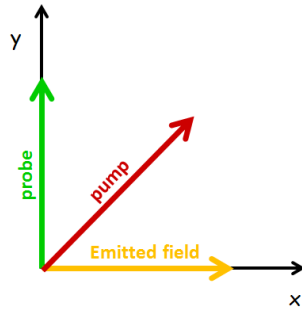


Figure 6.5: Polarization configuration: if the probe field is vertically polarized and the pump polarization form a  $45^\circ$  angle with the former, the emitted field is horizontally polarized.

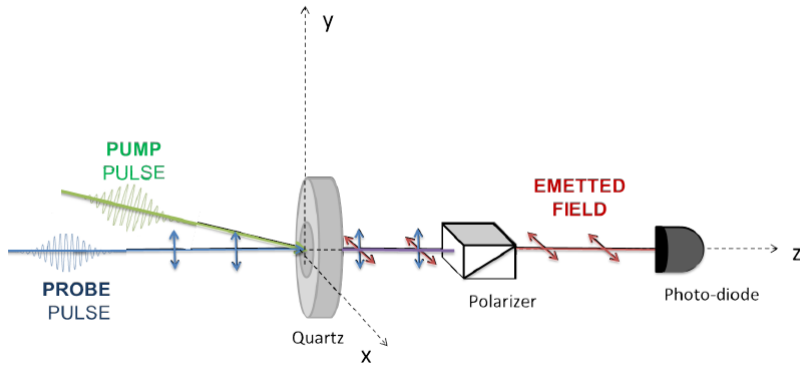


Figure 6.6: Our experimental configuration to detect the emitted field [17].

## 6.2 From the probe state to quantum fluctuation of the vibrational mode

### 6.2.1 Squeezing of the vibrational mode in photon number fluctuations

All measurements described in the previous chapters are implemented on the probe, which has interacted with the sample. The first ones (*Standard time resolved Raman Scattering*) provides the variation of the optical properties of the sample, as a consequence of the excitation of Raman modes due to the pump pulse, measured as modulation of the intensity of the signal. Thanks to the fast digitizer one can digitize hundreds of pulses for each time delay between the pump and the probe and get more information from the statistical analysis of the variance and higher momenta. The result of the transmittance measurement is predicted by semiclassical theories (such as four wave mixing, describe in chapter 3) and does not provide information on the quantum state of the probe. A preliminary information about it can be obtained by the Fourier analysis of the variance. As already anticipated a frequency component with twice the frequency of the oscillations of the emitted field is indicative of phonon squeezing. As schematized in Figure 6.7 the squeezed phonon mode has a variance in one of the quadratures which oscillates at twice the fundamental phonon frequency. It should be noticed that in our experiments we observe an oscillation at twice the phonon frequency in the fluctuation of the mean number of photons in the probe pulses as a function of the pump and probe delay. The central task of my work has been to investigate how the variance observed in the photon state could be representative of intrinsic quantum fluctuations on the state of the vibrational mode.

In order to better understand how the oscillation at double frequency of the variance is related to the squeezing of the vibrational mode we studied the amplitude of the double frequency component in the Fourier transform as a function of the intensity of the pump pulses. As described in section 1.2 it is expected that, while the generation of coherent vibrational states can

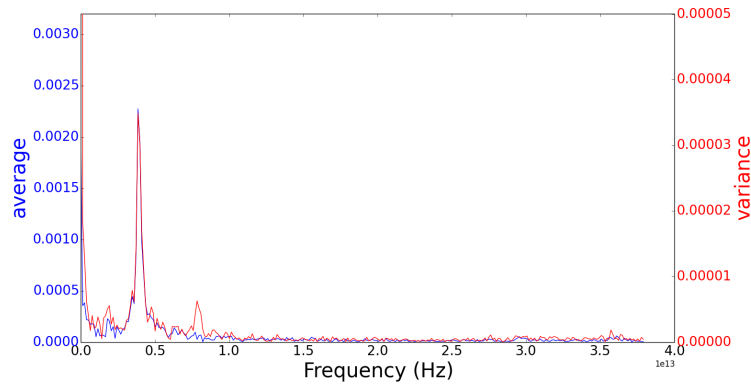
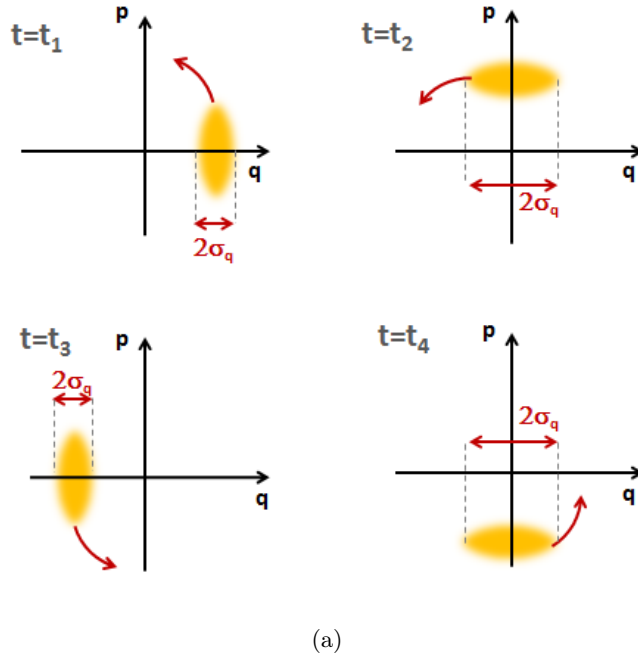


Figure 6.7: (a) Time evolution of a squeezed state due to a harmonic potential. The Wigner function rotates around the origin with a certain angular frequency  $\omega$ . The standard deviation, which can be seen as the projection on the axes of the width of the Wigner function, assume the same value twice during one period of the rotation, that is, varies with a frequency  $2\omega$ . An introduction to the time evolution of the Wigner function is treated in section 2.1.2. (b) Comparison between the Fourier transform of the signal and the variance. The peak at frequency  $2\omega$  is visible only in the latter.

be given by interaction terms which are linear in the phonon modes creation and annihilation operators ( $b^\dagger + b$ ), in order to obtain squeezing second order terms ( $(b^\dagger)^2 + b^2$ ) in the phonon latter operators are needed [22]. The results of such an analysis is given in Figure 6.8. We suppose the existence of a relation between the dependence of the Fourier component on the amplitude of the pump pulse and the squeezing of the phononic state. Future analyses will be made, in order to examine in depth this relation. An evidence of the squeezing in the phonon mode can be extracted by comparing the lifetime of the  $\omega$  ( $\sim 3.9$  THz) component of the oscillations in the variance with the  $2\omega$  one. In order to extract such information, we can multiply the signal with a gaussian function centered at a certain time delay and perform the Fourier transform of this product, in order to study the time evolution of the frequency components. The result is shown in Figure 6.9: one notice that while the component at the usual frequency  $\omega$  is visible at any time and decreases slowly in intensity, the peak at  $2\omega$  is weaker from the beginning and vanishes for times larger than  $2 ps$ .

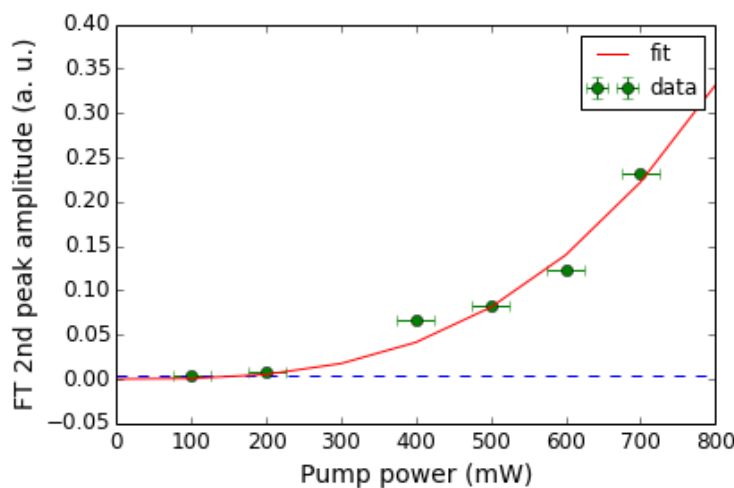


Figure 6.8: Intensity of the peak at frequency  $2\omega$  in the Fourier transform as function of the power of the probe. The blue dotted line represents the noise level.

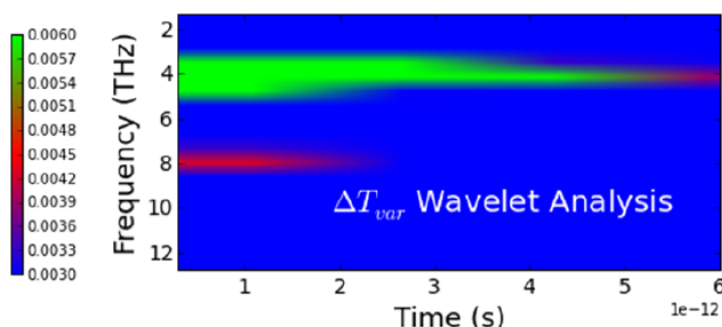


Figure 6.9: Time evolution of the frequency component in an Impulsive Stimulated Raman Scattering measurement.

### 6.2.2 Full quantum state reconstruction of the probe pulses

The same effective interaction terms between the phonon mode and the pump which is used to "prepare" the material in a quantum coherent/squeezed vibrational state can be used to manipulate the quantum state of the probe pulses. The quantum state reconstruction of the probe pulses is performed in a BHD configuration as described in chapter 4.1.3. The *Balanced Homodyne Detection measurements* provide a measure of the quadrature of the field from which one can reconstruct the Wigner function (see Appendix E). This probability distribution allows to make two equivalent analyses: since it gives a visual representation of the quantum state in phase space one can directly understand some feature of the analyzed radiation (number of photons and squeezing, for example). Moreover if the Wigner function is known one can calculate the expectation value of any operator, such as the mean number of photons or the squeezing parameter.

Some Wigner function at different times are shown in Figure 6.10<sup>1</sup>: oscillations of the mean values of  $q$  are connected to variations of intensity of the measured signal, while deformations in the shape may be connected to squeezing. In our results the mean value of  $q$  oscillates in time, as the intensity in the pump-probe measurement (see Figure 5.1); they are connected since the mean

<sup>1</sup>A video figuring the time evolution of the Wigner function can be found at [https://sites.google.com/site/danielefausti/educational-materials/Wigner\\_movie.wmv?revision=1](https://sites.google.com/site/danielefausti/educational-materials/Wigner_movie.wmv?revision=1)

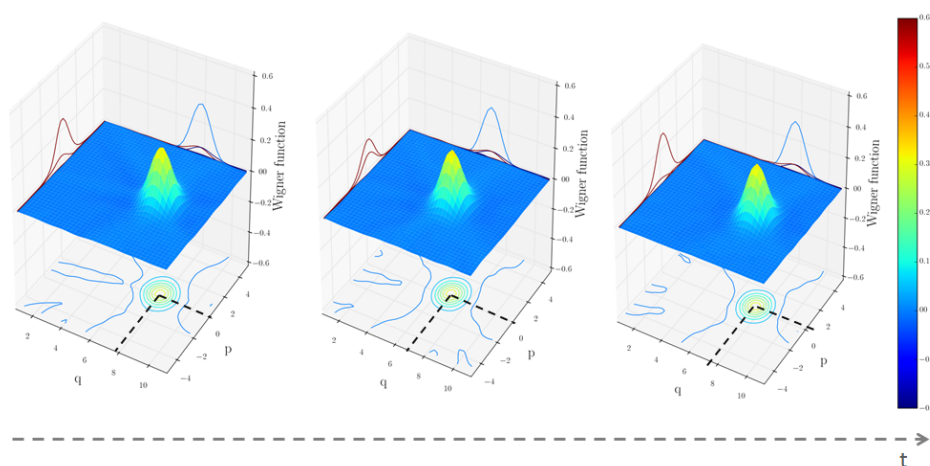


Figure 6.10: Wigner function of the probe pulse at three different time delays between the pump and the probe.

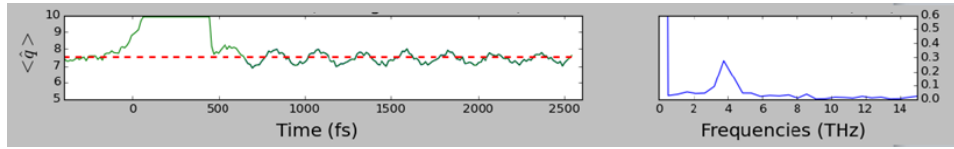
number of photons is  $\langle \hat{n} \rangle = \frac{q^2}{2}$ <sup>2</sup>. Differences in the standard deviation are not easily visible, since they are very small.

Quantum properties of the photon state can be measured calculating the expectation values of some observables: in particular we considered the number of photons, the values of  $q$  and  $p$ , their variances and the squeezing parameter  $\xi = \frac{1}{4} \ln \left( \frac{\sigma_p^2}{\sigma_q^2} \right)$ . The results are plotted in Figure 6.11. One can immediately notice that the number of photons shows the same oscillations of the Raman Scattering measurements (Figure 5.1) and present the same frequency component. The second spike of the variance in Fourier space is not visible, but we have important information about the squeezing parameter: it always positive, even if small, so we can say that the state is squeezed and the squeezing itself is modulated by the frequency of the Raman mode at about 3.9 THz.

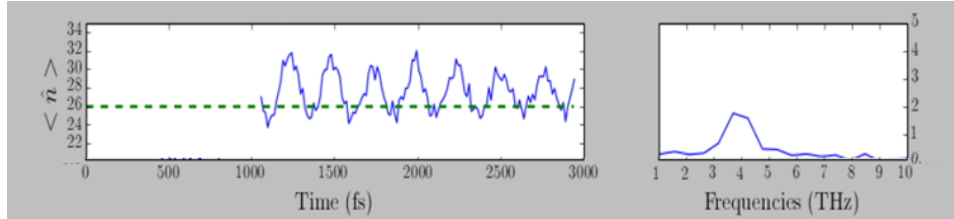
Finally we must specify the method of calculation of the expectation values.

<sup>2</sup>In general the number of photons depends on both coordinates  $p$  and  $q$  ( $\langle \hat{n} \rangle = \frac{q^2 + p^2}{2}$ ). In our case the mean value of the quadrature as function of the phase difference  $\Phi$  (see Figure 5.10) has always been fitted as a cosine with fixed phase. The result is a sort of rotation of the phase space, such that the so obtained  $q$ -axis has the direction of the line connecting the origin with the center of the Wigner function. That's why a displacement along the  $q$ -axis in our results is directly connected to the number of photons.

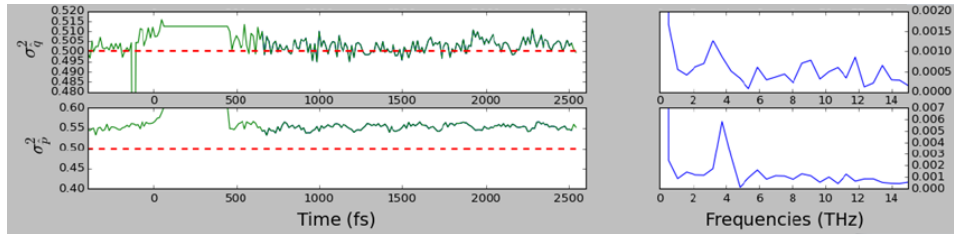
6.2. From the probe state to quantum fluctuation of the vibrational mode



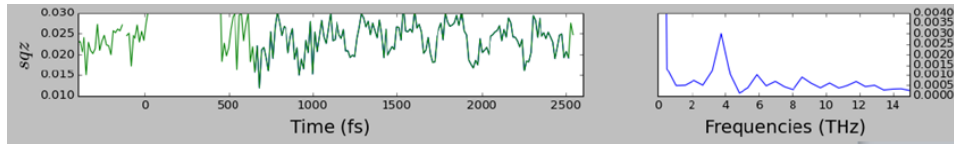
(a)



(b)



(c)



(d)

Figure 6.11: Expectation values calculated with the Wigner function of the signal: (a) coordinate  $q$ , (b) number of photons, (c) variances, both along  $q$  and  $p$  axes, (d) squeezing parameter. On the left side expectation values are shown, while on the right the Fourier transforms has been computed

The reconstruction of the Wigner function determines some artifacts which are not related to the photon state, but are difficult to "correct". One of them is the presence of many negative points (which are not present in a gaussian state), which appear with a certain regularity in the tails of the distribution and affect both the normalization of the function and the mean values. So we decided to fit the reconstructed Wigner function with a 2D gaussian and

to extract the expectation values directly from the fit parameters.

### 6.2.3 From photon to phonon quantum state detection

Raman active modes in samples have already been studied through ultrafast spectroscopic techniques [23, 24, 25, 26] and semiclassical theories (as the four wave mixing theory, described by S. Mukamel and reported in Chapter 3) have been developed in order to explain the experimental results and the relationship between the intensity of the detected signal and phononic excitations in the sample. In particular we know that the time evolution of ionic displacement is linearly mapped into the number of photons scattered by the sample (see section 3.4.1).

These theoretical treatments present anyway a limit: the radiation is described classically. If we want to measure a purely quantum property, as the squeezing, for example, a semiclassical theory is not adequate. In our specific case this means that we do not know how the phononic quantum noise is mapped in the electric field. As a consequence from the measurements described in the previous section we can, at least in principle, deduce only two kinds of information:

- in our configuration the pump pulse excites a Raman active E-mode at about 3.9 THz
- the quantum state of the *probe* after the interaction with the excited sample is squeezed and the squeezing parameter oscillates with the same frequency of the vibrational mode (see the discussion in the previous section).

For this reason the use of time resolved spectroscopic techniques to get information about quantum properties of the phononic field has been criticized in the past [2, 27]. In the following paragraph we are going to propose a model to describe the relation between the quantum state of phonons and of the probe [28]; simulation to verify its validity are still in progress.

Let us consider a time resolved ISRS<sup>3</sup> measurement step by step:

1. the pump pulse impinges on the sample and generates coherent phonons

---

<sup>3</sup>Impulsive Stimulated Raman Scattering

2. during the time delay between the pump and the probe the phononic states evolves thanks to interactions with the environment
3. the probe pulse impinges on the sample and interacts with its phononic state
4. the pump field is detected through BHD.

Our hypothesis is that the Hamiltonian which describes the effects of the pump on the sample is essentially the same that justifies the imprinting of the nature of the vibrations of ions in the material on the probe pulse. Let us try to write this Hamiltonian, starting the theory of the ISRS.

Since our pump pulse is not in resonance with electronic transitions in the  $\alpha$ -quartz and has a certain frequency dispersion, it can excite Raman active modes on the sample with frequency  $\Omega = \nu_1 - \nu_2$ , where  $\nu_1$  and  $\nu_2$  are both contained in the envelope of the pulse in frequency domain (see Figure 6.12). Moreover one can describe the interaction between the pump and the sample

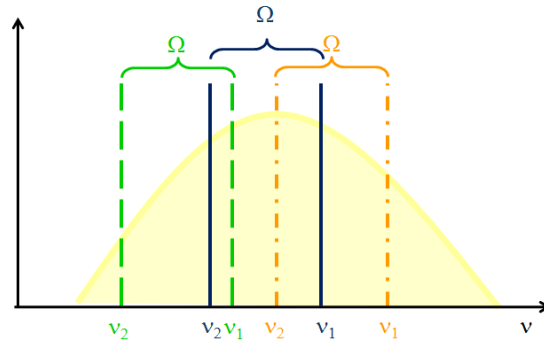


Figure 6.12: Envelope of the pump pulse in frequency domain. Three different couples of frequencies  $(\nu_1, \nu_2)$  for which  $\nu_1 - \nu_2 = \Omega$  are showed.

as the destruction of a photon with frequency  $\nu_1$  and the creation of a photon with energy  $h\nu_2$  and of a phonon with frequency  $\nu_1 - \nu_2$ . If we sum over all the couples  $(\nu_1, \nu_2)$  contained in the spectrum of the pump pulse, for which  $\nu_1 - \nu_2 = \Omega$ , in the limit of an instantaneous excitation one gets the following interaction Hamiltonian

$$H_{int} = \sum_{\nu_1 - \nu_2 = \Omega} \left( \gamma_S a_{\nu_1} a_{\nu_2}^\dagger b^\dagger + \gamma_A a_{\nu_1}^\dagger a_{\nu_2} b \right) \delta(t), \quad (6.3)$$

where  $a_\nu$  represents the annihilation operator of a photon with frequency  $\nu$ ,  $b$  is the same operator for a phonon with energy  $h\Omega$ , and  $\gamma$  are dimensional constants which reflects the effective coupling between photons and phonon. The first term in the sum represent exactly the situation described before, in which a phonon is created (Stokes Raman Scattering), while the second stands for the destruction of a photon ( $\nu_2$ ) and a phonon ( $\Omega$ ) and the creation of a higher energy photon ( $\nu_1$ ), which is an anti-stokes process. Note that in general  $\gamma_A$  the scattering intensities are related by [14]

$$\frac{I_{antistokes}}{I_{stokes}} = e^{-\frac{h\Omega}{k_B T}}, \quad (6.4)$$

(for  $T = 300$  K and  $\Omega = 3.9$  THz,  $\frac{I_{antistokes}}{I_{stokes}} \approx 0.5$ ). Finally the  $\delta$  function in equation 6.3 represents the impulsive character of the process.

Let us now write the quantum state of the total system (sample and radiation) for each step of the process listed before.

1. In the initial state the sample is in thermal equilibrium at temperature  $T$  and its quantum state can be described by the density operator of a thermal state  $\hat{\rho}_\beta$ , with  $\beta = (k_B T)^{-1}$  (see Appendix A), while the pump pulse is in a coherent state  $|\nu\rangle$ . The total initial state is

$$\hat{\rho}_0 = |\nu\rangle \langle \nu| \otimes \hat{\rho}_\beta. \quad (6.5)$$

When the pump impinges on the sample the state evolves instantaneously under the action of an operator

$$\begin{aligned} U &= e^{-i \int H_{int} dt} \\ &= e^{-i \sum_{\nu_1 - \nu_2 = \Omega} [\gamma_S a_{\nu_1} a_{\nu_2}^\dagger b^\dagger + \gamma_A a_{\nu_1}^\dagger a_{\nu_2} b]} \end{aligned} \quad (6.6)$$

and becomes

$$\hat{\rho}_1 = U \hat{\rho}_0 U^\dagger. \quad (6.7)$$

The density operator  $\hat{\rho}_1$  contains information both on phonon and photon states; since now we are interested only in phonon state, the photon degrees of freedom can be traced over and one gets

$$\hat{\rho}_1^{phon} = Tr_{phot} [\hat{\rho}_1]. \quad (6.8)$$

2. After the action of the pump, phonons interact with the environment and evolve in time. The time dependence of their density operator is due to the evolution of a coherent state and dissipative effects; standard techniques based on the Lindblad form allow to compute the quantum state  $\hat{\rho}_2(t)$  for a time  $t$  after the excitation.
3. As in point 1 the initial state of the interaction between the probe and the sample can be expressed as  $|\alpha\rangle\langle\alpha| \otimes \hat{\rho}_2^{phon}(t)$ , where  $|\alpha\rangle$  is the coherent photon state of the probe. The probing process is again described by the evolution under an unitary operator  $U'$ , which is similar to the  $U$  operator defined in point 1, but with different coupling constants  $\gamma$ . The result is the density operator

$$\hat{\rho}_3(t) = U' |\alpha\rangle\langle\alpha| \otimes \hat{\rho}_2^{phon}(t) U'^{\dagger}. \quad (6.9)$$

4. In the last step we detect the probe pulse. The density operator  $\hat{\rho}_3(t)$  is still a measure of the phonon and photon state, so, this time, phonon degrees of freedom can be traced over and one obtains

$$\begin{aligned} \hat{\rho}_4^{phot}(t) &= Tr_{phon} [\hat{\rho}_3] \\ &= Tr_{phon} \left[ U' |\alpha\rangle\langle\alpha| \otimes \hat{\rho}_2^{phon}(t) U'^{\dagger} \right]. \end{aligned} \quad (6.10)$$

Since the density operator (and consequently the Wigner function) completely characterizes the quantum state of a system, and, according to these model, the quantum state of the output signal is affected by the vibrational quantum state, we expect that also purely quantum properties can be detected through time resolved spectroscopy. In particular in our case this would mean that the phonon quantum state can be mapped on the photon one. Simulations based on this treatment are being executed in order to confirm its validity and to understand if the squeezing of light is visible only when a squeezing of the phonon state is present.

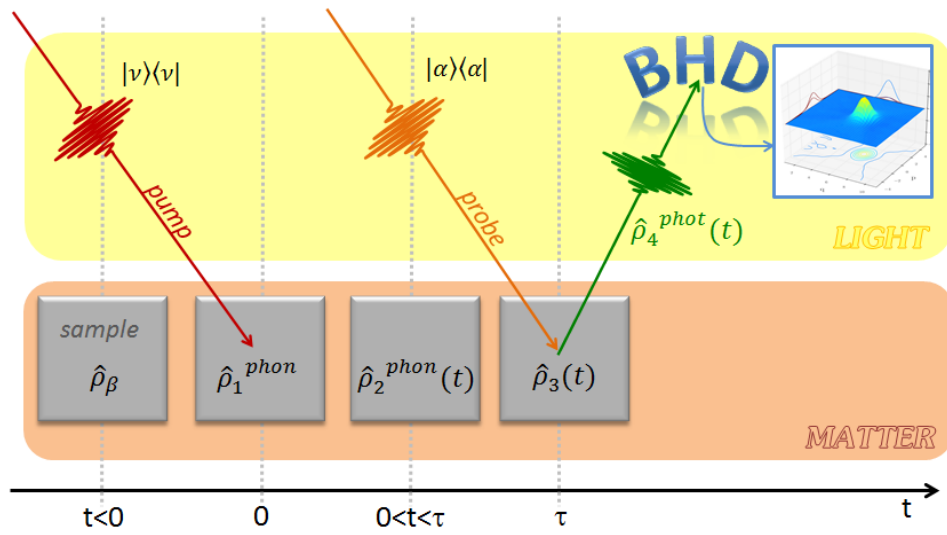


Figure 6.13: Simplified scheme of the model and the relation between phonon and photon quantum states.

# Appendix A

## Thermal states

The so called *thermal light* is the electromagnetic radiation emitted by a body at a certain temperature  $T$ . The radiation pattern consists of a spectrum of oscillating modes: each of them can be described as an harmonic oscillator with angular frequency  $\omega$ .

The probability of finding  $n$  photons in the  $i^{th}$  mode is given by the Boltzmann's law [29]

$$P_\omega(n) = \frac{e^{-\frac{E_n}{k_B T}}}{\sum_{k=0}^{\infty} e^{-\frac{E_k}{k_B T}}} \quad (\text{A.1})$$

where  $E_n = \hbar\omega (n + \frac{1}{2})$  is the quantized energy and  $k_B$  is the Boltzmann constant.

By substituting  $E_n$  in equation A.1 and keeping in mind the summation of a geometric progression  $\left( \sum_{j=0}^k x^j = \frac{1-x^{k+1}}{1-x}, \text{ for } 0 < x < 1 \right)$ , one gets

$$P_\omega(n) = e^{-\frac{\hbar\omega n}{k_B T}} \left( 1 - e^{-\frac{\hbar\omega}{k_B T}} \right). \quad (\text{A.2})$$

The mean photon number can be derived as

$$\begin{aligned} \langle \hat{n} \rangle &= \sum_{j=0}^{\infty} j P_\omega(j) \\ &= \frac{e^{-\frac{\hbar\omega}{k_B T}}}{1 - e^{-\frac{\hbar\omega}{k_B T}}}, \end{aligned} \quad (\text{A.3})$$

which is the so called Bose-Einstein distribution.

For the definition of density operator ( $\hat{\rho} = \sum_\omega P_\omega(n) |\psi_\omega\rangle \langle \psi_\omega|$ ), where the

possible values of  $\omega$  are supposed to be discrete and  $|\psi_\omega\rangle$  are the eigenstates of the harmonic oscillator hamiltonian with eigenvalues  $\hbar\omega (n + \frac{1}{2})$ , one gets

$$\begin{aligned}\hat{\rho}_T &= \sum_{\omega} \frac{e^{-\frac{E_n(\omega)}{k_B T}}}{\sum_k e^{-\frac{E_k(\omega)}{k_B T}}} |\psi_\omega\rangle \langle\psi_\omega| \\ &= \sum_i \frac{e^{-\frac{E_n(\omega)}{k_B T}}}{Tr\left(e^{-\frac{\hat{H}}{k_B T}}\right)} |\psi_\omega\rangle \langle\psi_\omega|.\end{aligned}\tag{A.4}$$

The Wigner function of a thermal state is a gaussian centered in the origin of the phase space, broader than the vacuum one.

# Appendix B

## Laser source

In order to perform our experiments we need a laser source that produces ultrashort pulses (10 – 100 fs) with a 250 KHz repetition rate (number of pulses per unit of time). Such repetition rate has been chosen as a trade off between the needs of acquiring a significant number of data (requiring high repetition rate), and high intensity per pulse needed for accessing large dynamical range in photoexcitation.

The laser system is made up of an oscillator that produces short low intense pulses and of an amplification system that increases their energy. A technique called Kerr Lens Mode-locking permits to obtain ultrashort pulses, with no active optical elements in the oscillator cavity. Finally the pulses are amplified with a chirped pulses amplification scheme. In the following section we are going to treat these techniques in more detail.

### B.1 Mode-Locking

Passive mode locking schemes are based on the geometrical properties of the resonant cavity of the laser system: in this chapter I'm going to show briefly a simplified model [30].

Let us consider the electric field inside the laser cavity as the sum of all its modes, that is all the modes with wavelength  $\lambda = \frac{2L}{m}$ , where  $L$  is the cavity length and  $m$  are integers known as mode orders. In simple lasers there is no

phase relation between the modes and interference effects produces an almost constant output intensity, called continuous wave. In Mode-Locked lasers the phase relation between the modes is forced to be fixed, in order to interfere constructively and to produce a train of pulses well separated in time.

The total electric field inside the cavity can be expressed as

$$E(t) = \sum_{n=-N}^N E_0 e^{i[(\omega_0+n\Delta\omega)t+n\varphi]} \quad (\text{B.1})$$

where  $n$  is the difference between the considered mode and the mode  $n_0$  with frequency  $\omega_0$  and

$$\Delta\omega = \frac{4\pi L}{c} \left( \frac{1}{n_0+n} - \frac{1}{n_0+n+1} \right) \approx \frac{4\pi L}{cn_0^2} \quad (\text{B.2})$$

In this expression we have supposed for simplicity that all modes have the same amplitude  $E_0$ .

We can rewrite the expression of the field this way

$$E(t) = e^{i\omega_0 t} A(N, t) \quad (\text{B.3})$$

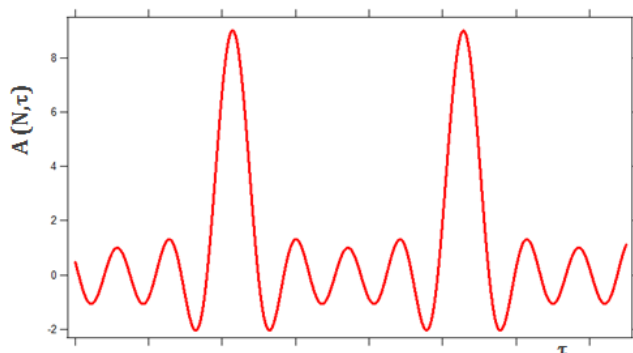
where  $A(N, t) = \sum_{n=-N}^N E_0 e^{in\tau}$ , with  $\tau = \Delta\omega t + \varphi$ , in order to consider only the quantity  $A(N, t)$  from now on. Rewriting the last expression, dividing the terms with positive  $n$  from the terms with negative  $n$  and computing the sum of the obtained geometric series, we finally get

$$A(N, \tau) = E_0 \frac{\sin\left(\frac{2N-1}{2}\tau\right)}{\sin\left(\frac{\tau}{2}\right)}, \quad (\text{B.4})$$

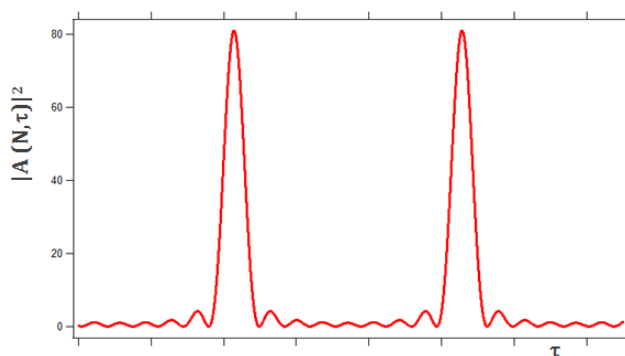
$A(n, \tau)$  and  $A(n, \tau)^2$  in function of  $\tau = \Delta\omega, t + \varphi$  are reported in Figure B.1

## B.2 Kerr lens mode-locking

The technique used to lock the modes is based on the so called Kerr Lens Effect, a nonlinear effect due to the properties of the active medium present in the laser system. A Kerr active medium has a refractive index which depends on the electromagnetic field intensity. As the beam in the cavity has a Gaussian power density distribution, it is much more intense in the center with respect to the edge and the refractive index will vary linearly with the



(a)



(b)

Figure B.1: Line shape of  $A(N, \tau)$  (a) and  $A(n, \tau)^2$  as function of  $\tau$ , for arbitrary values of  $N$ . They represent the time distribution of the pulses due to the Mode-Locking technique.

intensity across the beam profile [30]. In this way the active medium of the cavity works as a lens that focuses the beam at the center; since the Kerr effect depends on the intensity of the beam, pulsed and continuous wave modes are focused in different ways and, changing the geometry of the cavity it is possible to select only pulsed modes (Figure B.2). At the end of the cavity a mirror transmits partially the train of pulses, with repetition rate  $T^{-1} = \frac{c}{2L}$ .

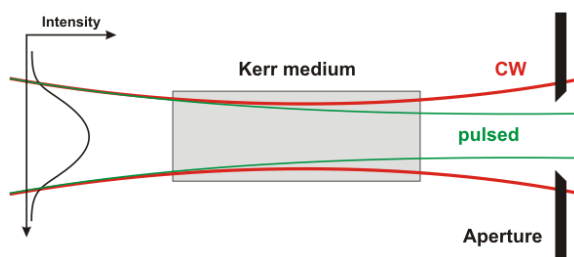


Figure B.2: Kerr lens scheme [31].

### B.3 Chirped pulse amplification

In order to amplify the laser pulses produced in the oscillator, the amplifier uses a scheme called *Chirped pulse amplification*. This technique is divided in three steps: stretching, amplification and compression.

In the first step the pulse is stretched in time through reflection and dispersion on gratings (different spectral components follow different path) , in order not to damage the crystal of the amplifier. Then the pulse is sent to the amplifier itself, where it can perform a certain number of cycles (it can be controlled) in order to produce an amplified pulse, but still spectrally and temporally spread. Finally the pulse is compressed through reflections on gratings (the inverse process with respect to what is happening into the stretcher).

### B.4 The laser system

We have described the general processes and techniques that allow us to obtain ultrashort laser pulses. Now we give the characteristics of our laser system. The mode-locked source is a Ti:Sapphire oscillator (Mira Seed), in which the active medium is Ti doped  $Al_2O_3$ ; it produces pulses with a wavelength centered at 800 nm and about 30 nm broad, with a 80 MHz repetition rate and output power approximately 800 mW. The oscillator is pumped by a  $Nd : YVO_4$  laser (Verdi V-18) which produces monochromatic continuous radiation with wavelength  $\lambda = 532$  nm. The pulses are stretched and sent to the amplifier RegA (which is also pumped by Verdi) and then recompressed. The final output is a pulsed beam of 250 KHz repetition rate (that is a pulse

every  $4\mu s$ ) and about 1.5 W mean power. The scheme of the laser system is shown in Figure (B.3).

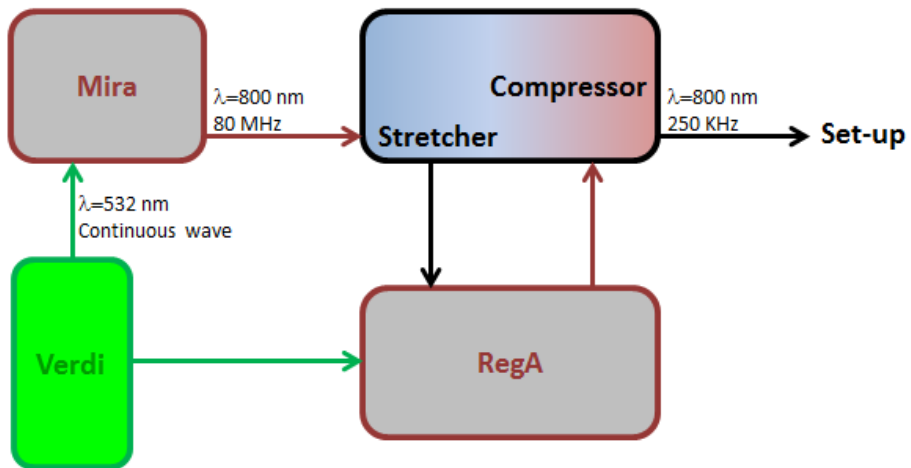


Figure B.3: Laser system scheme.



## Appendix C

# Autocorrelation

The Balance Homodyne Detection set-up is essentially a *Mach-Zehnder interferometer*, which measures the interference between two coherent elec-

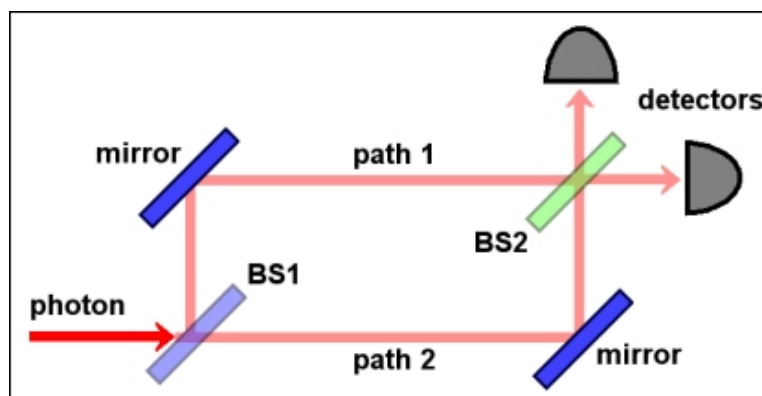


Figure C.1: Scheme of the Mach-Zehnder interferometer

tromagnetic fields coming from the same beam source. In practice the initial radiation is divided in two beams by the first beam splitter; both experience a reflection and finally interfere on the second beam splitter. Two photodetectors are put at the end: the first one measures the interference of the pulse transmitted by both the beam splitters with the one which has been reflected twice. They have the same phase and so we see a constructive interference. The other branch is the sum of the fields which have been first reflected and then transmitted or vice-versa: their phase difference is  $\pi$  and so one has destructive interference.

All previous considerations are based on the assumption that the optical paths of the beams after the first beam splitter have the same length. In order to reach this aim the set-up configuration is usually rectangular; moreover since we introduced some objects (the sample, half-wave plate and polarizers), one should pay attention on the modifications of the optical paths due to the different refractive indexes. That's why we introduced two wedge plates, which balance the paths. Nevertheless all these strategies are not enough to find the interference: one should move one of the mirrors to slightly vary the phase difference between the pulses. This is possible thanks to the piezoelectric translator.

In order to find the piezo positions for which the signal and the local oscillator interfere in the 50:50 beam splitter, one should perform a preliminary measure; it consists of a BHD scan (without pump pulse) on a large range of piezo positions (about  $100 \mu m$ ).

Let us try to understand what we expect from this measurement; notice that we can work in the classical regime of the interferometer, so the probe can be intense, in order to get higher signal. If the probe is a coherent state  $|\alpha\rangle$ , one gets, from equation 2.18

$$\hat{I}_\Phi = \sqrt{2}|z||\alpha| \cos \Phi, \quad (\text{C.1})$$

where  $\Phi$  is the phase difference between the signal and the local oscillator and  $z$  is the eigenvalue of the latter. This is a measure of the classical autocorrelation pattern of the pulse (Figure C.2). Note that for our experimental configuration

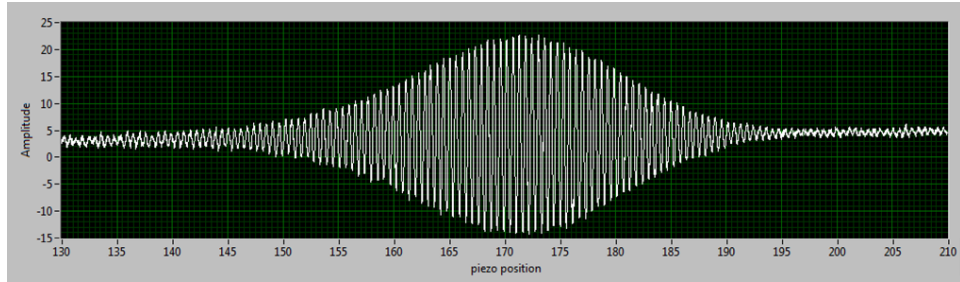


Figure C.2: Interferometric autocorrelation figure

a  $10 \text{ nm}$  step of piezo corresponds to a  $10\sqrt{2} \text{ nm}$  variation of the local oscillator optical path (see Figure C.3).

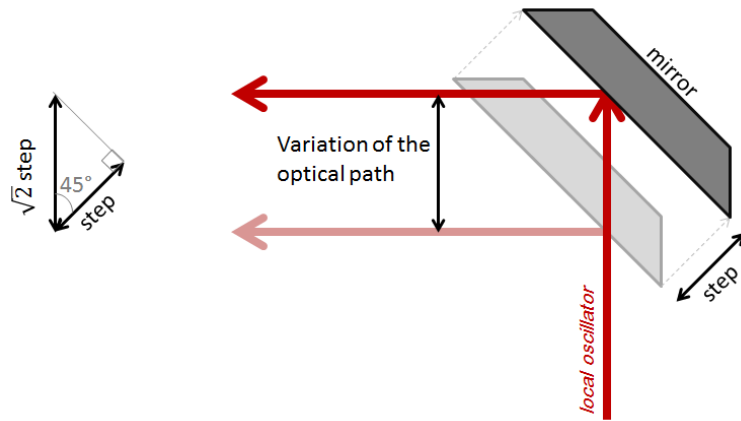


Figure C.3: Variation in the optical path of the local oscillator due to the position of the piezo. Two configurations of the mirror on the piezoelectric translator are shown, in order to compare the optical paths. Note that this figure is schematic and the scale is not exact; as a matter of fact the step of the piezo must be much smaller than the diameter of beam.



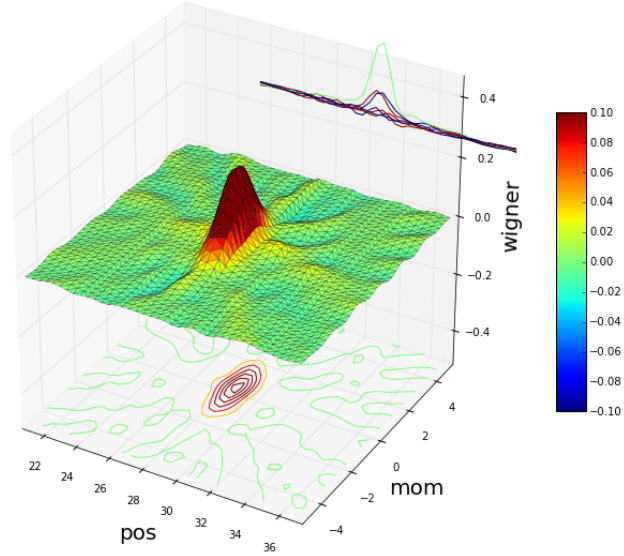
## Appendix D

# Systematic errors in BHD measurements

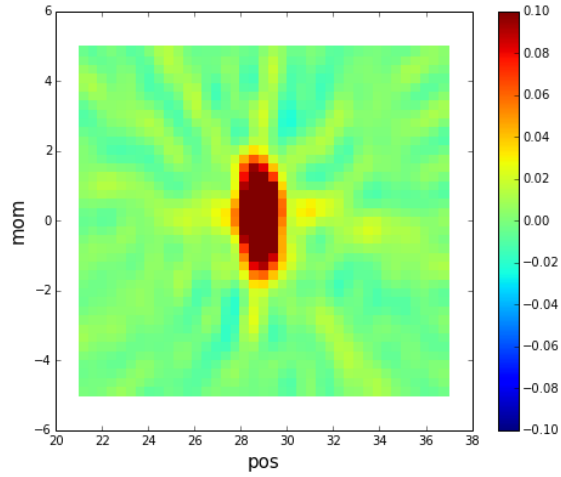
Performing measurements of time resolved Balance Homodyne Detection we noticed a suspect squeezing in many Wigner function, especially when the intensity of the probe was high. In order to verify this behavior we decided to execute the same measurement without the sample and we found out the same result (see Figure D.1). This proof demonstrated that there was a systematic error which affected the data.

The problem concerns the instability of the piezo read-out position: if we read the position of the piezoelectric translator (using an apposite software) we do not get always the same result. On the contrary one obtains a distribution around the mean value with standard deviation  $\sigma = 3$  nm [11].

In order to understand how uncertainty could affect our measurements, we decided to simulate it: we considered a quadrature of a coherent state and added to the position of the piezo (i.e. to the phase difference) a random number with gaussian distribution around zero and standard deviation of 3 nm. This modification is much more visible in correspondence of the phase difference for which the derivative  $\left| \frac{dx_\Phi}{d\Phi} \right|$  is maximum, since even a small error in the phase  $\Phi$  determines a considerable variation in  $x_\Phi$  (about  $\left| \frac{dx_\Phi}{d\Phi} \right| \cdot \Delta\Phi$ ). Therefore the variance increases around the points of maximum derivative, in absolute value, which occur with double frequency with respect to the same value of the quadrature and so this uncertainty entails a false squeezing in



(a)



(b)

Figure D.1: BHD measurement without sample, with a probe power of  $28 \mu W$ , which corresponds to an intensity of  $634 nJ/cm^2$ . In Figure (a) the Wigner function is represented, while its projection on the horizontal plane is plotted in (b).

the measured quantum state.

We also noticed that this effect depends on the probe power, so we performed several measurements without sample at different intensities and for each one

we calculated the squeezing parameter, which depends on the ratio between the standard deviations of the Wigner function along the p and the q axis. The squeezing parameter increases monotonically with the signal intensity; making the same calculation for the simulated data we got the same result and it confirms the hypothesis about the causes of the fictitious squeezing D.2. Since we cannot improve the sensibility of the piezoelectric translator, we decided to consider only low intensity data.

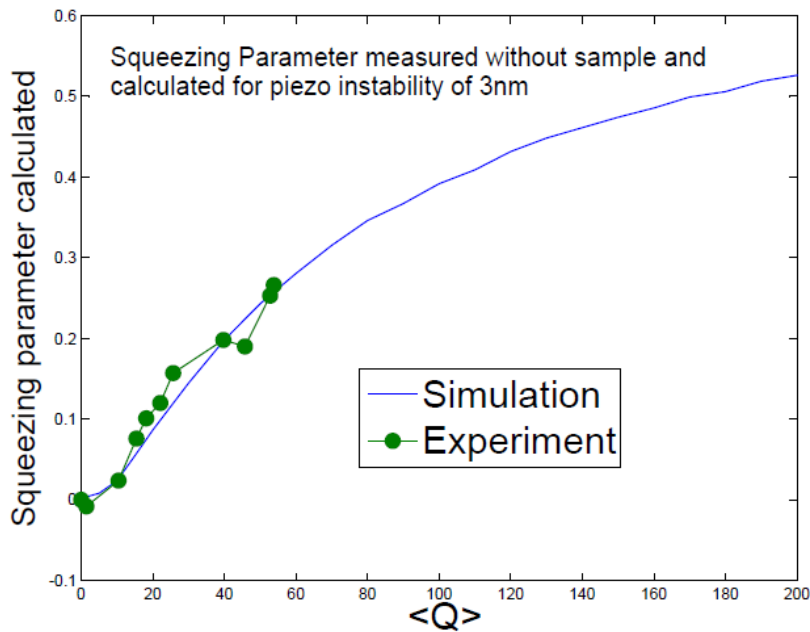
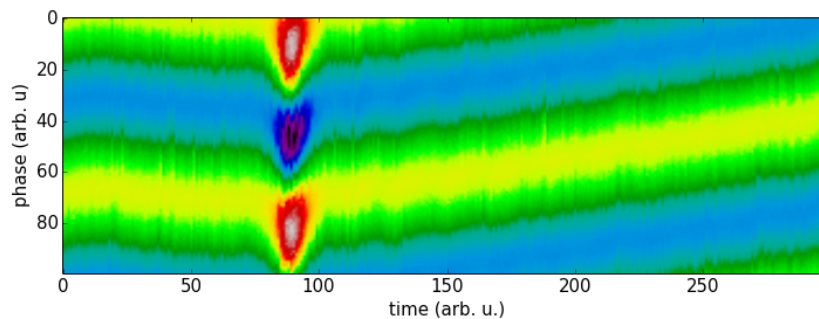


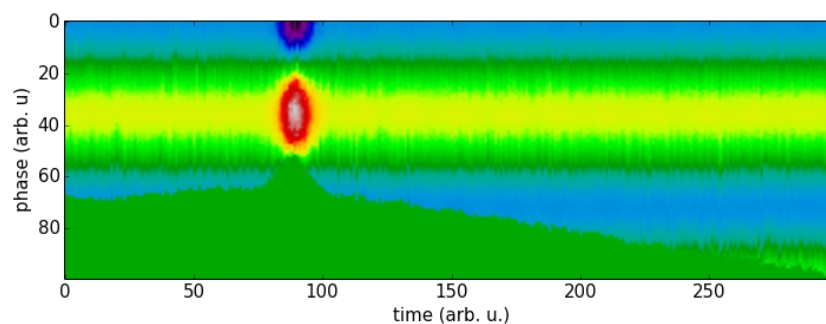
Figure D.2: Squeezing parameter as function of the number of photons of the signal. Green points represent experimental data, while the blue line is a simulation based on the hypothesis of a 3 nm uncertainty in the piezo position.

Another problem in BHD measurements is related to the phase in long experiments. This effect is visible in Figure D.3 (a) in which a shift of the phase is evident, whose cause is probably a variation of the difference between the optical path of the local oscillator and the signal. It might be caused by a variation of temperature, which modifies the optical paths (since the beams pass through some objects which can experience thermal expansion).

Since this shift of the phase is a systematic effect, we usually "correct" the



(a)



(b)

Figure D.3: Result of a time resolved balance homodyne detection measurement. In Figure (a) we notice a shift of the phase, which is "corrected" in (b).

image: we fit the columns of the image with a sine function and redefine a point of maximum (or minimum) of the sine function as the first point of the column. The result is shown in Figure D.3.b.

## Appendix E

# Wigner function reconstruction

Balance Homodyne Detection provides set of data of the form  $(x_\theta, \theta)$ , where  $x_\theta$  is the quadrature related to the phase difference  $\theta$  between the signal and the local oscillator, experimentally obtained by changing the piezoelectric translator position. Our aim is to get the Wigner function starting from these data, since it completely characterizes the quantum state of the signal we want to measure and allow to compute the expectation values of all the observables of the system.

The Wigner function is directly related to the quadrature  $x_\theta$ , and in particular to the marginal distribution  $pr(x_\theta, \theta)$  (see section 2.1.1) through the so called Radon transform

$$pr(x_\theta, \theta) = \int_{-\infty}^{+\infty} W_{det}(x_\theta \cos \theta - P_\theta \sin \theta, x_\theta \sin \theta + P_\theta \cos \theta) dP_\theta. \quad (\text{E.1})$$

The previous equation underlines that  $pr(x_\theta, \theta)$  is the integral projection of the Wigner function in a vertical plane which forms an angle  $\theta$  with the q-axis in phase space (Figure E.1). The subscript *det* stands for *detected* and refers to the fact that we deal with the reconstructed Wigner function and not the "real" one [32]. The difference between the two is due to the experimental conditions and limits; one can think that the detected Wigner is related to the real one by a convolution with a gaussian function which contains the efficiency of the detector (see Figure 2.4).

Several numerical methods exist to obtain the Wigner function starting from the experimental data. Some of them are classified as *inverse linear*

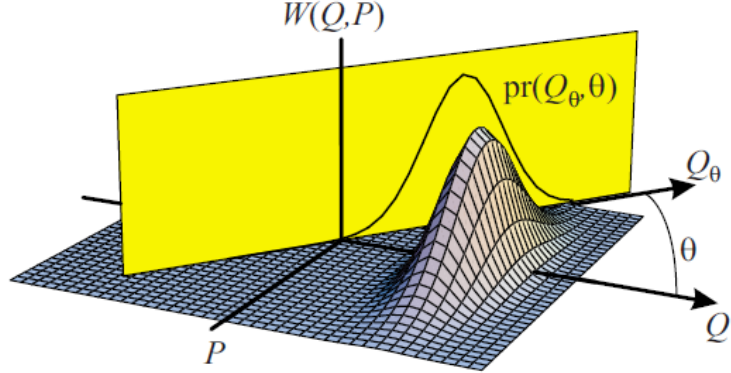


Figure E.1: Example of Wigner function and relative marginal  $pr(Q_\theta, \theta)$ , represented as projection on a plane rotated of an angle  $\theta$  with respect to the Q-axis. [32]

*transform techniques* and are based on the definition of marginals. Since the integration in equation E.1 is a linear operation, one can reverse it and reconstruct the function from the marginals. The numerical inversion of the Radon transform is well known in medical imaging, but we need a technique which takes into account also the efficiency of the detector.

The minmax reconstruction algorithm [33] satisfies the previous requests and provides a Wigner estimation

$$W_{h,M}^\eta(q, p) = \frac{1}{M} \sum_{i=1}^M K_{x_{\theta_i}, \theta_i}^{h,\eta}(q, p), \quad (\text{E.2})$$

with

$$K_{x_{\theta_i}, \theta_i}^{h,\eta}(q, p) = \int_{-\frac{1}{h}}^{\frac{1}{h}} dt \frac{|t|}{4\pi} e^{-it(q \cos \theta_i + p \sin \theta_i - \frac{x_{\theta_i}}{\sqrt{\eta}}) + t^2 \frac{1-\eta}{4\eta}}. \quad (\text{E.3})$$

The previous estimation depends on the data  $(x_{\theta_i}, \theta_i)$ , the detector efficiency  $\eta$ , the number of collected data  $M$  and an adaptive parameter  $h$ , necessary since the integrand diverges. The value of  $h$  which minimizes uncertainties [33] is

$$h = \sqrt{\frac{2\beta + 2\gamma}{\log N}}, \quad (\text{E.4})$$

where  $\beta$  depends on the class of the Wigner function and should be less than  $\frac{1}{4}$ , while  $\gamma = \frac{1-\eta}{4\eta}$  ( $\eta$  is the efficiency of the detector). Once the Wigner

---

function has been reconstructed, all expectation values of observables  $\hat{O}$  can be computed with the relation

$$\begin{aligned}
\langle \hat{O} \rangle_h &= \int dqdp O_W(q,p) W_{h,M}^\eta \\
&= \frac{1}{M} \sum_{i=1}^M \int dqdp O_W(q,p) K_{x_{\theta_i}, \theta_i}^{h,\eta}(q,p),
\end{aligned} \tag{E.5}$$

where  $O_W(q,p)$  is the Wigner transform of the operator  $\hat{O}$  (see section 2.1.1).



# Conclusions

A quantum state can be completely characterized by its Wigner function (WF), since it allows to compute the expectation value of any observable of the system. In addition to this the WF gives an immediate representation of the state characteristics: properties such as coherence or squeezing are visible in the WF shape in phase space.

Both photon and phonon fields are described with the quantum oscillator formalism and have eigenstates whose Wigner function is a gaussian in phase space. The quantum state of light can be detected through Balanced Homodyne Detection (BHD), while the detection of phonon quantum state is still a discussed topic.

In this thesis work we developed a set-up which connects time resolved techniques with BHD, in order to get a more profound analysis of the probe scattered in an Impulsive Stimulated Raman Scattering (ISRS) measurement. To test our new approach to pump and probe experiments we studied a representative sample for transparent materials such as  $\alpha$ -quartz, whose Raman active modes have been extensively studied with more standard approaches.

The measurements described in this thesis have been made possible by the use of a unique combination of the following instruments:

- a laser system which provides ultrashort pulses ( $\sim 100$  fs) with high repetition rate (250 KHz);
- a "home made" balanced differential detector with high efficiency (that is low electronic noise);

- a fast digitizer, which allows to analyze hundreds of equally prepared pulses, to average them and calculate variance and higher momenta in order to get statistical information too.

Performing "standard" time domain ISRS measurements we observed oscillations in the signal due to the mapping of the phonon state on the photon one, which has been theoretically demonstrated. From this measure one can obtain the frequency of the excited Raman mode ( $128 \text{ cm}^{-1}$  in our case). The analysis of the variance showed two Fourier components: one at the same frequency of the signal and the other at twice this frequency. The latter component is rationalized in terms of a squeezing of the excited vibrational state, which in our model is mapped onto a photon number fluctuation in the probe quantum state. The squeezing is confirmed by the Wigner function reconstruction of the probe state as a function of the delay time between the excitation and the instant in which the probe impinges on the sample. The calculation of the expectation value of the squeezing parameter demonstrates not only that it is not zero, but also that it oscillates at the frequency of the excited phononic mode.

To the best of our knowledge, a fully quantum description of how purely quantum phononic states (such as a squeezed one) are mapped on a photon field is not available. We developed a phenomenological model which describes the interaction of the two fields. Future investigations of such interactions will potentially enable a new approach to the manipulation of the quantum state of ultrashort pulses through time domain experiments.

# Riassunto

Uno stato quantistico può essere completamente caratterizzato dal suo *operatore densità*  $\hat{\rho}$ , dal momento che il valore di aspettazione di qualunque osservabile  $\hat{O}$  del sistema si ottiene dalla relazione  $\langle \hat{O} \rangle = Tr(\hat{\rho}\hat{O})$ . Il formalismo dell'operatore densità ha inoltre il vantaggio di descrivere anche stati misti, che non sono accessibili con l'usuale notazione delle funzioni d'onda nello spazio di Hilbert.

Analoghe proprietà caratterizzano la *funzione di Wigner*, una distribuzione di quasi-probabilità che dipende dalle coordinate dello spazio delle fasi  $q$  e  $p$ . La definizione di spazio delle fasi quantistico non è una semplice generalizzazione del caso classico, dal momento che nella quantizzazione del campo le variabili classiche vengono sostituite da operatori e quindi  $q$  e  $p$  saranno in questo caso gli autovalori di questi operatori. Inoltre la posizione e il momento non commutano e sono legati dal principio di indeterminazione di Heisenberg: da ciò consegue che uno stato non può essere definito univocamente (cioè con un punto nello spazio delle fasi). Per questo motivo uno stato quantistico viene rappresentato come un'area nello spazio delle fasi e non esiste una funzione che descriva la probabilità che il sistema abbia contemporaneamente posizione  $q$  e momento  $p$ , ma solo distribuzioni di probabilità per  $q$  e  $p$  separatamente. Per questo motivo la funzione di Wigner è definita di quasi-probabilità e può assumere valori negativi.

Tra le proprietà di questa distribuzione ricordiamo il fatto che i suoi marginali, cioè gli integrali su una delle dimensioni dello spazio delle fasi, sono la distribuzione di probabilità dell'altra variabile e che la conoscenza della funzione di Wigner permette di calcolare i valori di aspettazione di ogni osservabile del

sistema. Inoltre la rappresentazione di questa funzione nello spazio delle fasi esprime in maniera diretta le proprietà più rilevanti del sistema quantistico in esame.

In questo lavoro di tesi vengono trattati sia campi fononici che fotonici, entrambi descritti con il formalismo dell'oscillatore armonico, i cui autostati sono stati di Fock e stati gaussiani (la cui rappresentazione dello spazio delle fasi è appunto una gaussiana). Noi siamo interessati alla seconda categoria ed in particolare a stati che saturano il principio di indeterminazione: stati coerenti (in cui l'indeterminazione sulle due variabili è la stessa) e stati squeezed.

Lo stato quantistico della luce può essere ricostruito tramite tecniche di tomografia quantistica, come la *detezione omodina*: questa tecnica sperimentale prevede l'interferenza su un beam splitter 50:50 del campo che si desidera conoscere (segnale) con un fascio più intenso e noto (detto oscillatore locale). La differenza tra le intensità dei due fasci uscenti dal beam splitter è proporzionale alla quadratura di campo  $\hat{x}_\Phi = \frac{1}{\sqrt{2}} (\hat{a}e^{-i\Phi} + \hat{a}^\dagger e^{i\Phi})$  in funzione della differenza di fase  $\Phi$  tra il segnale e l'oscillatore locale, che può essere ottenuta variando il percorso ottico di uno dei due fasci. Da questa quantità è possibile ricostruire la funzione di Wigner del segnale.

Se la tecnica di deteazione dello stato quantistico della luce è ormai nota e spiegata teoricamente, dall'altro lato la completa caratterizzazione di stati fononici rappresenta ancora un argomento di discussione [2, 27] e non esiste ancora un modello teorico puramente quantistico che la descriva adeguatamente.

Al contrario modelli semiclassici per la deteazione di stati fononici sono stati ampiamente sviluppati. Un esempio sono le tecniche spettroscopiche basate sullo *scattering Raman stimolato*, che prevedono l'eccitazione di fononi nel campione con un impulso di luce intenso (pump) e lo studio della relativa variazione delle proprietà ottiche del sistema in funzione del tempo trascorso dall'eccitazione. Una trattazione formale, di cui riportiamo in seguito solo i punti fondamentali, è contenuta nel lavoro di S. Mukamel *Principles of Nonlinear optical spectroscopy* [1].

La spettroscopia ottica si propone di studiare le caratteristiche di un campione

---

analizzando la variazione delle proprietà della luce da lui riflessa o trasmessa. Per questo è necessario concentrarsi su una quantità che connetta le caratteristiche del sistema con la radiazione elettromagnetica: la polarizzazione. Ricordando che la polarizzazione  $P$  altro non è che il valore di aspettazione dell'operatore di dipolo  $V$  e che vale la relazione  $\langle \hat{V} \rangle = Tr \left( \hat{\rho} \hat{V} \right)$ , eseguendo uno sviluppo perturbativo dell'operatore densità  $\hat{\rho}$  in approssimazione di dipolo e di campi deboli, si ottiene l'ordine  $n$ -esimo dello sviluppo della polarizzazione

$$P^{(n)}(\mathbf{r}, t) = \int_0^{+\infty} dt_n \dots \int_0^{+\infty} dt_1 S^{(n)}(t_n, t_{n-1}, \dots, t_1) E(\mathbf{r}, t - t_n) \cdot \quad (\text{E.6}) \\ \cdot E(\mathbf{r}, t - t_n - t_{n-1}) \dots E(\mathbf{r}, t - t_n - t_{n-1} \dots t_1).$$

Nell'equazione precedente  $S^{(n)}(t_n, t_{n-1}, \dots, t_1)$  è la funzione di risposta del sistema, che dipende dal campione in esame, ed  $E(t)$  sono i campi elettrici che interagiscono con il sistema.

I processi connessi con l' $n - 1$ -esima componente della polarizzazione sono definiti processi di *n-wave mixing* e sono dovuti all'interazione di  $n - 1$  campi elettromagnetici con il campione. Nei materiali con simmetria per inversione la componente al secondo ordine della polarizzazione è nulla e quindi il primo contributo non lineare è legato a fenomeni del terzo ordine, cioè a processi di *four wave mixing*.

In questa trattazione l'impulso di pump dello Scatterig Raman Stimolato è rappresentato dai primi due impulsi che raggiungono il campione e per i quali non è previsto un preciso ordine temporale; la loro interazione genera una sorta di reticolo (con vettore d'onda pari alla differenza tra quelli dei due impulsi) dal quale il terzo impulso (probe) viene scatterato. La direzione e la polarizzazione del fascio scatterato forniscono le prime informazioni sul modo Raman eccitato dall'impulso di pump. La funzione di risposta dipende dal campione e nel caso di cristalli può essere calcolata a partire dal modello dell'oscilatore Browniano, che descrive la dinamica nucleare nel caso di oscillazioni coerenti e smorzate. Il risultato, nel caso impulsivo, prevede che il probe scatterato dal campione sia modulato da un segnale con frequenza pari a quella del modo Raman eccitato.

Nel nostro caso il campione è costituito da quarzo a temperatura ambiente

(detto  $\alpha$ -quartz) e per la nostra configurazione sperimentale il modo vibrazionale eccitato ha simmetria  $E$  e numero d'onda  $128 \text{ cm}^{-1}$ .

Scopo di questo lavoro di tesi è la combinazione delle due tecniche sperimentali (Detezione Omodina e Scattering Raman Stimolato) per ottenere un'analisi più completa dell'impulso di probe dopo l'interazione con il campione. In particolare non vogliamo solo misurare l'intensità del fascio, che, come anticipato, fornisce informazioni sull'energia del fonone eccitato, ma anche le fluttuazioni intrinseche dovute alla quantizzazione del campo elettromagnetico, la cui connessione con lo stato fononico non è ancora chiara.

Questo tipo di misura è stata resa possibile da una adeguata *strumentazione*, che comprende:

- un *sistema laser* che sfrutta la tecnica di Kerr Lens Mode Locking per produrre impulsi ultracorti ( $\sim 100 \text{ fs}$ ) con una repetition rate di 250 KHz (cioè un impulso ogni  $4 \mu\text{s}$ );
- un *detector differenziale bilanciato* costruito appositamente per eseguire queste misure, che presenta caratteristiche di elevata velocità dell'elettronica (tale da consentire la detezione di un impulso ultracorto ogni  $4 \mu\text{s}$  mantenendo separati i segnali) ed elevato rapporto tra shot noise e rumore elettronico, in modo da essere sensibile alle fluttuazioni dovute alla natura quantistica della luce;
- una *scheda di acquisizione* in grado analizzare centinaia di impulsi ugualmente preparati (necessari per la ricostruzione della funzione di Wigner) e di calcolarne la media, la varianza ed i momenti successivi per ottenere un'analisi statistica della misura.

Piccole modifiche al set-up ci hanno permesso di effettuare essenzialmente tre tipi di *misure*. La prima, una sorta di *detezione omodina senza l'oscillatore locale*, consiste in un processo di Scattering Raman Stimolato in cui il segnale finale è diviso da un beam splitter 50:50 in due fasci che vengono misurati dal detector differenziale.

Non è difficile immaginare che una misura di questo tipo dovrebbe fornire

---

una differenza di intensità media nulla; quest'ipotesi è confermata anche dalla teoria alla base della detezione omodina (basta sostituire all'oscillatore locale il vuoto). Al contrario il risultato di questa misura è un'intensità media che, dopo l'arrivo del pump sul campione, oscilla alla frequenza del modo Raman eccitato. L'analisi della varianza fornisce lo stesso risultato, ma in questo caso le oscillazioni presentano una differenza di fase rispetto a quelle della media. La varianza inoltre presenta un'altra componente di Fourier a una frequenza circa doppia rispetto a quella del modo vibrazionale. Le misure sono state ripetute e presentano sempre lo stesso risultato. Probabilmente la presenza di segnale è dovuta a un semplice sbilanciamento tra i due rami in uscita dal beam splitter, che produrrebbe appunto risultati simili. Tuttavia questa ipotesi non spiega il comportamento della varianza, che resta un problema aperto.

La seconda è una misura di *Scattering Raman Stimolato risolto in tempo*: l'intensità del probe scatterato dal campione in seguito all'eccitazione di modi Raman viene misurata dal detector. Il risultato di questo tipo di misura è l'oscillazione dell'intensità alla frequenza del solito modo Raman a  $128 \text{ cm}^{-1}$ . Anche la varianza presenta lo stesso comportamento dell'intensità, compresa la fase. In condizioni di rumore sufficientemente basso si nota una seconda componente di Fourier nella varianza ad una frequenza doppia rispetto a quella del modo Raman.

Questo effetto può essere spiegato con uno squeezing dei fotoni di probe: l'evoluzione temporale di un autostato dell'Hamiltoniana dell'oscillatore armonico quantistico (e quindi anche dei fotoni) nello spazio delle fasi è infatti rappresentata da un'area che ruota attorno all'origine degli assi. Se lo stato è squeezed, e quindi la deviazione standard (rappresentata nello spazio delle fasi dalla larghezza della distribuzione) lungo  $q$  è diversa da quella lungo  $p$ , si può facilmente vedere che la varianza oscilla al doppio della frequenza.

L'ipotesi di squeezing è confermata dalla terza misura, una *Detezione Omodina risolta in tempo*. Si tratta di una normale misura di tomografia quantistica effettuata a diversi ritardi temporali  $\tau$  tra il pump ed il probe. Il risultato è un grafico tridimensionale in cui la quadratura di campo dipende sia dalla fase relativa tra segnale e oscillatore locale (come normalmente

accade nella detezione omodina), che dall'intervallo di tempo  $\tau$ . Fissando la fase tra i due impulsi è possibile studiare la dipendenza temporale della quadratura di campo: anche questa grandezza presenta le tipiche oscillazioni per tempi successivi rispetto all'arrivo del pump.

Fissando invece il tempo otteniamo misure della quadratura in funzione della fase tra il probe scatterato e l'oscillatore locale, che ci permettono di ricostruire la funzione di Wigner al tempo fissato. Ripetendo questa operazione per tutti gli intervalli temporali  $\tau$  otteniamo l'evoluzione temporale dello stato quantistico del probe. Da una prima analisi delle funzioni di Wigner notiamo subito un'oscillazione del numero di fotoni (che equivale ad una variazione della distanza dall'origine dello spazio delle fasi) e un leggero squeezing (la figura risulta schiacciata lungo la direzione della variabile  $q$ ). Per avere un'analisi più quantitativa basta utilizzare le funzioni di Wigner ottenute per calcolare il valore di aspettazione delle osservabili che ci interessano, quali il numero di fotoni, le varianze e il parametro di squeezing. I primi due riflettono il comportamento osservato nelle misure di Scattering Raman risolto in tempo, mentre l'ultimo mostra oscillazioni alla solita frequenza di circa 3.9 THz, ma i suoi valori, per quanto piccoli, non raggiungono mai lo zero.

Come anticipato non esiste una teoria quantistica che descriva l'interazione tra il campo vibrazionale e quello elettromagnetico. Pertanto se da un lato è noto che i modi vibrazionali si mappano sull'intensità del fascio scatterato, dall'altro non sappiamo come l'indeterminazione dei primi modifichi lo stato quantistico dei fotoni.

Abbiamo quindi tentato di sviluppare un modello fenomenologico che descriva questa interazione, basato sull'ipotesi che l'Hamiltoniana utilizzata per descrivere l'interazione tra il pump e il campione nello stato iniziale sia valida anche per quella tra il probe ed il campione. Il processo totale è stato poi suddiviso in più fasi (arrivo del pump sul campione, interazione con l'ambiente durante l'intervallo tra pump e probe, arrivo del probe, misura e caratterizzazione dello stato quantistico del segnale), per ognuna delle quali abbiamo ottenuto l'operatore densità  $\rho$ . Da questa formulazione sembra evidente che lo stato quantistico del probe sia influenzato da quello fononico, sebbene non sia ancora chiaro quali possano essere le conseguenze.

---

Scopo delle prossime simulazioni numeriche sarà capire quali siano gli effetti di uno stato fononico coerente e squeezed sullo stato quantistico della luce in questo tipo di esperimenti e se effettivamente informazioni sullo stato quantistico vibrazionale possano essere accessibili con misure di ottica quantistica risolte in tempo.



# Bibliografia

- [1] Shaul Mukamel. *Principles of Nonlinear optical spectroscopy*. Oxford University Press, 1995.
- [2] O. V. Misochko. «Nonclassical states of lattice excitations: squeezed and entangled phonons». In: *Physics-Uspokhi* 56 (2013), pp. 868–882.
- [3] Scully e Zubairy. *Quantum Optics*. Cambridge University Press, 1997.
- [4] Robert W. Boyd. *Nonlinear Optics*. Academic Press, 2007.
- [5] Wolfgang P. Schleich. *Quantum Optics in Phase Space*. Wiley-VCH, 2001.
- [6] Ulf Leonhardt. *Measuring the Quantum State of Light*. CAMBRIDGE STUDIES IN MODERN OPTICS, 1997.
- [7] J. G. Snijders. «Quantum statistical response function». 1998. URL: <http://theochem.chem.rug.nl/publications/PDF/ft328.pdf>.
- [8] Peter Hamm. «Principles of Nonlinear Optical Spectroscopy: A Practical Approach». 2005. URL: <http://www.mitr.p.lodz.pl/evu/lectures/Hamm.pdf>.
- [9] E. P. Wigner. «On the Quantum Correction Fro Thermodynamic Equilibrium». In: *Physical Review* 40 (1932), p. 749.
- [10] URL: <http://www.iqst.ca/quantech/wigner.php>.
- [11] Martina Esposito. «Design and experimental realization of a pulsed homodyne detector for optical quantum states characterization». Università degli Studi di Trieste, 2012.
- [12] A. Ferraro, S. Olivares e M. G. A. Paris. *Gaussian states in quantum information*. Bibliopolis, Napoli, 2005.

## BIBLIOGRAFIA

---

- [13] M. Esposito et al. «Pulsed homodyne Gaussian quantum tomography with low detection efficiency». In: *New Journal of Physics* 16 (2014).
- [14] Mark Fox. *Optical properties of solids*. Oxford Master Series in Condensed Matter Physics, 2010.
- [15] H. Hansen. «An ultra-sensitive pulsed balanced homodyne detector : Application to time-domain quantum measurements». In: *Optics letter* 26.21 (2001), p. 1714.
- [16] Francesco Randi. «Pulsed homodyne detection for quantum state reconstruction applied to ultrafast non-equilibrium spectroscopy». Università degli Studi di Trieste, 2013.
- [17] Martina Esposito. «Excitation of coherent phonons in alpha-quartz by Impulsive Stimulated Raman Scattering». 2014.
- [18] J. F. Scott e S. P. S. Porto. «Longitudinal and Transverse Optical Lattice Vibrations in Quartz». In: *Physical Review* 161 (1967), p. 903.
- [19] D. Underwood A. Rundquist J. Broman e D. Blank. «Polarization-dependent detection of impulsive stimulated Raman scattering in alpha-quartz». In: *Journal of Modern Optics* 52 (2006), pp. 2501–2510.
- [20] URL: <http://www.chemguide.co.uk/atoms/structures/giantcov.html>.
- [21] URL: <http://wps.prenhall.com/wps/media/objects/3311/3391416/blb1107.html>.
- [22] X. Hu e F. Nori. «Phonon Squeezed States: Quantum Noise Reduction in Solids». In: *Physica B* 263-264 (1999).
- [23] Keith A. Nelson Lisa Dhar John A. Rogers. «Time-resolved vibrational spectroscopy in the impulsive limit». In: *Chem. Rev* 94.1 (1994), 157–193.
- [24] D.M. Fritz et al. «Ultrafast Bond Softening in Bismuth: Mapping a Solid's Interatomic Potential with X-rays». In: *Science* 315.5812 (2007), pp. 633–636.
- [25] E. Papalazarou et al. «Coherent Phonon Coupling to Individual Bloch States in Photoexcited Bismuth». In: *Phys. Rev. Lett.* 108.25 (2012).

- 
- [26] et al. J. J. Li. «Optical Probing of Ultrafast Electronic Decay in Bi and Sb with Slow Phonons». In: *Phys. Rev. Lett.* 110.4 (2013).
- [27] A. Hussain e S. R. Andrews. «Absence of phase-dependent noise in time-domain reflectivity studies of impulsively excited phonons». In: *Phys. Rev. B* 81.22 (2010).
- [28] Kelvin Rubén Titimbo Chaparro. «Creation and detection of squeezed phonons in pump and probe experiments: a fully quantum treatment». Università degli Studi di Trieste, 2015.
- [29] Mark Fox. *Quantum Optics. An introduction*. Oxford Master Series in Physics, 2006.
- [30] Daniele Fausti. «Dinamiche elettroniche di superficie». Università Cattolica Brescia, 2003.
- [31] URL: [http://en.wikipedia.org/wiki/Kerr-lens\\_modelocking](http://en.wikipedia.org/wiki/Kerr-lens_modelocking).
- [32] A. I. Lvovsky e M. G. Raymer. «Continuous-variable optical quantum state tomography». In: *Review of modern physics* 81 (2009), pp. 299–332.
- [33] L. Artiles C. Butucea M. Guta. «Minmax and adaptive estimation of the Wigner function in quantum homodyne tomography with noisy data.» In: *The Annals of Statistics* 35.2 (2007).
- [34] Hans A. Bachor e Timothy C. Ralph. *A Guide to experiments in Quantum Optics*. WILEY-VCH, 2004.
- [35] S. Tomsovic O. Bohigas e D. Ullmo. «Manifestations of classical phase space structures in quantum mechanics». In: *PHYSICS REPORTS* 223.2 (1993), pp. 43–133.
- [36] M. O. Scully M. Hillery R. O’Connell e E. P. Wigner. «Distribution functions in physics: fundamentals». In: *PHYSICS REPORTS* 106.3 (1984), pp. 121–167.



# Ringraziamenti

Le prime persone da ringraziare sono sicuramente Martina e Daniele, perchè hanno cominciato a sopportarmi ben prima dell'inizio di questo lavoro; perchè quando non sapevo cosa scegliere (come sempre!) sono stati capaci di mostrarmi le alternative cercando di indirizzare la mia scelta il meno possibile, perchè alla fine "te la devi sentire tu". Per avermi inserita in un progetto che esisteva già indipendentemente da me e per il quale forse non ho fatto abbastanza... Perchè sono sempre riusciti a convincermi che in laboratorio stava andando tutto bene, quando secondo me stava andando tutto male, annientando i miei dubbi con il loro entusiasmo. Perchè dopo aver distrutto la bozza di un capitolo della tesi ti dicono "secondo me è scritto bene!" e perchè sono più preoccupati loro del mio futuro di quanto lo sia io. Ma soprattutto perchè, nonostante il mio carattere spesso non lo permetta, hanno fatto molto di più di quanto sia richiesto a un relatore e un correlatore.

Ringrazio il prof. Fulvio Parmigiani per i confronti schietti e costruttivi, che lasciano da parte la retorica per andare al nocciolo della questione.

Grazie a Ghil e Franz per le pause, i pranzi e gli altri momenti passati assieme, perchè la loro assoluta incapacità di "staccare la spina" persino in queste situazioni ha prodotto ottimi consigli anche per il nostro esperimento...

A Fabio Benatti, Roberto Floreanini, Kelvin e Klaus per i confronti e le discussioni che di certo non finiranno con questa tesi.

Grazie a Giovanni Franchi, perchè senza le sue competenze e la sua voglia di accettare nuove sfide non avremmo mai raggiunto efficienze così alte nell'esperimento.

A tutti i componenti del gruppo *T-Rex*, per il loro modo di interpretare la

vita in laboratorio e per non avermi mai fatto sentire “l’ultima arrivata”.

Un grazie a tutti coloro che hanno condiviso questi cinque anni (e qualche mese...) di studi a Trieste: ai miei compagni di banco (praticamente fissi!) sia della triennale che della magistrale, a chi ha trascorso con me interi pomeriggi in laboratorio (ed interi weekend a scrivere relazioni!), a chi mi ha fatto scoprire quanto possa essere costruttivo (e produttivo!) studiare assieme e a chi mi ha ospitato, o si è offerto di ospitarmi, perchè “dopo una certa ora non ci sono più treni”.

Un grazie alla mia famiglia, senza la quale, ovviamente, non sarei qui. Per i consigli, il supporto, che non ha mai sconfinato nella “bugia a fin di bene” e per aver sempre pensato a ciò che non avevo tempo di fare io perchè “la Francy deve studiare”.

Ringrazio tutte le persone che mi hanno sempre accompagnato anche al di fuori dell’università, quelli che quando scendi dal treno, magari alle otto di sera, ti fanno sentire che la tua giornata comincia adesso!

Quelli che solo guardandoti in faccia capiscono cosa è il caso di dirti in quel momento e cosa è il caso di rinviare...

Quelli che ti aiutano a sollevare lo zaino quando è troppo pesante (e non solo metaforicamente!!!) e chi “ha una marcia in più e vince in partenza”.

A chi abita un po’ più lontano e con mezzi più o meno tecnologici trova il modo di contattarti per chiederti semplicemente “come va?”.

Un grazie a chi mi cerca anche quando forse un po’ mi nascondo; a chi dopo un weekend di studio e panico da esame ti propone una cena assieme, perchè “tanto dovresti cenare comunque!” e a chi invece preferisce essere rincorso, perchè mi ha insegnato, forse involontariamente, che ci sono dei motivi per cui vale la pena avere (costantemente!) un po’ di fiatone.

Grazie a chi ti ritiene un genio solo perchè sei iscritto al corso di Laurea in Fisica e a quelli per cui i tuoi studi non fanno nessuna differenza; anzi quando scoprono cosa fai nella vita rispondono: “Wow, anch’io da grande voglio studiare ginnastica!”.

A chi di questa tesi leggerà solo i ringraziamenti, perchè crede di non poter

---

capire altro, e a chi non leggerà neanche quelli, perchè “la gratitudine si vede nei fatti e non con qualche parola”.

Infine ringrazio chi, leggendo, si sarà riconosciuto in molte delle cose che ho scritto, perchè significa che ha fatto molto per me. Ma soprattutto ringrazio chi non ricorda di aver fatto o detto niente di tutto questo, non solo perchè in questo modo sottolinea l'efficienza della mia memoria a lungo termine (il che aumenta non di poco la mia autostima!!!), ma anche perchè dimostra di aver agito spontaneamente, senza averci pensato troppo, senza ritenere questo favore un sacrificio, senza aspettarsi niente in cambio...